

**THEORETICAL INVESTIGATION OF CONFORMATIONS AND  
ENERGIES OF METAL-FREE ORGANIC DYE FOR  
DYE-SENSITIZED SOLAR CELLS BY DFT / TDDFT STUDY**

**RATTANAWALEE RATTANAWAN**

**A THESIS SUBMITTED IN PARTIAL FULFILLMENT OF THE REQUIREMENTS  
FOR THE DEGREE OF MASTER OF SCIENCE**

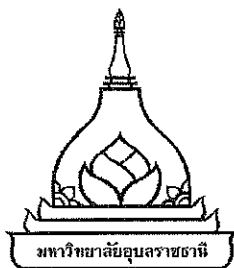
**MAJOR IN CHEMISTRY**

**FACULTY OF SCIENCE**

**UBON RATCHATHANI UNIVERSITY**

**YEAR 2012**

**COPYRIGHT OF UBON RATCHATHANI UNIVERSITY**



**THESIS APPROVAL**  
**UBON RATCHATHANI UNIVERSITY**  
**MASTER OF SCIENCE**  
**MAJOR IN CHEMISTRY FACULTY OF SCIENCE**

**TITLE** THEORETICAL INVESTIGATION OF CONFORMATIONS AND ENERGIES OF  
METAL-FREE ORGANIC DYE FOR DYE-SENSITIZED SOLAR CELLS BY  
DFT / TDDFT STUDY

**NAME** MS.RATTANAWALEE RATTANAWAN

**THIS THESIS HAS BEEN ACCEPTED BY**

.....  
(ASST.PROF.DR.SIRIPORN JUNGSTUTIWONG) CHAIR

.....  
(DR.SUPAWADEE NAMUANGRUK) COMMITTEE

.....  
(DR.TINNAGON KEAWIN) COMMITTEE

.....  
(ASST.PROF DR.CHAN INNTAM) COMMITTEE

.....  
(ASST.PROF.DR.JANPEN INTARAPRASERT) DEAN

**APPROVAL BY UBON RATCHATHANI UNIVERSITY**

.....  
(ASSOC.PROF.DR.UTITH INPRASIT)

VICE PRESIDENT FOR ACADEMIC AFFAIRS

FOR THE PRESIDENT OF UBON RATCHATHANI UNIVERSITY

ACADEMIC YEAR 2012

## ACKNOWLEDGMENTS

I would like to thank my advisor Asst.Prof.Dr.Siriporn Jungsuttiwong for her excellent guidance, constant encouragement, and invaluable discussions during the course of research.

I wish to express Dr.Tinnagon Keawin and Asst.Prof.Dr.Chan Inntam for all of comment and excellent suggestions throughout my study. Thank you so much to Thailand Graduate Institute of Science and Technology (TGIST) for research scholarship to me.

I would also like to thank Assoc.Prof.Dr.Vinich Promarak for experiment data.

I am very thankful to thank Dr.Supawadee Namuangrak for serving on my thesis examination as chairperson and for constructive supervision and suggestion.

I would also like to thank Mr.Thanisorn Yakhantip for PC computer clustering.

I am grateful to all members in the Center for Organic Electronic and Alternative Energy, Department of Chemistry, Faculty of Science, Ubon Ratchathani University. Many thank to my sister, brother and everyone who contributed their time and advice to my project.

Finally, my graduation would not be achieved without best wish from my parents who help me for everything and always gives me greatest love, encouragement and financial support everything during my study.

(Miss Rattanawalee Rattanawan)

Researcher

## บทคัดย่อ

ชื่อเรื่อง : การศึกษาสมบัติทางโครงสร้างและพลังงานของสีย้อมไวแสงอินทรีย์ที่ปราศจากโลหะเพื่อใช้ในเซลล์แสงอาทิตย์ชนิดสีย้อมไวแสงโดยใช้ระเบียบวิธีดีเอฟที/ทีดีดีเอฟที

โดย : รัตนาวลี รัตนวัน

ชื่อปริญญา : วิทยาศาสตร์มหาบัณฑิต

สาขาวิชา : เคมี

อาจารย์ที่ปรึกษา : ผู้ช่วยศาสตราจารย์ ดร. ศิริพร จิงสุทธีวงษ์

ศัพท์สำคัญ : ทฤษฎีเค้นซิต์ฟังก์ชันแนล ทฤษฎีไฮมิดเพนเด็นต์-เค้นซิต์ฟังก์ชันแนล สีย้อมไวแสงที่ปราศจากโลหะ

ในงานวิจัยนี้ได้ทำการศึกษาสมบัติทางโครงสร้างและค่าพลังงานของโมเลกุลสีย้อมไวแสงที่ปราศจากโลหะโดยใช้ระเบียบวิธีทางเคมีควอนตัม ระเบียบวิธีเค้นซิต์ฟังก์ชันแนล และไฮมิดเพนเด็นต์-เค้นซิต์ฟังก์ชันแนล ถูกนำมาใช้ในการคำนวณ โครงสร้างและพลังงานของโมเลกุลที่เป็นอนุพันธ์ของคูมาริน อนุพันธ์ของไดเมททิลอะนิลีน และอนุพันธ์ของคาบาโซล-ฟลูออรีน โดยทำการศึกษาผลของหมู่ให้อิเล็กตรอน หมู่เชื่อมต่อและหมู่รับอิเล็กตรอนที่แตกต่างกัน โครงสร้างที่สถานะพื้นถูกคำนวณที่ระดับ B3LYP/6-31G(d,p) โดยใช้โปรแกรม Gaussian 03 สมบัติในการส่งผ่านอิเล็กตรอนภายใน โมเลกุลสีย้อมและค่าพลังงานกระตุ้นถูกคำนวณโดยใช้ระเบียบวิธีไฮมิดเพนเด็นต์-เค้นซิต์ฟังก์ชันแนล (TDDFT) ที่ระดับเดียวกับการคำนวณในสถานะพื้น ผลการคำนวณแสดงให้เห็นว่ามีการส่งผ่านประจุภายในโมเลกุลซึ่งสอดคล้องกับการส่งผ่านอิเล็กตรอนจากระดับพลังงาน HOMO ไปยังระดับพลังงาน LUMO นอกจากนี้ยังได้เปรียบเทียบผลที่ได้จากการคำนวณและผลที่ได้จากการทดลอง พบว่าผลที่ได้จากการคำนวณมีแนวโน้มที่สอดคล้องกับการทดลองสามารถกล่าวได้ว่าการคำนวณโดยระเบียบวิธีไฮมิดเพนเด็นต์-เค้นซิต์ฟังก์ชันแนลสามารถทำนายสมบัติทางโครงสร้างและพลังงานของโมเลกุลสีย้อมไวแสงที่ปราศจากโลหะในเซลล์แสงอาทิตย์ชนิดสีย้อมไวแสงได้

**ABSTRACT**

**TITLE** : THEORETICAL INVESTIGATION OF CONFORMATIONS AND ENERGIES  
OF METAL-FREE ORGANIC DYE FOR DYE-SENSITIZED SOLAR CELLS  
BY DFT / TDDFT STUDY

**BY** : RATTANAWALEE RATTANAWAN

**DEGREE** : MASTER OF SCIENCE

**MAJOR** : CHEMISTRY

**ADVISOR** : ASST.PROF.DR.SIRIPORN JUNGSTIWIWONG

**KEYWORDS** : DENSITY FUNCTIONAL THEORY / TIME-DEPENDENT DENSITY  
FUNCTIONAL THEORY/ METAL - FREE ORGANIC DYE

The conformations, electronic and optical properties of metal free organic dyes have been investigated by Density functional theory (DFT) and Time-dependent DFT (TDDFT) calculation. The effects of different donors, different linkers and different acceptors have been performed on the coumarin derivatives, *N,N*-dimethylaniline and carbazole-fluorene derivative. The ground state structures were optimized at the B3LYP/6-31G (d,p) level of theory implemented in Gaussian 03 program. The intramolecular charge transfer (ICT) properties were evaluated by single point energy calculation using TDDFT at the same basis set. Our results show that the ICT character involves primarily the promotion of an electron from the HOMOs to the LUMOs. The calculation results were compared with the experimental data. We also found that the calculation results are in good agreement with experimental results. The TDDFT calculations can predict the properties of structure and energy of organic materials for DSCs applications.

# CONTENTS

	PAGES
ACKNOWLEDGMENTS	I
THAI ABSTRACT	II
ENGLISH ABSTRACT	III
CONTENTS	IV
LIST OF TABLES	VI
LIST OF FIGURES	VIII
LIST OF ABBREVIATIONS	XI
CHAPTER	
1 INTRODUCTION	
1.1 General Introduction	1
1.2 Objectives of this research	15
2 COMPUTATIONAL DETAIL	
2.1 Hartree–Fock Theory	17
2.2 Density functional theory	24
2.3 Time-dependent density functional theory	31
3 COUMARIN DERIVATIVES	
3.1 Introduction	33
3.2 Method	35
3.3 Results and discussion	36
3.4 Conclusion	50
4 <i>N,N</i> -DIMETHYLAMINOPHENYL DERIVATIVES	
4.1 Introduction	51
4.2 Method	52
4.3 Results and discussion	53
4.4 Conclusion	61

**CONTENTS (CONTINUED)**

	<b>PAGES</b>
<b>5 CARBAZOLE-FLUORENE DERIVATIVES</b>	
5.1 Introduction	62
5.2 Method	63
5.3 Results and discussion	64
5.4 Conclusion	71
<b>6 CONCLUSIONS</b>	
6.1. Coplanarity of the D- $\pi$ -A structure	72
6.2 Intramolecular charge transfer	74
6.3 Energy Gap	76
6.4 Light Harvesting Efficiency	78
6.5 TiO <sub>2</sub> adsorption	80
<b>REFERENCES</b>	<b>83</b>
<b>APPENDIX</b>	<b>89</b>
<b>VITEA</b>	<b>107</b>

## LIST OF TABLES

TABLE	PAGES
3.1 Selected inter-ring distances (Å) and dihedral angles (°) of O-CT1A, O-CT2A, O-CTPA, O-CT3A and O-CT2PA calculated by B3LYP/6-31G(d,p) calculations	37
3.2 Summarizes the energies and percentage contribution of frontier molecular orbital of O-CT1A, O-CT2A, O-CTPA, O-CT3A and O-CT2PA calculated by B3LYP/6-31G(d,p)	39
3.3 The calculated HOMO-LUMO energy gap of O-CT1A, O-CT2A, O-CT3A, O-CTPA and O-CT2PA	40
3.4 The excitation energies, oscillator strengths and molecular compositions for the 2 lowest states by TD-B3LYP/6-31G(d,p)	43
3.5 The excitation energies, oscillator strengths and molecular compositions for the 2 lowest states by TD-B3LYP/6-31G(d,p)	43
3.6 Selected inter-ring distances (Å) and dihedral angles (°) of N-CT2A and N-CT3A by B3LYP/6-31G(d,p).	45
3.7 Summarizes the energies and character of frontier orbital of N-CT2A and N-CT3A calculated by B3LYP/6-31G(d,p)	47
3.8 The calculated HOMO-LUMO energy gap of N-CT2A and N-CT3A	47
3.9 The excitation energies, oscillator strengths and molecular compositions for the 2 lowest states by TD-B3LYP/6-31G(d,p)	49
4.1 Selected inter-ring distances (Å) and dihedral angles (°) of PTPA, PT2A, PT2PA and PT3A by B3LYP/6-31G(d,p).	54
4.2 Summarizes the energies and percentage contribution of frontier orbital of PTPA, PT2A, PT2PA and PT3A calculated by B3LYP/6-31G(d,p)	56
4.3 The calculated HOMO-LUMO energy gap of PTPA, PT2A, PT2PA and PT3A	57



## LIST OF TABLES (CONTINUED)

TABLE	PAGES
4.4 The excitation energies, oscillator strengths and molecular compositions for the 2 lowest states by TD-B3LYP/6-31G (d,p)	59
5.1 Selected inter-ring distances (Å) and dihedral angles (°) of TK1 and TK2 by B3LYP/6-31G (d,p)	65
5.2 Summarizes the energies and character of frontier orbital of TK1 and TK2 calculated by B3LYP/6-31G(d,p)	66
5.3 The calculated HOMO-LUMO energy gap of TK1 and TK2	66
5.4 The excitation energies, oscillator strengths and molecular compositions for the lowest states by TD-B3LYP/6-31G (d,p) (solvent)	70
6.1 Selected inter-ring distances (Å) and dihedral angles (°) of O-CT3A, N-CT3A and PT3A calculated by B3LYP/6-31G (d,p) calculations	73
6.2 Summarizes the energies and character of frontier orbital of -CT3A, N-CT3A and PT3A calculated by B3LYP/6-31G (d,p)	75
6.3 The calculated HOMO-LUMO energy gap of O-CT3A, N-CT3A and PT3A	78
6.4 The excitation energies, oscillator strengths and molecular compositions for the 2 lowest states of O-CT3A, N-CT3A and PT3A by TD-B3LYP/6-31G (d,p)	80
6.5 Selected bond length (Å) and adsorption energy (kcal/mol) of O-CT3A, N-CT3A and PT3A complex calculated by Dmol <sup>3</sup> calculation	82

## LIST OF FIGURES

FIGURE	PAGES
1.1 (a)-Typical of DSCs and (b) energy level diagram of DSCs	3
1.2 Molecular structure of N3, N719, Z907 and Black dye	5
1.3 Molecular structure of NKX-2311 and TPA2	6
1.4 Molecular structure of the coumarin derivatives	7
1.5 Molecular structure of the two triphenylamine-based dyes	7
1.6 Molecular structure of organic sensitizers	11
1.7 The Jablonski diagram	14
1.8 Franck – Condon energy diagram	14
1.9 Molecular structures of coumarin derivatives	15
1.10 Molecular structures of dimethylaniline derivatives	16
1.11 Molecular structures of carbazole-fluorene derivatives	16
3.1 Coumarin derivatives	34
3.2 Sketch map structures of the target molecule <i>O</i> -Coumarin and <i>N</i> -Coumarin	35
3.3 The optimize structure of <i>O</i> -CTA, <i>O</i> -CT2A, <i>O</i> -CTPA, <i>O</i> -CT3A and <i>O</i> -CT2PA by calculated by B3LYP/6-31G(d, p) level of theory	37
3.4 Frontier molecular orbital of <i>O</i> -CTA, <i>O</i> -CT2A, <i>O</i> -CTPA, <i>O</i> -CT3A and <i>O</i> -CT2PA calculated by B3LYP/6-31G(d,p) level of theory	40
3.5 (a) Molecular orbital energy diagram of <i>O</i> -CT1A, <i>O</i> -CT2A and <i>O</i> -CT3A and (b) Molecular orbital energy diagram of <i>O</i> -CTPA and <i>O</i> -CT2PA	41
3.6 Calculated absorption spectra of <i>O</i> -CT1A, <i>O</i> -CT2A, <i>O</i> -CTPA, <i>O</i> - CT3A and <i>O</i> -CT2PA by B3LYP/6-31G(d,p)	44
3.7 Sketch map structure of target molecule <i>N</i> -CT2A and <i>N</i> -CT3A	45
3.8 The optimize structure <i>N</i> -CT2A and <i>N</i> -CT3A by calculated by B3LYP/6-31G(d, p) level of theory	45

## LIST OF FIGURES (CONTINUED)

FIGURE	PAGES
3.9 Frontier molecular orbital of N-CT2A and N-CT3A calculated by B3LYP/6-31G(d,p) level of theory	47
3.10 Molecular orbital energy diagram of N-CT2A and N-CT3A	48
3.11 Calculated absorption spectra of N-CT2A and N-CT3A by B3LYP/6-31G(d,p)	49
4.1 <i>N,N</i> -dimethylaniline derivatives	52
4.2 Sketch map structure of target molecule PTPA, PT2A, PT2PA and PT3A	52
4.3 The optimize structure of PTPA, PT2A, PT2PA and PT3A by calculated by B3LYP/6-31G(d, p) level of theory	54
4.4 Frontier molecular orbital of PTPA, PT2A, PT2PA and PT3A calculated by B3LYP/6-31G(d,p) level of theory	56
4.5 Molecular orbital energy diagram of PTPA, PT2A, PT2PA and PT3A	58
4.6 (a) Calculated absorption spectra of PTPA and PT2PA and (b) calculated absorption spectra of PT2A and PT3A by TD-B3LYP/6-31G(d,p)	60
5.1 Sketch map structure of molecule MK-2, D1, D2 and D3	62
5.2 Sketch map structure of target molecule TK1 and TK2	63
5.3 The optimize structure of TK1 and TK2 by calculated by B3LYP/6-31G(d,p) level of theory	65
5.4 Frontier molecular orbital of TK1 and TK2 calculated by B3LYP/6-31G (d,p) level of theory	68
5.5 Molecular orbital energy diagram of TK1 and TK2	69
5.6 Calculated absorption spectra of TK1 and TK2 by TD-B3LYP/6-31G (d,p)	70

## LIST OF FIGURES (CONTINUED)

FIGURE	PAGES
6.1 The structure of O-CT3A, N-CT3A and PT3A by calculated B3LYP/ 6-31G (d,p)	72
6.2 The optimize structure of O-CT3A, N-CT3A and PT3A by calculated B3LYP/ 6-31G (d,p)	73
6.3 Frontier molecular orbital of O-CT3A, N-CT3A and PT3A calculated by B3LYP/ 6-31G (d,p)	76
6.4 The charge density difference of O-CT3A, N-CT3A and PT3A calculated by B3LYP/6-31G (d,p). The contour thresholds for molecular orbitals and density differences are 0.02 and 0.0004 a.u., respectively. The yellow and blue colors indicate a decrease and increase of charge densities, respectively	76
6.5 Frontier molecular orbital of O-CT3A, N-CT3A and PT3A calculated by B3LYP/ 6-31G (d,p)	77
6.6 Calculated absorption spectra of O-CT3A, N-CT3A and PT3A by B3LYP/6-31G (d,p)	79
6.7 Structure of O-CT3A, N-CT3A and PT3A adsorbed on $(\text{TiO}_2)_{38}$ surface by Dmol <sup>3</sup> calculation	81

## LIST OF ABBREVIATIONS

## ABBREVIATION FULL WORD

Å	Angstroms
$\lambda_{ab}$	Absorption wavelength
B3LYP	Becke's three parameter hybrid functional using the Lee-Yang-Parr functional
CB	Conduction band
°	Degree of angle
DFT	Density functional theory
DSCs	Dye sensitized solar cells
eV	Electron volt
$\lambda_{em}$	Emission wavelength
$E_{gab}$	Energy gab
$\Delta E_{H-L}$	HOMO-LUMO gap
HOMO	Highest occupied molecular orbital
LUMO	Lowest unoccupied molecular orbital
TDDFT	Time dependent density functional theory
nm	Nanometers

## CHAPTER 1

### INTRODUCTION

#### 1.1 General introduction

##### 1.1.1 Dye-sensitized solar cells (DSCs)

Dye-sensitized solar cells (DSCs), an alternative to the conventional solar cell, were developed by O'regan and Gratzel [1]. They have been increasing interest in DSCs because of their high photoelectric conversion efficiency, simple assemble technology and potential low cost. In these cells, the sensitizer is one of the key components for high power-conversion efficiency. Among the material tested so far, ruthenium polypyridyl complexes have shown outstanding charge-transfer properties. Overall energy conversion efficiency greater than 10% was achieved with two excellent dyes, N3 and N719 [2]. However, ruthenium complex dyes are not suitable for cost-effective and environmentally friendly photovoltaic system because ruthenium is a rare and expensive metal, which limits the potentially wide application of these complexes [3].

Since metal free sensitizers are being investigated as alternative sensitizers for DSCs applications. Most of the reported highly efficient metal free dyes could be classified as electron donor acceptor  $\pi$ -conjugated (D- $\pi$ -A) compounds [4]. For further development of highly efficient dye in DSCs, the dye must be designed to absorb most of the radiation of sun light in visible and near-IR region to produce a large photocurrent response. In addition, suitable energy level and location of highest occupied molecular orbital (HOMO) and lowest occupied molecular orbital (LUMO) of the dye are required to match the  $I/I_3^+$  redox potential and conduction band edge level of the  $TiO_2$  semiconductor, respectively [5].

Currently, molecular modeling techniques and especially quantum chemistry offer a competitive alternative for the interpretation of the experimental data. Therefore the theoretical investigations of the physical properties of dye sensitizers are very important in order to disclose the relationship among the performance, structures and the properties. It is also helpful to design and synthesis novel sensitizers with higher performance. The density functional theory

(DFT) and time-dependent density functional theory (TDDFT) methods were performed to theoretically investigate the ground-state and excited-state electronic structures. The theoretical prediction will be useful and helpful for the design and synthesis of novel molecular materials. In this work, we have studied the electronic structure and the optical properties of organic sensitizer. First, we consider the geometry of the organic dyes in the electronic ground state using DFT method. Second, we explore the optical response of the different structures using TDDFT [6]. The aim of this work is to understand the physical-chemical aspects that govern the light absorption process in the organic metal free dye to find the parameters that affect to the efficiency of these dyes as DSCs sensitizers.

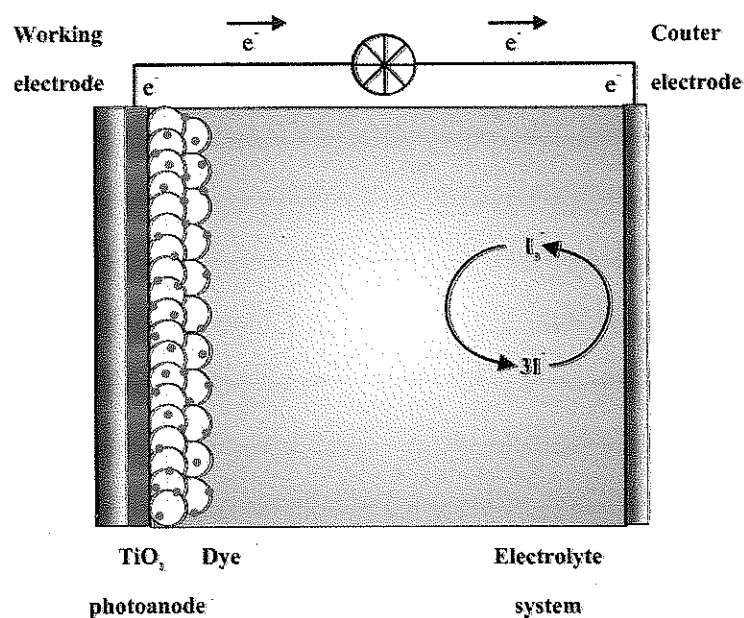
### 1.1.2 Basic principle of DSCs

The typical DSCs consist of three main components: (i) organic sensitizer coating with wide band gap semiconductor which is placed in contact with a redox electrolyte, the material of choice has been  $\text{TiO}_2$  (anatase), (ii) an electrolyte solution containing redox couple such as  $\text{I}^-/\text{I}_3^-$ , the regeneration of the sensitizer by iodide intercepts the recapture of the conduction band electron by the oxidized dye and (iii) a counter electrode which is a platinized conductive glass substrate shown in Figure 1.1 (a). The iodide is regenerated by the reduction of tri-iodide at the counter-electrode the circuit being completed via electron migration through the external load. The voltage generated under illumination corresponds to the difference between the fermi level of the electron in the solid and the redox potential of the electrolyte. Overall the device generates electric power from light without suffering any permanent chemical transformation [7].

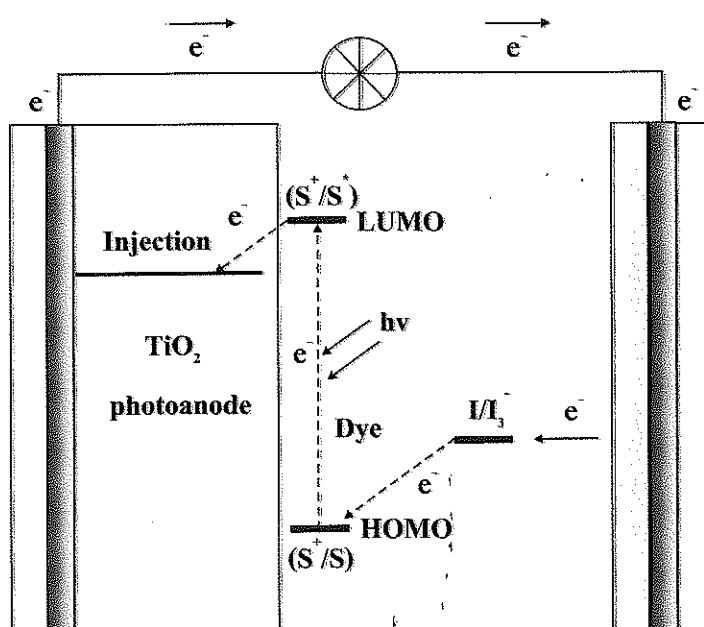
As shown in Figure 1.1 (b), the DSCs process is initiated by dye absorb photons which excite the dye molecule from the ground state to the excited state, and the resultant excited dye molecule injects an electron to the conduction band (CB) of  $\text{TiO}_2$ . The resultant oxidized dye molecule is quickly reduced to its original state by  $\text{I}^-$  ions in the electrolyte. When  $\text{I}^-$  is oxidized to its oxidized form  $\text{I}_3^-$  and the latter is reduced back to  $\text{I}^-$  through accepting electrons at the counter electrode. The electric circuit is completed by diffusion of  $\text{I}^-$  and  $\text{I}_3^-$  from and to the counter electrode, respectively.

To improve the efficiency of DSCs, the highest occupied molecular orbital (HOMO) and the lowest unoccupied molecular orbital (LUMO) of dyes must be situated under  $\text{I}^-/\text{I}_3^-$  redox couple and placed above the CB of the  $\text{TiO}_2$  semiconductor to produce regeneration

and efficient electron injection. In addition, the solar spectrum of dye should be sensitive to cover UV/visible and near-IR range to increase broad-band light harvesting [8].



(a)



(b)

**Figure 1.1** (a) Typical of DSCs and (b) energy level diagram of DSCs



### 1.1.3 Metal-free organic sensitizer

The ideal sensitizer for DSCs converting standard global AM 1.5 sunlight to electricity should absorb all light below a wavelength of about 920 nm. In addition, it must also carry attachment groups such as carboxylate to the semiconductor oxide surface. The energy level of the excited state should be well matched to the lower bound of the conduction band of the oxide to minimize energetic losses during the electron transfer reaction. Its redox potential should be sufficiently positive that it can be regenerated via electron donation from the redox electrolyte. Therefore, much effort has been put into improve the power conversion efficiency. Moreover, it did not take much time for the scientific community to prove the DSCs are alternatives to the conventional first- and second-generation silicon solar cells. In fact, the DSCs technology works well, even in diffused light conditions, unlike the first-and second-generation photovoltaic devices [9, 10].

The sensitizer is one of the key components in achieving high efficiency and durability of DSCs devices. The extensively used charge-transfer sensitizers employed so far in such cells are ruthenium complex producing solar energy-to-electricity conversion efficiencies of 11% shown in Figure 1.2. Although ruthenium complexes have shown very good efficiency, there are certain limitations in the practical application of these complexes for DSCs. The first problem is the rarity of the ruthenium metal as a results it is very expensive. Secondly, these complexes have a lack of absorption in the red region of the visible spectrum and also relatively low molar extinction coefficients. The third drawback is that the metal complex-based sensitizers involve careful synthesis and tricky purification steps. A new class of compounds such as metal-free organic dye was developed. Organic sensitizer is indeed possible to tune the absorption and electrochemical properties in a desired manner through suitable molecular design strategies. More interestingly, the high molar extinction coefficient of these metal-free sensitizers is particularly attractive because they enhance the conversion efficiency [11, 12].

The donor-spacer-acceptor (D- $\pi$ -A) system is the basic structure for designing the metal-free dyes due to the effective photo induced intramolecular charge transfer properties. Most of the organic sensitizers applied in DSCs have three important parts: 1) the electron donor 2) the electron acceptor and 3) the linker units for the  $\pi$ -conjugation to enhance the molar absorption coefficient. Thus, it is interesting to study the influence of the electron donor,

the electron acceptor, and the linker separately in metal-free dyes with a general structure donor–linker–acceptor [13].

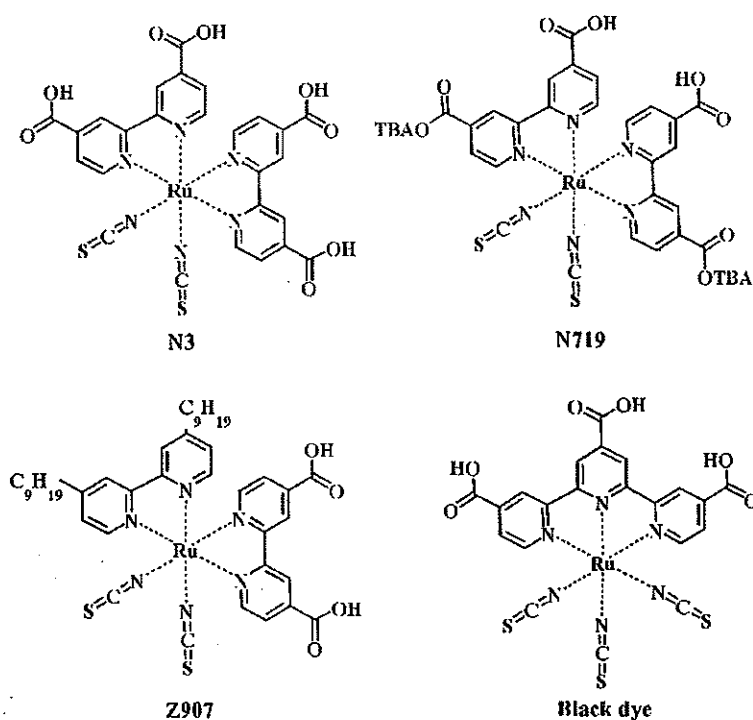
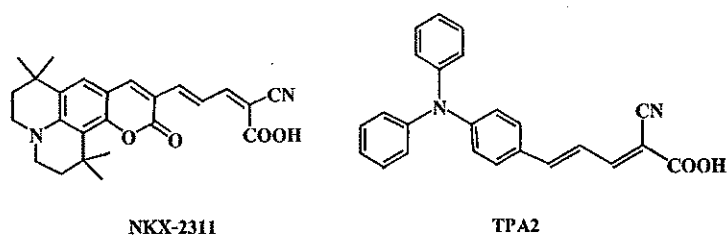


Figure 1.2 Molecular structure of N3, N719, Z907 and Black dye

### 1.1.3.1 Donor part

The dye consists of an electron-donating group,  $\pi$ -spacer and electron acceptor. The influent of different section cause significant differences in photovoltaic character [14]. Kohjiro Hara and coworker developed a class of coumarin derivatives. The novel coumarin dyes for use in DSCs were studied, they employed methine unit ( $-\text{CH}=\text{CH}-$ ) connecting both the cyano ( $-\text{CN}$ ) and carboxyl ( $-\text{COOH}$ ) groups into the coumarin framework expanded the  $\pi$ -conjugation in the dye and thus resulting in a wide absorption in the visible region. A HOMO-LUMO calculation indicated that the electron moves from the coumarin framework to the  $-\text{CH}=\text{CH}-$  unit by photoexcitation of the dye (a  $\pi$ - $\pi^*$  transition). These novel dyes performed as efficient photosensitizers for DSCs. Under optimized condition, the device based on dye molecule NKX-2311 gave 6.0 % efficiency [15]. The structure of NKX-2311 shown in Figure 1.3 which carboxyl group is directly connected to the  $-\text{CH}=\text{CH}-$  unit, this is advantage for effective electron

injection from the dye into the conduction band of  $\text{TiO}_2$ . Moreover triphenylamine has widely been used as an electron donor for metal-free organic sensitizers due to its excellent electron-donating capability and aggregation resistant non-planar molecular configuration. Recently, triphenylamine-based dyes, TPA2, shown in the Figure 1.3 were designed and synthesized. These results suggested that the commercial application of organic dyes in DSCs is promising [16].



**Figure 1.3** Molecular structure of NKX-2311 and TPA2

#### 1.1.3.2 Linker

Moreover the effect of different electron-donating cause significant differences in photovoltaic character,  $\pi$ -spacer is also play a crucial role in determining the solar energy-to-electricity conversion efficiency of DSCs. The thiophene units are used to provide conjugation between the donor and the anchoring groups as well as to increase the molar extinction coefficient of the dye. The absorption maximum of metal-free organic dyes gradually red-shifts with size expansion of their conjugate system by increasing the number of methine units. A drawback related to these dyes that they are liable to experience  $\pi$ -stacked aggregation on  $\text{TiO}_2$  surfaces. Rocio Sanchez-de-Armas and coworker compare similar sensitizers in Figure 1.4. In this series the  $\pi$  electron system increases, the main band becomes wider, the maximum position of the main band and the absorption spectra slightly red-shift, the light harvesting process is more favorable when the absorption spectra is lower and the first band in the spectrum becomes wider extending into the visible region. This modification improves the performance of coumarin dye. Therefore efficiencies up to 7.7% have been reached in DSCs based on coumarin dyes containing two thiophene units [17, 18].

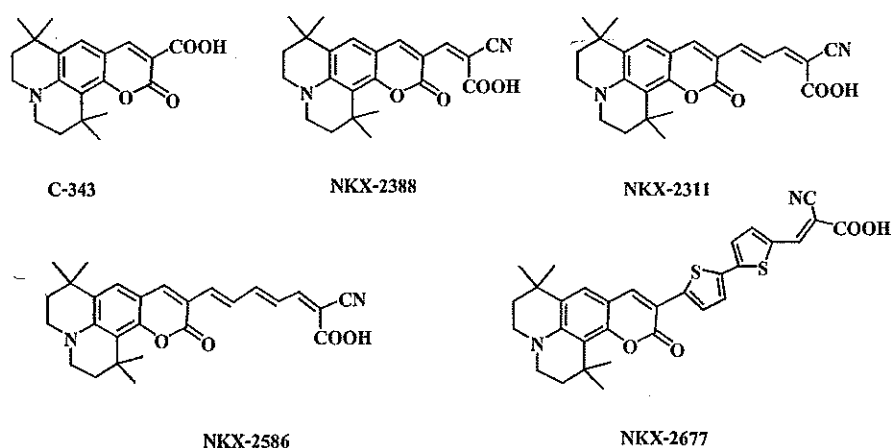


**Figure 1.4** Molecular structure of the coumarin derivatives

### 1.1.3.3 Acceptor

The excited electrons on the dye molecules are injected to the semiconductor film through the acceptor moiety. The acceptor part has significant influence on the photovoltaic properties of the dyes. For example, Wei Xu and co-work designed and synthesized two novel organic dyes (TPAR11 and TC12) in Figure 1.5 containing styryltriphenylamine as the donor part and rhodanine-3-acetic acid or cyanoacrylic acid as the electron acceptor. The influence of two different acceptor moieties on the optical and electrochemical characters of the dyes and the performances of the DSCs were studied [19]. A molecular-orbital calculation shows that the delocalization of the excited state for TPAR11 is broken between the 4-oxo-2-thioxothiazolidine ring and the acetic acid, which affects the electron movement from dye molecule to the semiconductor film [20].

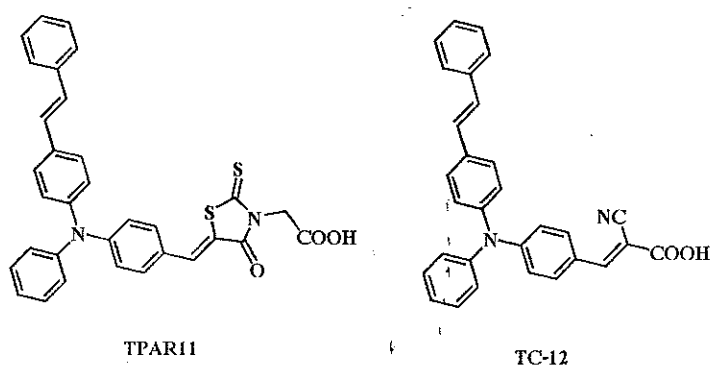


**Figure 1.5** Molecular structure of the two triphenylamine-based dyes

#### 1.1.4 Theoretical investigation on metal-free organic sensitizer

Theoretical calculations can be of great help in the design of new solar cell sensitizers with improved characteristics, thereby providing a deep understanding of the character of the excited states involved in the absorption and injection processes.

Juan Pei and coworker have designed and synthesized a new TPA derivative (TPAR14). The geometrical and electronic properties of the TPAR14 were performed with the Gaussian 03 program package. The calculation was optimized by means of the B3LYP method (Becke three parameters hybrid functional with Lee–Yang–Perdew correlation functionals) in combination with the Pople 6-31+G(d) atomic basis set. The excitation transitions of TPAR14 as shown in Figure 1.6 was calculated using time-dependent density functional theory (TD-DFT) calculations with B3LYP/6-31+G(d). Molecular orbitals were visualized using Gaussview. The calculation results shown that two phenyl of the diphenylvinyl part are arranged in an out-of-plane fashion to minimize the steric hindrance. The rhodanine-3-acetic acid group was found to be essentially coplanar with the neighboring phenyl of TPA unit, reflecting the strong conjugation across the phenyl ring. The HOMO is to a large extent distributed over the system between the donor and acceptor groups. However, the LUMO reflecting the excited state of the dye under light illumination is delocalized across the linker and acceptor group. This distribution of HOMO and LUMO levels is separated in the compound, indicating that the HOMO to LUMO transition can be considered as a charge-transfer transition. Assuming similar molecular orbital geometry when anchored to  $\text{TiO}_2$ , the position of the LUMO close to the anchoring group enhances the orbital overlap with the titanium 3d orbitals and favors electron injection. TD-DFT calculations on a B3LYP/6-31+G(d) level of theory show two transitions with large oscillator strengths ( $f > 0.1$ ), consistent with the absorption spectrum. The lowest transition is calculated at 2.18 eV and corresponds to an ICT excitation from HOMO to LUMO. Density functional theory calculation shows that the electron distribution is shifted from the donor unit to the electron acceptor under light irradiation, which favors efficient ICT [21].

Zhongquan Wan and coworker have reported the calculation results of the organic sensitizer with different arylamine donor as shown in Figure 1.6. The geometries and energies were optimized by density functional theory (DFT) calculations. Gaussian 03 package was used for density functional theory (DFT) calculations. The geometries and energies of the

organic dyes were determined using the B3LYP method with the 6-31G (d,p) basis set. The HOMO is mainly located on the electron donating group and linker, and the LUMO is mainly located in electron withdrawing groups through the linker. It reveals that the benzene linker is essentially coplanar with cyanoacetic acid group. There are effective electron separations between HOMO and LUMO of these dyes induced by light irradiation. The influence of the different arylamine electron donors on the photophysical, electrochemical properties and photovoltaic performances were studied by spectral, electrochemical, photovoltaic experiments, and density functional theory calculations. These findings reveal that different electron donors in organic sensitizers cause significant differences in photovoltaic performance [22].

Ho Wan Ham and Young Sik Kim have designed and studied new indoline dyes as shown in Figure 1.6 that exhibit high efficiency. Density functional theory (DFT) and time-dependent DFT (TDDFT) calculations were performed on the ground state of the indoline dyes. This computational procedure allows us to provide a detailed assignment of the excited states involved in the absorption process. The geometries in the gas phase were optimized by the DFT method using the B3LYP exchange-correlation function together with a 6-31G(d) basis set in the Gaussian 03 program package. Electronic populations of the HOMO and LUMO were calculated to show the position of the localization of electron populations along with the calculated molecular orbital energy diagram. At the ground-state-optimized geometries were performed TDDFT calculations at the B3LYP/6-31G(d) level of theory. Solvation effects were included by the conductor-like polarizable continuum model (CPCM), as implemented in the G03 program package. Calculation of the lowest singlet-singlet excitations at the ground-state-optimized geometries allowed us to simulate the portion of the absorption spectrum. The calculated electronic structure in terms of molecular orbital energies and localization is consistent with the experimental results. The good agreement between the experimental and TDDFT calculated absorption spectra of the D149 sensitizer allowed us to provide a detailed assessment of the main spectral features of a series of dye sensitizers [23].

Haining Tian and coworker have studied the effect of the electron donating groups, C1-1, D5 and TH208, on device performance as shown in Figure 1.6. To get a further insight into the difference in performance of DSCs based on organic dyes, density functional theory (DFT) calculations were performed at a B3LYP/6-31+g(d) level for the geometry

optimization. The HOMO is mainly located on the electron donating group and  $\pi$ -spacer, and the LUMO is located in electron withdrawing groups through the  $\pi$ -spacer. It reveals that the thiophene  $\pi$ -spacer is essentially coplanar with cyanoacrylic acid group. There are effective electron separations between HOMO and LUMO of these dyes induced by light irradiation. The result suggests that the nonplanar structures of organic sensitizers could be further designed to complete the monomolecular adsorption without suppressor and obtain the more prominent performance of DSCs [24].

Xiaobing Cheng and coworker investigated on the geometrical structures of the three dyes by using density functional theory (DFT) calculations and time-dependent DFT (TDDFT) calculations of the excited states at the B3LYP/6-31 +G(d) level with the Gaussian 03 program package. To gain insight into the geometrical, electronic, and optical properties of the dyes XS28-XS30 as shown in Figure 1.6, DFT calculations and time-dependent DFT (TDDFT) calculations of the excited states were performed. From the calculation result shown that the HOMO orbital of XS28-XS30 is of  $\pi$ -character and is delocalized over the entire molecule with maximum components on donor units. The LUMO orbital is, on the other hand, a single  $\pi^*$  orbital delocalized across the cyclopentadithiophene and cyanoacrylic acid groups with sizable contributions from the latter. This distribution of HOMO and LUMO levels is separated in the molecule of compound, indicating that transition from HOMO to LUMO can be considered as a charge-transfer transition. In addition, this spatially directed separation of HOMO and LUMO is an ideal condition for dye-sensitized solar cells, which not only facilitates the ultrafast interfacial electron injection but also slows down the recombination of the injected electron with the oxidized dyes. These results suggest that the sensitizers based on functionalized cyclopentadithiophene unit are promising candidates for DSCs [25].

Surya Prakash Singh and coworker have reported the calculation results of TPA1-CN1-R1 and TPA1-CN1-R2 as shown in Figure 1.6 to understand the nature of the optical transitions, results obtained by DFT and TDDFT methods are analyzed. Geometrical parameters of the molecules optimized at the RB3LYP/6-31 G(d,p) level. As expected the molecules are not planar but slightly twisted with respect to the central plane. This twisting could be dependent on the solvent and thus charge transfer would be angle dependent. The stimulated absorption spectra of both the dyes were calculated. The solvent phase (THF) TDDFT spectrum closely matches

with the experimental observation. The computed vertical excitations show that the singlet singlet transition is dominated in both molecules by charge transfer from the donor moieties to the acceptor moieties [26].

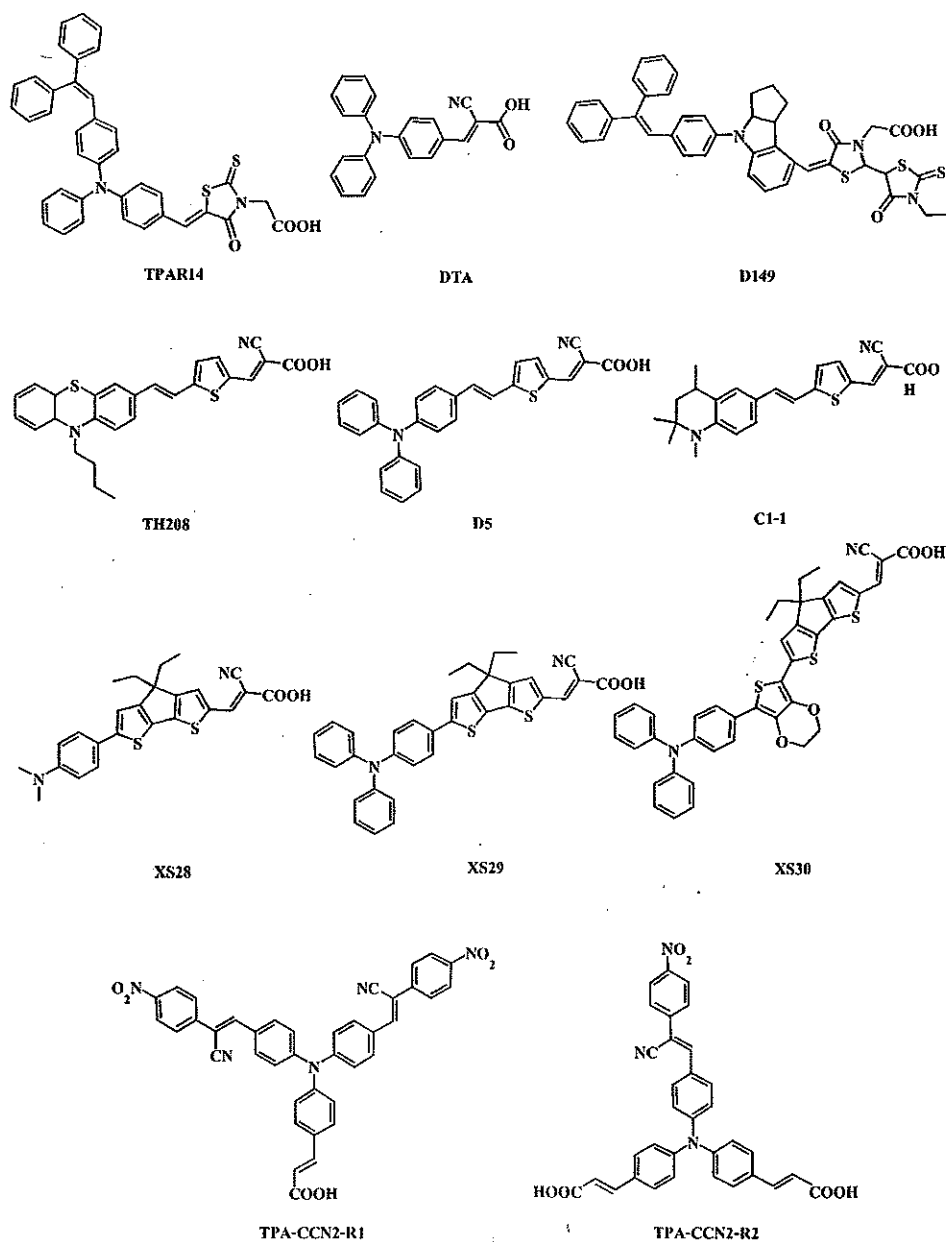


Figure 1.6 Molecular structure of organic sensitizers.



### 1.1.5 Photochemistry

Photochemistry is the study of chemical reaction that proceeds with the absorption of light by atom or molecule. Chemical reactions occur when a molecule is provided the activation energy. In case of photochemical reactions light provides the activation energy. Simplistically, light is one mechanism for providing the activation energy required for many reactions. The absorption of a photon of light by a reactant molecule may also permit a reaction to occur not just by bringing the molecule to the necessary activation energy, but also by changing the symmetry of the molecule's electronic configuration, enabling an otherwise inaccessible reaction path. Photochemical reactions involve electronic reorganization initiated by electromagnetic radiation. The reactions are several orders of magnitude faster than thermal reactions; reactions as fast as  $10^{-9}$  seconds and associated processes as fast as  $10^{-15}$  seconds are often observed. The ease of electronic transition from the ground to a higher excited state dictates whether the observed wavelength is in the UV-Vis region. UV and Vis spectra offer valuable information for identifying compounds, especially by the use of their emission. The photoabsorption properties of a D- $\pi$ -A dye are associated with intramolecular charge transfer (ICT) excitation from the donor to the acceptor moiety of the dye, resulting in efficient electron transfer through the acceptor moiety from the excited dye into the semiconductor CB [27, 28].

#### 1.1.5.1 The Jablonski Diagram

The energy gained by a molecule when it absorbs a photon causes an electron to be promoted to a higher electronic energy level. The Jablonski as shown in Figure 1.7 illustrates the principal photophysical radiative and non-radiative processes displayed by organic molecules in solution. The symbols  $S_0$ ,  $S_1$ ,  $T_2$ , etc., refer to the ground electronic state ( $S_0$ ), first excited singlet state ( $S_1$ ), second excited triplet state ( $T_2$ ), and so on. The horizontal lines represent the vibrational levels of each electronic state. Straight arrows indicate radiative transitions and curly arrows indicate non-radiative transitions. The boxes detail the electronic spins in each orbital, with electrons shown as up and down arrows, to distinguish their spin. Note that all transitions from one electronic state to another originate from the lowest vibrational level of the initial electronic state. For example, fluorescence occurs only from  $S_1$ , because the higher singlet states ( $S_2$ , etc.) decay so rapidly by internal conversion that fluorescence from these states cannot compete [29].

### 1.1.5.2 Electronically excited states

The absorption of a UV or visible photon by a molecule produces an electronically excited state. Electron excitation is the movement of an electron to a higher energy state. This can either be done by photoexcitation (PE), where the original electron absorbs the photon and gains all the photon's energy or by electrical excitation (EE), where the original electron absorbs the energy of another, energetic electron. Within a semiconductor crystal lattice, thermal excitation is a process where lattice vibrations provide enough energy to move electrons to a higher energy band. When an excited electron falls back to a lower energy state again, it is called electron relaxation. This can be done by radiation of a photon or giving the energy to a third spectator particle as well. In physics there is a specific technical definition for energy level which is often associated with an atom being excited to an excited state [30].

### 1.1.5.3 Energy level diagram

One way to view the properties of molecular excited states is shown by the potential energy diagram in Figure 1.7. This diagram, known as a *Franck-Condon* energy level diagram, shows potential energy curves for the ground state ( $S_0$ ), and first excited singlet state ( $S_1$ ) of an organic molecule as a function of nuclear configuration. These curves are sometimes referred to as potential energy wells, because of their shape. The horizontal lines within each curve represent the vibrational levels of each electronic state. The lowest vibration state for each energy level is designated as 0, and the levels above it are successively 1, 2, etc. The band assignments in brackets (e.g., (0, 1)) indicate, respectively, the vibration level of the initial state, and of the final state involved in a transition [31].

The horizontal axis is the nuclear configuration which can be thought of as the distance between nuclei. When considering two atoms bonded to each other, the bottom of the well corresponds to the equilibrium bond length. Because excitation involves the movement of charge density into an antibonding orbital, the equilibrium bond length in  $S_1$  is generally longer than in  $S_0$ . The absorption of light takes place on a much faster time scale ( $\sim 10^{-15}$  s) hence the initially formed excited state must have the same nuclear configuration as the ground state. This transition is called the vertical or *Franck-Condon* transition, and results in the molecule having excess vibrational energy. The excess vibrational energy can be dissipated through the process of vibrational relaxation, i.e., the process of internal conversion, which returns

the molecule to the lowest vibrational level of  $S_1$ . Fluorescence usually occurs from the lowest vibrational level of  $S_1$ . Because these transitions occur at lower energies than absorption that is observed at longer wavelengths ( $\pi$ ) than absorption (i.e. lower energy), as shown in the lower right corner of Figure 1.8.

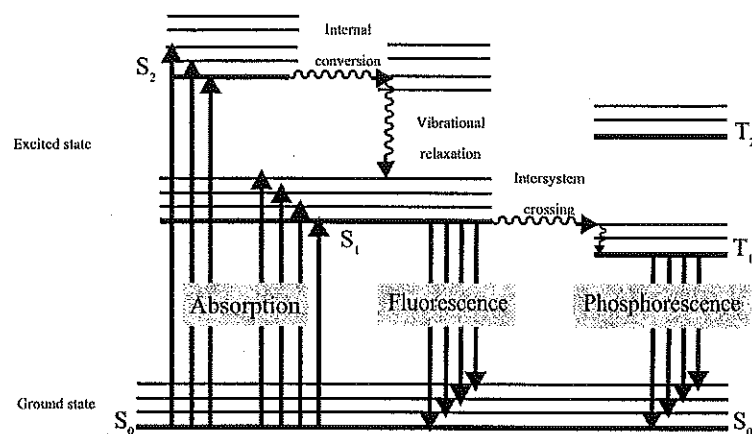


Figure 1.7 The Jablonski Diagram

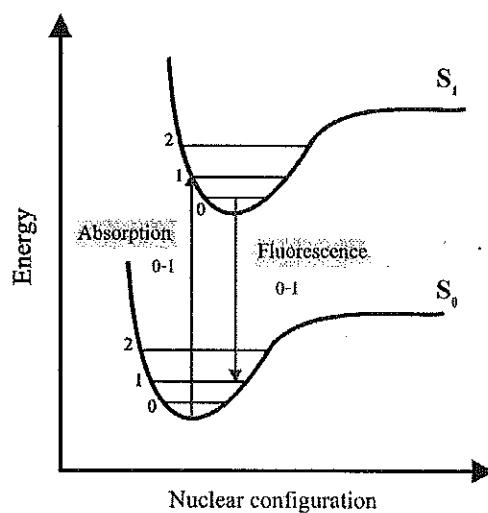
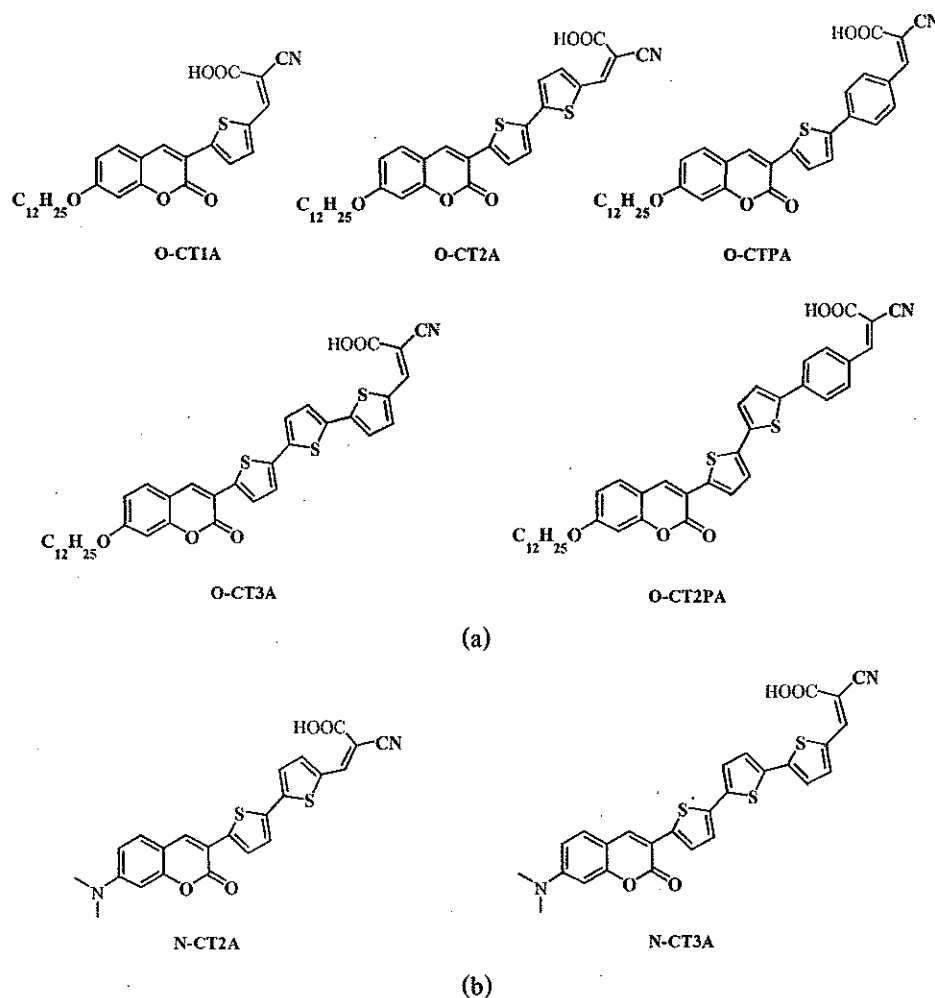


Figure 1.8 Franck-Condon energy level diagram

## 1.2 Objectives of this research

1.2.1 To investigate the effect of electron donating capability of coumarin derivatives by comparing between two different donor, *O*-coumarin and *N*-coumarin as shown in Figure 1.9, to improve the structural and optical properties of these dyes for using in highly efficient DSCs.



**Figure 1.9** Molecular structures of (a) *O*-coumarin and (b) *N*-coumarin derivative

1.2.2 To investigate the effect of conjugated spacer on dimethylaniline derivatives by substituting different linker and increasing number of thiophene units as shown in Figure 1.10 to improve the intramolecular charge transfer, optical properties and energy gap of dyes for using in highly efficient DSCs.

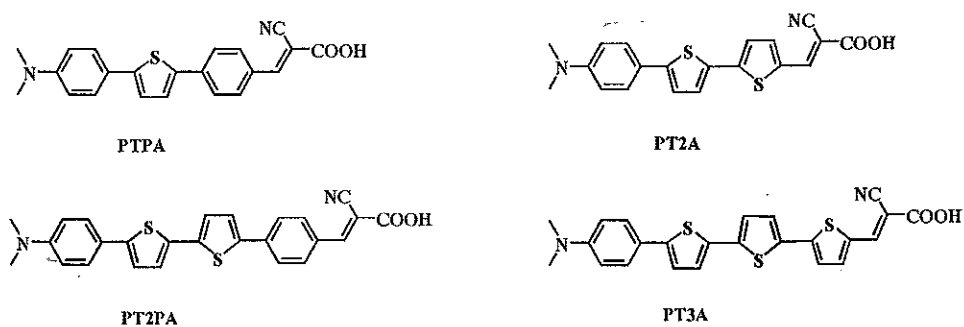


**Figure 1.10** Molecular structures of dimethylaniline derivatives

1.2.3 To investigate the effect of anchoring group on carbazole-fluorene derivatives by introducing different anchoring unit (acrylic acid and cyanoacrylic acid) as shown in Figure 1.11 to improve the electronic properties, energy gap and the injection of electron from LUMO level of dye to conduction band of  $\text{TiO}_2$  of dyes for using in highly efficient DSCs.

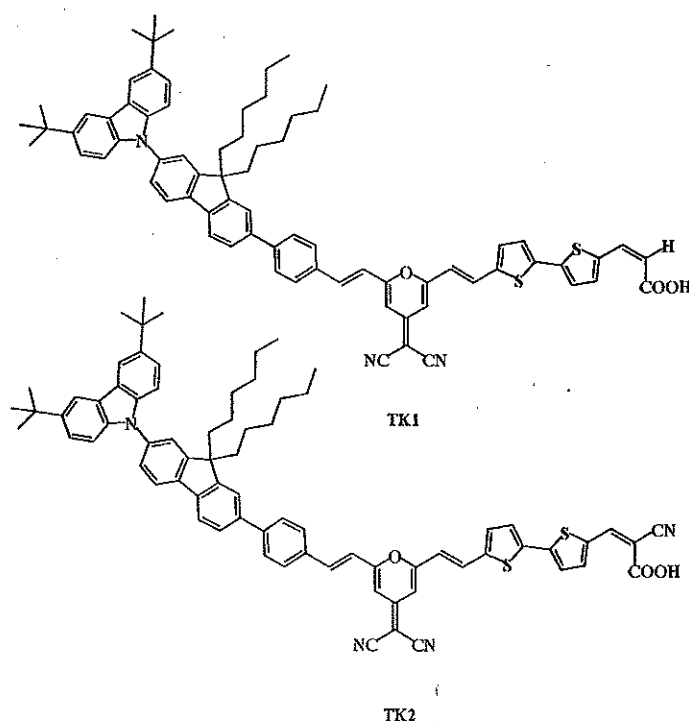


**Figure 1.11** Molecular Structures of carbazole-fluorene derivatives

## CHAPTER 2

### COMPUTATION DETAIL

Recently, the computational chemistry has reached a consensus on a relatively well-defined range of computational methods suitable for studying electronic and optical properties of dyes used in DSCs. For this reason, calculations by different groups are often comparable in terms of accuracy and expected discrepancy from experiment. In practice, geometry optimization is performed using Density Functional Theory (DFT), and Time-Dependent Density Functional Theory (TDDFT) is used to describe the excited states and optical properties of the optimized molecules. [32]

#### 2.1 The Hatree-Fock Theory

##### 2.1.1 Hamiltonian operator for many-electron system

The quantum chemical methods are based on finding solution to the Schrodinger wave equation on molecular orbital theory.

$$H\Psi = E\Psi \quad (1)$$

Where H is Hamiltonian operator which gives the kinetic and potential energies of the system. The Hamiltonian operator for many electrons system can be written

$$\hat{H} = -\sum_{i=1}^n \frac{1}{2} \nabla_i^2 - \sum_{A=1}^K \frac{1}{2M} \nabla_A^2 - \sum_{i=1}^n \sum_{A=1}^K \frac{Z_A}{r_{iA}} + \sum_{i=1}^n \sum_{j < i}^n \frac{1}{r_{ij}} + \sum_{A=1}^K \sum_{B < A}^K \frac{Z_A Z_B}{R_{AB}} \quad (2)$$

In Equation 2, the first and second term represent the kinetic energies of electron and nucleus, respectively. The third term is the electron-nucleus attraction. The forth term corresponds to the electron-electron repulsion and the fifth the nuclear-nuclear repulsion.

### 2.1.2 Born-Oppenheimer Approximation

The Born-Oppenheimer Approximation is central to quantum chemistry. Since nuclei are much heavier than the electron one can treat electrons as if they are moving in the field of fixed nuclei. With this approximation, the five terms in Equation 2 can be reduced to three and the Schrodinger equation for nuclei and electron can be solved separately.

$$\hat{H} = -\sum_{i=1}^n \frac{1}{2} \nabla_i^2 - \sum_{i=1}^n \sum_{A=1}^K \frac{Z_A}{r_{iA}} + \sum_{i=1}^n \sum_{j < i}^n \frac{Z_A}{r_{ij}} \quad (3)$$

Within this approximation, the kinetic energy of the nuclei can be neglected to be constant. The remaining terms are called the electronic Hamiltonian or Hamiltonian describing the motion of N electrons in the field of M point charge.

$$\hat{H}_{elec} \psi_{elec} = E_{elec} \psi_{elec} \quad (4)$$

In the Hartree Approximation the n-electron wavefunction  $\psi^{HP}$  is simply written as a product of one-electron wavefunctions  $\phi_i$

$$\psi^{HP}(x_1, x_2, \dots, x_n) = \phi_1(x_1) \phi_2(x_2) \dots \phi_n(x_n) \quad (5)$$

Such a many-electrons wavefunction is termed a Hartree product, with electron being described by the orbital  $\phi_1$ , electron two being described by the orbital  $\phi_2$ , ect. Using the Hartree product, the energy is just the sum of orbital energies.

$$E = \epsilon_1 + \epsilon_2 + \dots + \epsilon_n \quad (6)$$

The orbital energies are obtained from

$$h(i) \phi_j(x) = \epsilon_j \phi_j(x) \quad (7)$$

Where  $h(i)$  is the one electron Hamiltonian operator which is function of coordinates of each electrons.

### 2.1.3 The Slater Determinant

Hartree product  $\psi^{HP}$  does not satisfy the asymmetry principle. That is the interchange of two electron coordinates does not lead to change in sign of the wave function, in the Hartree – Fock theory the wavefunction is given by the Slater determinants of  $n$  spin-orbital

$$\psi(x_1, x_2 \dots x_n) = \frac{1}{\sqrt{n!}} \begin{vmatrix} \phi_1(x_1) & \phi_2(x_1) & \dots & \phi_n(x_1) \\ \phi_1(x_2) & \phi_2(x_2) & & \phi_n(x_2) \\ \vdots & \vdots & & \vdots \\ \phi_1(x_n) & \phi_2(x_n) & & \phi_n(x_n) \end{vmatrix} \quad (8)$$

$\frac{1}{\sqrt{n!}}$  is the normalization constant for  $n$ -electron system

A short hand notation for Slater determinant is written using only the diagonal element.

$$\psi(x_1, x_2 \dots x_n) \equiv |\phi_1(x_1) \phi_2(x_2) \dots \phi_n(x_n)\rangle \quad (9)$$

The antisymmetric property of Slater determinant is  $|\dots \phi_i \dots \phi_j \dots\rangle = -|\dots \phi_j \dots \phi_i \dots\rangle$

The Slater determinant is accepted to be simplest antisymmetric wavefunction which can be used to describe the ground state of an  $n$ -electron system.

By using Slater determinant the Pauli Exclusion Principle is automatically satisfied from the most important property of determinant, namely the determinant is zero if two rows or two columns of the determinant are exactly the same. In other words, no two electrons are allowed to occupy the same spin orbital since this will lead to zero value of the wave function.

### 2.1.4 The Hartree – Fock Equations [33]

The Hartree-Fock method seeks to approximately solve the electronic Schrodinger equation and it assumes that the wavefunction can be approximated by a single Slater determinant made up of one spin orbital per electron. Since the energy expression is symmetric, the variational theorem holds, and so we know that the Slater determinant with the lowest energy is as close as we can get to the true wavefunction for the assumed functional form of a single Slater



determinant. The Variational principle states that if a normalized wavefunction  $|\tilde{\phi}\rangle$  that satisfies the appropriate boundary condition is given, the expectation value of the Hamiltonian is upper bound to the exact ground state energy. That is, if  $\langle\tilde{\phi}|\tilde{\phi}\rangle = 1$  then

$$\langle\tilde{\phi}|\hat{H}|\tilde{\phi}\rangle \geq E_0 \quad (10)$$

The equality holds only when  $|\tilde{\phi}\rangle$  is identical to the exact wavefunction  $|\phi\rangle$ . The problem of minimizing a function subject to a constraint of normalization is solved by Lagrange's method of undetermined multipliers. According to the variational principle, the orbitals are those which minimize the electronic energy  $E$ , which is defined by

$$\begin{aligned} E &= \langle\psi|\hat{H}|\psi\rangle \\ &= \sum_a^N \langle\psi|\hat{H}|\psi\rangle + \frac{1}{2} \sum_{a,b}^N (\langle ab|ab\rangle - \langle ab|ba\rangle) \\ &= \sum_a^N h_{aa} + \frac{1}{2} (J_{ab} - K_{ab}) \end{aligned} \quad (11)$$

Where  $h_{aa}$  is a core Hamiltonian for an electron, describing its kinetic energy and potential energy in the field of the nuclei and  $J_{ab}$  and  $K_{ab}$  is the coulombic energy and exchange energy, respectively. By a linear variational method, the orbitals can be systematically varied with the constraint that they remain orthonormal until the energy  $E_0$  is a minimum.

For a given single determinant  $|\psi\rangle \equiv |\phi_1\phi_2\ldots\phi_a\phi_b\ldots\phi_n\rangle$  the energy is a function of the orbital  $\{\phi_i\}$ . We need to minimize  $E$  with respect to the orbital, subject to the constraints that the orbitals remain orthonormal,

$$\int dx(1)\phi_a^*(1)\phi_b(1) = \langle\phi_a|\phi_b\rangle = \delta_{ab} \quad (12)$$

Using the variational principle, the best orbitals that minimize  $E$  are obtained from

$$\left[ \hat{h}(1) + \sum_{b=1}^N J_{ab}(1) - K_{ab}(1) \right] \phi_a(1) = \sum_{b=1}^N \epsilon_{ab} \phi_b(1) \quad (13)$$

The Coulomb operator, corresponding to the classical electronic interaction, is defined by

$$\hat{J}_{ab}(1)\phi_a(1) = \left[ \int dx_2 \phi_b^*(2) r_{12}^{-1} \phi_b(2) \right] \phi_a(1) \quad (14)$$

And the non-local potential operator describing the exchange term interaction, is

$$\hat{K}_{ab}(1)\phi_a(1) = \left[ \int dx_2 \phi_b^*(2) r_{12}^{-1} \phi_b(2) \right] \phi_b(1) \quad (15)$$

Equation 4 can be written in a short form of

$$\hat{F}|\phi_a\rangle = \sum_{b=1}^N \epsilon_{ab} |\phi_b\rangle \quad (16)$$

The Fock operator,  $\hat{F}$ , is an effective one electron operator, describing the kinetic energy of an electron, the attraction of all the nuclei and the repulsion of all the outer electrons (via  $\hat{J}$  and  $\hat{K}$ ) called the Fock operator, of the form

$$\hat{F}(1) = \hat{h}(1) + \sum_{b=1}^N \hat{J}_b(1) - \hat{K}_{ab}(1) \quad (17)$$

Equation 16 is not in the canonical eigenvalue form. The reason is that any single determinant wavefunction formed from a set of orbitals retains a certain degree of flexibility in the orbitals. It is always possible to find a unitary matrix  $U$  such that the transformation diagonalizes  $\epsilon$ . A new set of orbitals  $\{\phi'_a\}$  can be obtained from an old set  $\{\phi_a\}$  by a unitary transformation, i.e.  $\phi'_a = \sum_b \phi_b U_{ba}$  the equation 14 can be written in the canonical form without changing the expectation value of energy.

$$\hat{F}|\phi'_a\rangle = \epsilon_a |\phi'_a\rangle \quad (18)$$

Where  $\epsilon_a$  is the orbital of  $\phi_a$ . From Equation 9 the total electronic energy  $E$  is given by

$$E = \sum_a^N \frac{1}{2} (h_{aa} + \epsilon_a) \quad (19)$$

Since the Fock operator has a function dependence, through the Coulomb and Exchange operators, on the solution of  $\{\phi_i\}$  of the pseudo-eigenvalue equation, thus the Hartree-Fock equations are really nonlinear equations and will need to be solved by iterative procedures.

### 2.1.5 The Roothan Equation

Numerical solution of Equation 9 is usually found by expanding the orbitals in a basis set;

$$\phi_i = \sum_v^M C_{vi} \chi_v \quad (20)$$

In equation 20, the unknown HF orbitals  $\phi_i$  are written as a linear expansion in  $M$  known basis function  $\chi_v$ . If the set of  $\chi_v$  is complete, it would be an exact expansion. Equation 16 can be thus written as

$$\hat{F} \sum_v^M C_{vi} \chi_v = \epsilon_i \sum_v^M C_{vi} \chi_v \quad (21)$$

Multiplying from the left by a specific basis function and integrating yields the Roothan-Hall equations which can be shown in a matrix form of

$$\sum_v C_{vi} \int dr_i \chi_\mu^*(1) \hat{F}(1) \chi_v(1) = \epsilon_i \int dr_i \chi_\mu^*(1) \hat{F}(1) \chi_v(1) \quad (22)$$

Two matrices are defined here as the overlap matrix  $S$  and the Fock matrix  $F$ . The Fock matrix has elements

$$F_{\mu\nu} = \int dr_i \chi_\mu^*(1) \hat{F}(1) \chi_\nu(1) = \langle \chi_\mu | \chi_\nu \rangle \quad (23)$$

And the overlap matrix S has element

$$S_{\mu\nu} = \int dr_i \chi_\mu^* \chi_\nu = \langle \chi_\mu | \chi_\nu \rangle \quad (24)$$

Although the basis function  $\{\chi_\nu\}$  is assumed to be normalized and linearly independent, they are not in general orthogonal. The diagonal elements  $S_{\mu\nu}$  are unitary and the off-diagonal elements are numbers less than one in magnitude. Equation 24 can thus be written in a short form of Roothaan equation as

$$\sum_\nu F_{\mu\nu} C_{\nu i} = \epsilon_i \sum_\nu S_{\mu\nu} C_{\nu i} \quad i = 1, 2, 3, \dots, M \quad (25)$$

If a system is close-shell the sum over N occupied spin orbitals included an equal sum over those with the  $\alpha$  spin function and those with the  $\beta$  spin function, i.e.,

$\sum_b^N \rightarrow \sum_{b(\alpha)}^{N/2} + \sum_{b(\beta)}^{N/2}$  the Fock operator then has a form of

$$\hat{F}(1) = \hat{h}(1) + \sum_{a=1}^{N/2} 2\hat{J}_a(1) - \hat{K}_a(1) \quad (26)$$

The Fock matrix F is the matrix representation of the Fock operator in the basis  $\{\chi_\mu\}$ , i.e.,

$$\begin{aligned} F_{\mu\nu} &= \int dr_i \chi_\mu^*(1) \hat{F}(1) \chi_\nu(1) + \sum_{a=1}^{N/2} \int dr_i \chi_\mu^* [2\hat{J}_a(1) - \hat{K}_a(1)] \chi_\nu(1) \\ &= H_{\mu\nu}^{core} + \sum_{a=1}^{N/2} 2\langle \mu a | \nu a \rangle - \langle \mu a | a \nu \rangle \end{aligned} \quad (27)$$

Where a core-Hamiltonian matrix is integral involving the one-electron operator describing the kinetic energy and the nuclear attraction of an electron. By inserting the linear expansion for the molecular orbitals into the two-electron terms one gets

$$\begin{aligned}
F_{\mu\nu} &= H_{\mu\nu}^{core} + \sum_a \sum_{\lambda\sigma}^{N/2} c_{\lambda\sigma} c_{\lambda\sigma}^* \left[ 2\langle \mu\sigma | v\lambda \rangle - \langle \mu\sigma | \lambda\nu \rangle \right] \\
&= H_{\mu\nu}^{core} + \sum_{\lambda\sigma} P_{\lambda\sigma} \left[ \langle \mu\sigma | v\lambda \rangle - \frac{1}{2} \langle \mu\sigma | \lambda\nu \rangle \right] \\
&= H_{\mu\nu}^{core} + G_{\mu\nu}
\end{aligned} \tag{28}$$

P is the density matrix,  $P_{\lambda\sigma} = 2 \sum_{\mu\sigma}^{N/2} c_{\mu\sigma} c_{\nu\sigma}^*$  and G is the two-electron part of the Fock matrix.

The Roothaan equations are nonlinear and can be written in a matrix form of

$$FC = SC \in \tag{29}$$

## 2.2 Density functional theory [36]

Density functional theory-based methods ultimately derive from quantum mechanics research from the 1920's, especially the Thomas-Fermi-Dirac model. The DFT approach is based on a strategy of modeling electron correlation via general functionals of the electron density.

### 2.2.1 Hohenberg-Kohn theorems

Such methods owe their modern origins to Hohenberg-Kohn theorem, published in 1964, which demonstrated the existence of a unique functional which determines the ground state energy and density exactly. In the quantum mechanics Hamiltonian, the kinetic energy of electron and electron-electron interaction ( $V_{ee}$ ) adjust themselves to the external potential ( $V_{ex}$ ) to get the lowest total energy. Thus, the external potential can be uniquely determined from knowledge of the electron density. The Hohenberg-Kohn theorem states that if N interacting electrons move in an external potential  $V_{ext}$ , the ground state electron density  $\rho(r)$  minimized the functional

$$E[\rho] = F[\rho] + \int \rho(r) V_{ext}(r) dr \tag{30}$$

where  $F[\rho]$  is a universal functional of  $\rho(r)$  and the minimum value of the functional E is  $E_0$ , the exact ground-state electronic energy.

$$\hat{F} = \hat{T}_e + \hat{V}_{ee} = \sum_i -\frac{1}{2}\nabla_i^2 + \sum_{i \neq j} \frac{1}{|r_i - r_j|} \quad (31)$$

And by using the variation principle, the density can be obtained.

### 2.2.2 The Kohn – sham Equation

Kohn and Sham (1965) introduce a method based on the Hohenberg-Kohn theorem that allows one to minimize the functional  $E[n(r)]$  by varying  $\rho(r)$  overall the densities containing N electron. The derived a coupled set of differential equations enabling the ground state density  $\rho(r)$  to be found. Kohn and sham separated  $F[\rho(r)]$  in Equation into three distinct part, so that the functional E becomes.

$$E[\rho] = T_s[\rho(r)] + \frac{1}{2} \iint \frac{\rho(r)\rho(r')}{|r_i - r_j|} dr dr' + E_{xc}\rho(r) + \int \rho(r)V_{ext}(r)dr \quad (32)$$

Where  $T_s[\rho(r)]$  is defined as the kinetic energy of non-interacting electron gas with density  $\rho(r)$ ,

$$T_s[\rho(r)] = -\frac{1}{2} \sum_i \psi_i^*(r) \nabla^2 \psi_i(r) dr \quad (33)$$

And  $E_{xc}\rho(r)$  is the exchange-correlation energy functional. Introducing a normalization constraint on the electron density,  $\rho(r)dr = N$ , by the Langrange's method of undetermined multiplier, we obtain

$$\delta \left\{ E[\rho(r)] - \mu \left[ \int \rho(r)dr - N \right] \right\} = 0 \quad (34)$$

When  $\mu$  is an undetermined Lagrangmultiplie. The number of electrons in the system is constant so  $\delta N = 0$  then equatio reduce to

$$\delta E[\rho(r)] - \mu \delta \left( \int \rho(r)dr \right) = 0 \quad (35)$$

Using the definition of the differential of the functional  $\delta F = \int \frac{\delta F}{\delta f(x)} \delta f(x) dx$  and the fact that the differential and the integrals may be interchange,

$$\int \frac{\delta E[\rho(r)]}{\delta \rho(r)} \delta \rho(r) dr - \mu \int \delta \rho(r) dr = 0 \quad (36)$$

$$\int \left\{ \frac{\delta E[\rho(r)]}{\delta \rho(r)} - \mu \right\} \delta \rho(r) dr \Rightarrow \frac{\delta E[\rho(r)]}{\delta \rho(r)} = \mu \quad (37)$$

Equation 34 may now be rewritten in terms of an effective potential,  $V_{eff}(r)$ ,

$$\frac{\delta T_s[\rho(r)]}{\delta \rho(r)} + V_{eff}(r) = \mu \quad (38)$$

Where

$$V_{eff}(r) = V_{ext}(r) + \int \frac{\rho(r')}{|r-r'|} + V_{xc}(r) \quad (39)$$

And

$$V_{xc}(r) = \frac{\delta E_{xc}[\rho(r)]}{\delta \rho(r)} \quad (40)$$

### 2.2.3 Exchange and correlation

Hohenberg and Kohn demonstrated that  $E_{xc}$  is determined entirely by the electron density. In practice,  $E_{xc}$  is usually approximated as an integral involving only the spin densities and possibly their gradient.  $E_{xc}$  is usually divided into separate part, referred to as the exchange and correlation part, but actually corresponding to the same-spin and mixed-spin interaction, respectively:

$$E_{xc}[\rho] = E_x[\rho] + E_c[\rho] \quad (41)$$

All three terms are again functionals of the electron density, and functional defining the two components on the right side of equation are termed exchange functional and

correlation functional, respectively. The form of  $E_{xc}$  is in general unknown and its exact value has been calculated for only a few very simple systems. In the density functional theory, the exchange functional is always defined as follow

$$E_x[\rho] = \langle \phi[\rho] | \hat{V}_{ex} | \phi[\rho] \rangle - U[\rho] \quad (42)$$

When  $U[\rho]$  is the Hartree price of the coulomb potential. The correlation term is defined as the remaining unknown price of the energy:

$$E_c[\rho] = F[\rho] - T_s[\rho] - U[\rho] - E_x[\rho] \quad (43)$$

For calculations in which the energy surface is quantity of primary interest DFT offers a practical and potential highly accurate alternative to the wavefunction discussed above. In practice, the unility of the theory rest on the approximation used for  $E_{xc}$ .

#### 2.2.3.1 The Local Density Apporoximation

The generation of approximations for  $E_{xc}$  has lead to large and still expanding field of research. Thomas and Fermi studied the Homogeneous electron gas in early 1920's the orbital of system are, plane waves. If the electron interaction is approximate by the classical Hatree potential the total energy functional can be readily computed. Under these condition the dependence of kinetic and exchange energy on the density of electron gas can be extracted and expressed in term of local functions of the density. This suggests that inhomogeneous system might approximate the function as an integral over a local function of the charge density. Using the kinetic and exchange energy densities of the non-interacting homogeneous electron gas this leads to;

$$T[\rho(r)] = 2.87 \int \rho^{5/3}(r) dr$$

And,

$$E_x[\rho] = 0.74 \int \rho^{4/3}(r) dr \quad (44)$$



These results are highly suggestive of a representation for  $E_{xc}$  in an inhomogeneous system. The local exchange correlation energy per electron might be approximate as a simple function of the local charge density. That is, approximation of the form;

$$E_{xc}^{LDA}[\rho(r)] = \int \epsilon_{xc}(\rho(r))\rho(r)dr \quad (45)$$

With the LDA  $\epsilon_{xc}$  is a function of only the local value of the density. It can be separate into exchange and correlation contribution;

$$\epsilon_{xc}(\rho) = \epsilon_x(\rho) + \epsilon_c(\rho) \quad (46)$$

The Dirac form can be used for

$$\epsilon_x(\rho) = -C\rho^{1/3} \quad (47)$$

Where for generality a free constant, C, has been introduced rather than that determined for the homogeneous electron gas. This function is form is much more widely applicable than is implied from its derivation and can be established from scaling arguments. The functional form for the correlation energy is unknown and has been simulated for the homogeneous electron gas in numerical quantum Monte Carlo calculations which yield essentially exact results. The resultant exchange correlation energy has been fitted by a number of analytic forms all of which yield similar results in practice and are collectively referred to as LDA functional.

### 2.2.3.2 The Generalised Gradient Approximation

The local density approximation can be considered to be the zeroth order approximation to the semi- classical expansion of the density matrix in term of density and its derivatives. A natural progression beyond the LDA is that gradient expansion approximation in which first order gradient terms is the expression are include. In the generalized gradient approximation (GGA) a function a functional from is adopted which ensure the normalization condition and that the exchange hole is negative definite. This lead to an energy functional that

depends on both the density and its gradient but retains the analytic properties of the exchange correlation hole inherent in the LDA.

An approach to improving the LDA, so call generalized gradient approximation (GGA), is to include gradient correlations by making  $E_{XC}$  a functional of the density and its gradient:

$$E_{XC}^{GGA}[\rho(r)] = \int \epsilon_{XC}(\rho(r)) \rho(r) dr + \int F_{XC}[\rho(r)|\nabla\rho(r)|] d \quad (48)$$

Where  $F_{XC}$  is a correction chosen to satisfy one or several known limits for  $E_{XC}$ . Clearly, there is no unique recipe for  $F_{XC}$ , and several functional is currently a currently a very active area of research and although incremental improvements are likely, it is far from clear whether the research will be successful in providing the substantial increase in accuracy that is desired.

### 2.2.3.3 Hybrid Functionals [34]

There is an exact connection between the non interacting density functional system and the fully interacting many body system via integration of the the work done in gradually turning on the electron electron interaction. The adiabatic connection approach allow the exact functional to be formally written as

$$E_{XC}[\rho] = \frac{1}{2} \int d\vec{r} d\vec{r}' \int_{\lambda=0}^1 d\lambda \frac{\lambda e^2}{|\vec{r} - \vec{r}'|} \left[ \langle \rho(\vec{r}) \rho(\vec{r}') \rangle_{\rho, \lambda} - \rho(\vec{r}) \delta(\vec{r} - \vec{r}') \right] \quad (49)$$

Where the expectation value  $\langle \dots \rangle_{\rho, \lambda}$  is the density-density correlation functional and is computed at density  $\rho(r)$  for a system described by effective potential;

$$V_{eff} = V_{en} + \sum_{i \neq j} \frac{\lambda e^2}{|\vec{r}_i - \vec{r}_j|} \quad (50)$$

Thus the exact energy could be computed if one knew the variation of density density correlation function with the coupling constant,  $\lambda$ . The LDA recoved by replacing the pair correlation function with that for the homogeneous electron gas. The adiabatic integration

approach suggests a difference approximation for the exchange–correlation functional. At  $\lambda=0$  the non-interacting system corresponds identically to Hartree–Fock ansatz, while the LDA and GGA functional are constructed to be excellent approximations for the fully interacting homogeneous electron gas—that is, a system with  $\lambda=1$ . It is therefore not unreasonable to approximate the integral over the coupling constant as a weighted sum of the end point—that is, we might set:

$$E_{XC} \approx aE_{Fock} + bE_{EX}^{GGA} \quad (51)$$

Within the coefficients are to be determined by reference to a system for which the exact results is known. Becke adopted this approach in the definition of a functional with coefficients determined by a fit to the observe atomization energies, ionization potential, proton affinities and total atomic energies for a number of small molecules.

Hybrid functional of this type is now very widely used in chemical applications with the B3LYP functional being the most notable. Computed binding energies, geometries and frequencies are systematically more reliable than the best GGA functional. A Becke–style three-parameter functional may be defined via the following expression:

$$E_{XC}^{B3LYP} = (1-a)E_{XC}^{LCD} + aE_{XC}^{\lambda=0} + bE_X^{B88} + cE_C^{LYP} + (1-c)E_C^{LCD} \quad (52)$$

Here, the parameter  $C_0$  allows any admixture of Hartree–Fock and LDA local exchange to be used. In addition, Becke’s gradient correction to LDA exchange is also included, scaled by the parameter  $c_X$ . Similarly, the VWN3 local correlation functional is used and it used, and it may be optionally corrected by the LYP correction via the parameter the parameter  $c_C$ . In B3LYP functional, the parameters values are those specified by Becke, which he determined by fitting to the atomization energies, ionization potential, proton affinities and first-row atomic energies in the G1 molecule set:  $c_0=0.20$ ,  $c_X=0.72$  and  $c_C=0.81$ . Note that Beck used the Perdew–Wang 1991 correlation functional in his original work rather than VWN3 and LYP. The fact that the same coefficients work well with different functional reflects the

underlying physical justification for using such a mixture of Hartree-Fock and DFT exchange first pointed out by Becke.

### 2.3 Time-dependent density functional theory [35]

The Time-Dependent extension of DFT (TDDFT) has become the method of choice. This is due to its accuracy coupled with its reasonable scaling with the systems dimensions. TDDFT can be as accurate as correlated ab initio techniques for the description of excited states, displaying a much lower computational cost. TDDFT is still limited to excited state having a single-excitation character and various problems of current XC functional have been highlighted for long-range charge transfer excitations in which the starting and arriving orbitals of given transition do not overlap significantly. Nevertheless, TDDFT is currently successfully applied to study of organic molecule and systems containing transition metal centers. Considering the ground state geometry the excited state geometry, TDDFT can simulate absorption spectra. This opens the way to calculations of emission spectra and excited state dynamics. Furthermore, efficient procedures for calculations of dense spectra have recently been reported.

Density functional theory (DFT) in its usual time-independent form is essentially a ground state theory and, as such, excludes the interaction of matter with time-dependent fields. There is generally no rigorous way, for example, to calculate electronic excitation energies due to photoabsorption. Standard DFT can be extended to excited states representing the lowest state of a given space-spin symmetry. The description of time-dependent phenomena, including photoexcitation, was incorporated properly into DFT by Runge and Gross who generalized the Hohenberg-Kohn theorem to time-dependent densities and potentials. It makes sense to distinguish between two main types of time-dependent DFT (TDDFT) calculations. The overwhelming majority of applications deal with relatively weak electric fields, e.g. photoabsorption spectra, which can be treated as a small perturbation within linear response theory. The other branch solves the TDDFT equations in the time domain to dynamically propagate electrons and nuclei. In the present article we will limit the discussion to the linear response aspect, the particular focus being on electronic excitation.

### 2.3.1 Time-Dependent Kohn-Sham Theory

According to the Runge-Gross theorem there is a one to one correspondence between the time-dependent external potential,  $V_{ext}(r, t)$  and the time-dependent electron density,  $\rho(r, t)$ , for a fixed initial state. This can be seen as a generalization of the usual Hohenberg-Kohn theorem for electronic ground states. Similar to the static case, one can cast the many-electron problem into the Kohn-Sham non-interacting electrons from assuming non-interacting v-represent ability. The latter assumption means that the density of the interacting system can be reproduced by the non-interacting potential,  $V_s$ , i.e.

$$\rho(r, t) = \sum_i^{occ} |\phi_i(r, t)|^2 \quad (53)$$

where the orbital  $\phi_i(r, t)$  satisfy the time – dependent Kohn – sham equations

$$i \frac{\partial}{\partial t} \phi_i(r, t) = \left( -\frac{\nabla^2}{2} + V_s[\rho](r, t) \right) \phi_i(r, t) \quad (54)$$

With

$$V_s[\rho](r, t) = V_{ext}[\rho](r, t) + \int dr' \frac{(r', t)}{|r - r'|} + V_{xc}[\rho](r, t) \quad (55)$$

Defining the exchange-correlation potential  $V_{xc}[\rho](r, t)$ . In the usual adiabatic approximation, the exchange-correlation potential is taken to be simply the derivative of the static ground state exchange-correlation energy,  $E_{xc}$  with respect to the density,

$$V_{xc}[\rho](r, t) \approx \frac{\delta E_{xc}[\rho]}{\delta \rho} \quad (56)$$

## CHAPTER 3

### COUMARIN DERIVATIVES

#### 3.1 Introduction to coumarin sensitizer

Coumarin derivatives are used in a wide range of applications, such as dye-sensitized solar cells (DSCs) and dye lasers. Coumarin dyes, for example coded as coumarin 343 is good organic sensitizer for efficient electron injection from the dye to the conduction band of semiconductors. Electron-transfer processes in the C343 semiconductor systems have been studied. They found that the charge injection from the C343 dye to the conduction band (CB) of the  $\text{TiO}_2$  occurs on a time scale of ca. 200 fs. It is attributed to strong electronic coupling between the dye and  $\text{TiO}_2$  energy levels. However, the efficiency based on C343 is lower than the efficiencies of DSCs based on Ru-complex owing to the former's lack of absorption in the visible region [36]. Therefore, the absorption spectra of organic dyes must be developed to have the broadened and red-shifted absorption spectra for highly efficient of solar-cell performance in terms of harvesting sunlight. Kohjiro Hara and coworker developed a class of coumarin derivatives. The coumarin dyes modified with thiophene moieties were sensitized and their high performance in DSCs was investigated. DSCs based on the coumarin dyes gave good performance in terms of incident photon-to-current conversion efficiency (IPCE) in the range of 400-800 nm. They found that a solar energy to electricity conversion efficiency of 7.4% was obtained with a device of NKX-2677 based dye [37]. Currently, theoretical investigation on physical properties of organic dye in order to disclose the relationship among performances, structures and optical properties. Kang Deuk Seo and coworker examined the excitation energy of coumarin dyes containing a low-band-gap chromophore of ethylenedioxythiophene (EDOT) by using DFT and TDDFT study. The dyes comprise a coumarin moiety as the electron donor and a cyanoacrylic acid moiety as electron acceptor in D- $\pi$ -A system shown in Figure 3.1. The calculation results are in good agreement with experimental data. As the calculation results, the solar cell based on HKK-CM1 sensitizer shows better photovoltaic performance with the overall conversion efficiency of 6.07% HKK-CM2 and HKK-CM3 based solar cells.

Even though HKK-CM2 and HKK-CM3 have more extended aromatic units than HKK-CM1, the degree of  $\pi$ -conjugation in HKK-CM2 and HKK-CM3 is less efficiency than that of HKK-CM1 due to the relatively larger torsion angle between the plane of the donor and that of the acceptor [38]. Later, Julien Preat and coworker investigated on UV absorption spectra of coumarin derivatives with the theoretical methods. In the density functional theory framework, various basis sets as well as several functionals have been tested. It turns out that the Becke-Lee-Yang-Parr functional (B3LYP) combined with the 6-311+G (2d,2p) basis set provides reliable absorption spectra when the solvent effects are included in the model [39]. Nowadays, Saurabh Agrawa and coworker have investigated the two coumarins, NKX-2311 and NKX-2593 by using TDDFT. The two sensitizers differ only in their linker moieties and are shown to have different absorption spectra when adsorbed on to the  $\text{TiO}_2$  surface. Knowledge of different light absorption and charge transfer (CT) behavior within these complexes is useful for further improving the performance of organic dyes presently being designed and investigated worldwide [40].

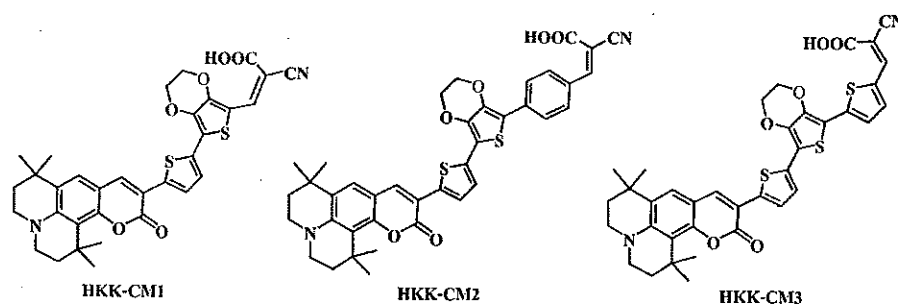


**Figure 3.1** Coumarin derivatives

In this chapter, the investigation of D- $\pi$ -A systems, especially the molecular structure of the ICT states is an important point of discussion. Herein, theoretical calculations were performed to study the ground-state structures and optical properties of *O*-Coumarin and *N*-Coumarin sensitizer. The series of conjugated metal-free organic dyes containing coumarin unit (*O*-Coumarin and *N*-Coumarin) as electron donor, thiophene and phenyl as linker and cyanoacrylic acid as electron acceptor as shown in Figure 3.2. The influence of increasing thiophene units for improving the absorption spectra of coumarin derivatives and the difference linker (thiophene and phenyl) were investigated. Moreover, the effect of different donor between *O*-Coumarin and *N*-coumarin, were studied.

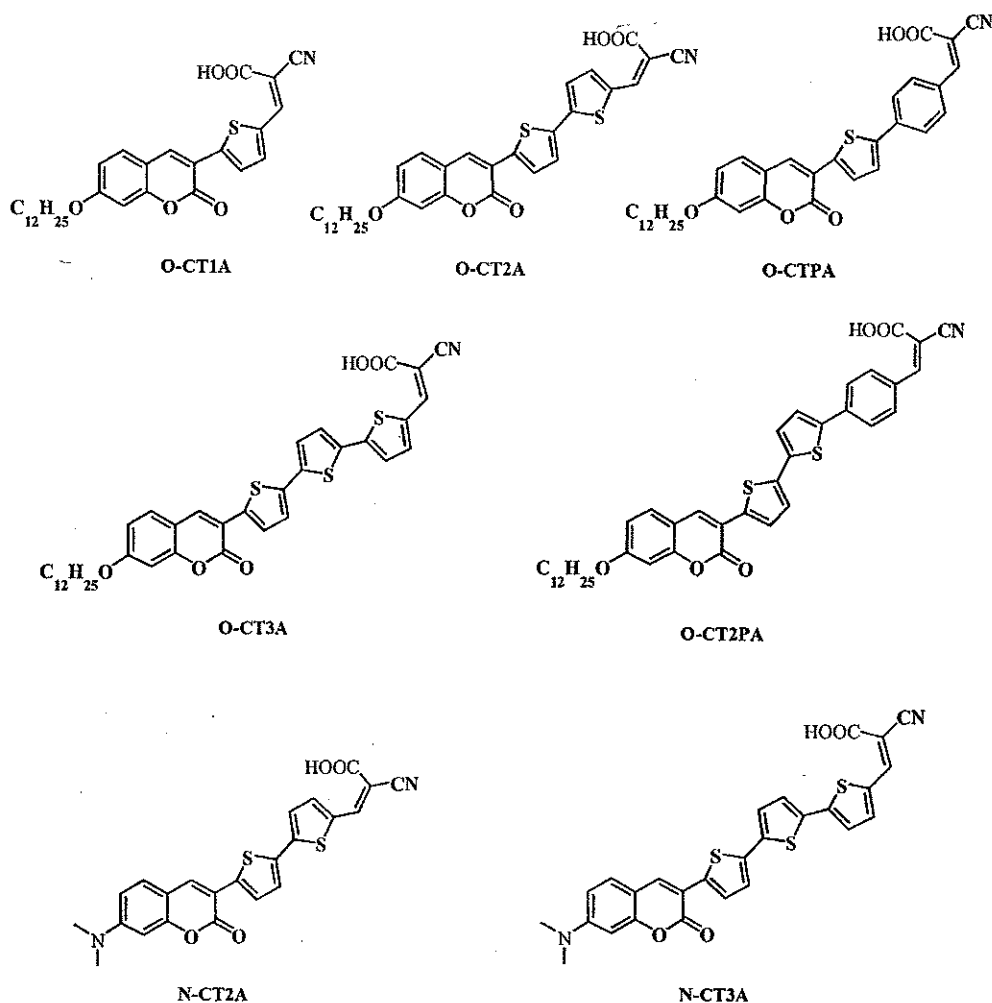


**Figure 3.2** Sketch map structures of the target molecule *O* - Coumarin

### 3.2 Method

To gain insight into the factor responsible for the absorption spectral, we perform density functional theory (DFT) and time-dependent DFT (TDDFT) calculations on the ground state of organic dyes. The ground state structure of *O*-Coumarin and *N*-Coumarin were optimized by the DFT method using the B3LYP exchange-correlation function with 6-31G (d,p) basis set. Electronic population of the HOMO and LUMO were calculated to show the position of localization of electron populations along with the calculated molecular orbital energy diagram. The electronic absorption spectra require calculation of the allowed excitation and oscillator strengths, these calculations were carried out using TDDFT with the same basis set and exchange-



correlation functional. The absorption spectra of all organic dyes were calculated using the Swizard program and the results were compared with the experimental data. Solvent effect for dichloromethane was included by means of the conductor-like polarizable continuum model (C-PCM). This computational approach allows us to provide a detailed assignment of the excited state involved in the absorption process. All calculations were carried out using the Gaussian 03 program package.

### 3.3 Results and discussion

#### 3.3.1 *O*-Coumarin derivatives

##### 3.3.1.1 Optimized structure

The structures of organic dye used in this study are shown in Figure 3.2. The optimized geometries of O-CTnA and O-CTnPA in the gas phase obtained by DFT/6-31G (d,p) are shown in Figure 3.3 and the selected inter-ring distances and dihedral angles are listed in Table 3.1.

To understand the influence of different linker, the dihedral angles of *O*-Coumarin dyes were analyzed. The dihedral angle between C-T in O-CT1A, O-CT2A and O-CT3A are -0.00, -0.16 and 3.51 degree respectively, T-T dihedral angle were calculated to be 0.18 and -3.69 degree for O-CT2A and O-CT3A, respectively. The calculation result show that the dihedral angle between donor and linker is coplanar. Moreover, T-A dihedral angle are found to be 0.00-0.02 degree indicating the cyanoacrylic acid group was located to be coplanar with the thiophene. From the results, we found that the donor and acceptor moieties are fully conjugated as demonstrated by the co-planarity of the donor, linker and acceptor.

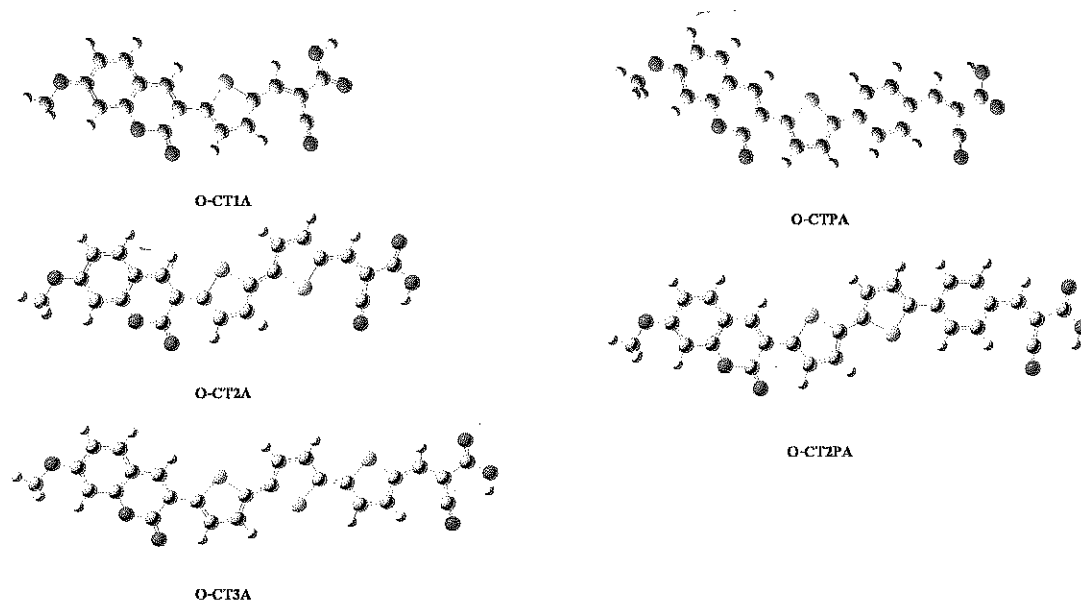


**Figure 3.3** The optimize structure of O-CT1A, O-CT2A, O-CT3A, O-CTPA and O-CT2PA by calculated B3LYP/6-31G (d,p) level of theory

**Table 3.1** Selected inter-ring distances (Å) and dihedral angles (°) of O-CT1A, O-CT2A, O-CT3A, O-CTPA and O-CT2PA calculated by B3LYP/6-31G (d,p) calculations

Molecules		C-T	T1-T2	T2-T3	T1-P	T-A
O-CT1A	Dihedral ( $\Phi$ )	-0.00	-	-	-	0.00
	Distance ( $r$ )	1.46	-	-	-	1.43
O-CT2A	Dihedral ( $\Phi$ )	-0.16	0.18	-	-	-0.01
	Distance ( $r$ )	1.46	1.44	-	-	1.42
O-CT3A	Dihedral ( $\Phi$ )	3.51	-9.94	3.69	-	-0.28
	Distance ( $r$ )	1.46	1.44	1.44	-	1.42
O-CTPA	Dihedral ( $\Phi$ )	5.70	-	-	-17.24	3.60
	Distance ( $r$ )	1.46	-	-	1.46	1.45
O-CT2PA	Dihedral ( $\Phi$ )	-2.01	11.65	-	-16.83	0.66
	Distance ( $r$ )	1.46	1.44	-	1.46	1.46

Note: C is coumarin, P is phenyl, T is thiophene, A is acceptor

When the thiophene ring was replaced by phenyl ring, T-P dihedral angle was found to be -17.24 and -16.83 degree for O-CTPA and O-CT2PA respectively. Since

the effect of steric repulsion between the hydrogen atoms of thiophene and benzene, the dihedral angle between thiophene and phenyl is not fully coplanar. The non-planar structure affects the delocalization of electron from donor to acceptor cannot smoothly. It is noted that the optimized geometries, the T-T dihedral angle of ink in O-CT1A, O-CT2A and O-CT3A is smaller than the T-P dihedral angle in O-CTPA and O-CT2PA. From the calculation results, we found that coumarin dyes with thiophene-thiophene linker is more coplanar than that of the coumarin dyes with thiophene-phenyl linker. The results suggesting that the strong conjugated effects are formed. This conjugation is very helpful for efficient transfer in conjugate chains. Furthermore, dye with a more planar  $\pi$ -conjugated chain may have a better DSCs performance.

### 3.3.1.2 Electronic structure

To gain insight into the geometrical and electronic structures of the dyes, molecular orbital and density of state were performed by using B3LYP/6-31G (d,p) level of theory. The frontier molecular orbital of the dyes are shown in Figure 3.4. The calculated the HOMOs level, the LUMOs level and percentage contribution of frontier molecular orbital of O-CTnA (n=1-3) and O-CTnPA (n=1-2) are listed in Table 3.2. From the results can be seen that the HOMOs level are a delocalized  $\pi$  orbital over the coumarin and thiophene unit, whereas the LUMOs level are  $\pi^*$  orbital which  $\pi$ -electron was localized in thiophene ring, phenyl ring and cyanoacrylic group. Therefore, this distribution of the HOMO and LUMO is separated in the donor and acceptor part of compounds, indicating that the HOMO $\rightarrow$ LUMO transition can be considered as an intramolecular charge transfer (ICT) transition. To obviously explain the charge separation, the electron density of each part was shown in Table 3.2.

Electron density distribution of HOMO state for O-CT1A, O-CT2A and O-CT3A is mainly located at the coumarin which is calculated to be 58%, 30% and 25% and the thiophene moieties are calculated to be 30%, 58% and 68%, respectively. These results indicate that the electron density of HOMO is mainly located on donor part. For the LUMOs level, the percentage contributions of cyanoacrylic acid are calculated to be 43%, 35% and 36% for O-CT1A, O-CT2A and O-CT3A, respectively, which is mainly delocalized on acceptor part. From these results, the excited electrons are shifted from the electron donor moiety to the electron acceptor unit implying that the single excited state of these molecules could be considered as the intramolecular charge transfer from donor to acceptor along through the  $\pi$ -conjugated skeleton.

**Table 3.2** Summarizes the energies and character of frontier orbital of O-CT1A, O-CT2A, O-CT3A, O-CTPA and O-CT2PA calculated by B3LYP/6-31G (d,p)

Molecule	Molecular orbital	Molecular Energy (eV)	percentage composition		
			Donor	Linker	Acceptor
O-CT1A	LUMO	-2.69	26	31	43
	HOMO	-5.44	58	30	12
O-CT2A	LUMO	-2.78	18	47	35
	HOMO	-5.25	30	58	12
O-CT3A	LUMO	-2.80	7	58	36
	HOMO	-5.12	25	68	7
O-CTPA	LUMO	-2.69	17	41	42
	HOMO	-5.25	38	55	6
O-CT2PA	LUMO	-2.69	7	51	42
	HOMO	-5.09	29	68	3

For the series of different  $\pi$ -spacer, phenyl ring instead of thiophene unit which are composed of O-CTPA and O-CT2PA dyes, the HOMOs level are a delocalized  $\pi$  orbital over the donor and  $\pi$ -spacer, while the LUMOs level is a  $\pi^*$  orbital that localized in  $\pi$ -spacer and acceptor unit. The percentage contributions of coumarin are calculated to be 38% and 29% and the electron density of thiophene are calculated to be 55% and 68% for O-CT1PA and O-CT2PA, respectively. For the LUMOs level, the percentage contributions of cyanoacrylic acid are calculated to be 42% for both of CT1PA dyes and CT2PA dye. It was found that the excited electrons transfer from the electron donor to the electron acceptor unit indicating that the excited state of these organic dye could be considered as the ICT along the  $\pi$ -conjugated backbone. Moreover, comparing between O-CT2A and O-CTPA, the percentage contributions results have been shown that electron contribution of linker in both dyes are slightly different. Therefore, it is clearly concluded that thiophene ring is appropriate linker for improving the dye efficiency of our dye molecules.

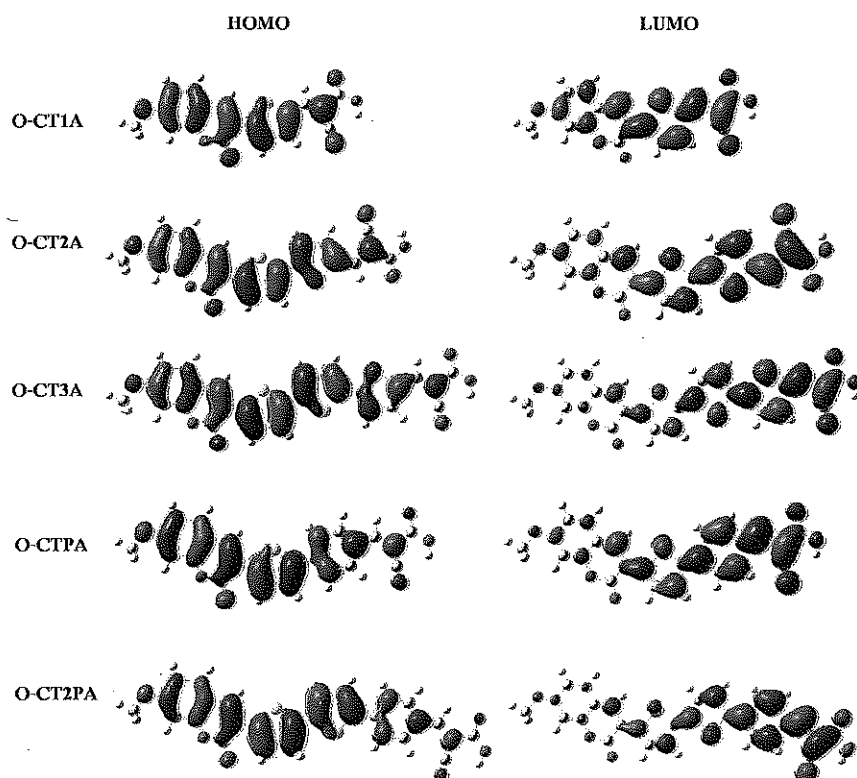


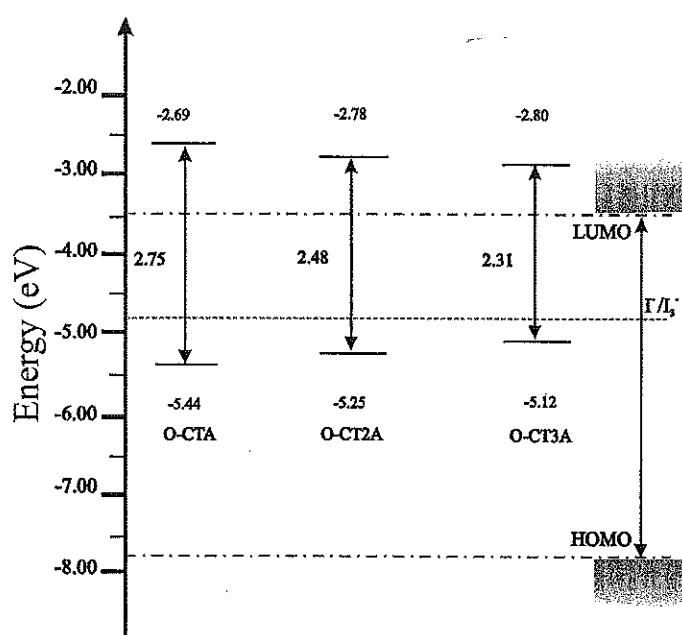
**Figure 3.4** Frontier molecular orbital of O-CT1A, O-CT2A and O-CT3A, O-CTPA and O-CT2PA calculated by B3LYP/6-31G (d,p) level of theory

**Table 3.3** The calculated HOMO-LUMO energy gap of O-CT1A, O-CT2A, O-CT3A, O-CTPA and O-CT2PA

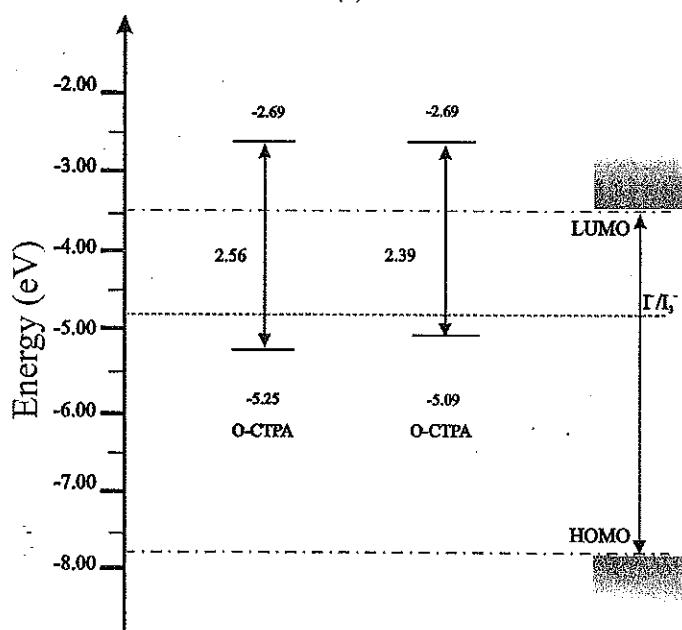
Molecule	$\Delta_{\text{HOMO-LUMO}}^{\text{a}}$ (eV)	Expt. <sup>b</sup> (eV)
O-CT1A	2.75	2.53
O-CT2A	2.48	2.48
O-CT3A	2.31	2.38
O-CTPA	2.77	2.58
O-CT2PA	2.50	2.46

<sup>a</sup>Calculations are performed with B3LYP/6-31G (d,p) in gas phase.

<sup>b</sup>Experimental  $\Delta_{\text{HOMO-LUMO}}$  estimated from the onset of the absorption spectra  $E_{\text{g}}$  (eV) =  $1240/\lambda_{\text{onset}}$  in dilute  $\text{CH}_2\text{Cl}_2$  solution.



(a)



(b)

**Figure 3.5** (a) Molecular orbital energy diagram of O-CT1A, O-CT2A and O-CT3A and  
 (b) Molecular orbital energy diagram of O-CTPA and O-CT2PA

From the calculated results as presented in Table 3.3 the HOMO-LUMO gaps of the dye O-CT1A, O-CT2A, O-CT3A, O-CTPA and O-CT2PA are calculated as 2.75, 2.48, 2.32, 2.77 and 2.50 eV, respectively. The energy level of O-CT1A, O-CT2A, O-CT3A, O-CTPA and O-CT2PA as shown in Figure 3.5, the HOMO-LUMO gap of O-CT3A is smallest, compared with those of O-CT1A and O-CT2A, respectively, indicating that increasing the number of the thiophene units increases the HOMO level and narrows the HOMO-LUMO gap. Moreover, comparing the HOMO-LUMO gap between O-CTnA and O-CTnPA dye, we found that introducing thiophene substituent has remarkable influence on the LUMOs level. The LUMOs of O-CTPA and O-CT2PA with phenyl group is destabilized by 0.12 – 0.14 eV compared to the corresponding O-CT2A and O-CT3A respectively. Therefore, the LUMOs level of O-CT2A and O-CT3A with thiophene was closer conduction band of  $\text{TiO}_2$  than those of CTPA and O-CT2PA, respectively.

### 3.3.1.3 Absorption spectra

TDDFT calculations on a B3LYP/6-31G(d,p) level of theory show transitions with large oscillator strengths consistent with the absorption spectrum. The absorption spectra of all compounds are shown in Figure 3.6. Their optical characteristics are listed in Table 3.4. The main absorption peak of O-CT1A, O-CT2A and O-CT3A are 477.0 nm, 544.0 and 605.7 nm, respectively. The main absorption spectra could be attributed to the intramolecular charge transfer (ICT) between the donor and the acceptor which is consistent with the assignment to the transition from the ground state ( $S_0$ ) to the first singlet excited state ( $S_1$ ).

For O-CTPA and O-CT2PA, the main absorption spectrum is around 515.6 and 574.7 nm, respectively. This result can be attributed to the ICT character from the donor part to the acceptor. The calculated results by using TDDFT, we found that the calculated data have the same tendency with the experiment. Beside the calculated absorption spectra of O-CT2A exhibit red-shifted compared to the absorption of O-CT1PA. It should be noted that improving conjugation system by the addition of thiophene unit is more suitable than phenyl unit.

**Table 3.4** The excitation energies, oscillator strengths and molecular compositions for the 2 lowest states by TD-B3LYP/6-31G(d,p) (solvent)

Molecule	State	Excitation energy (eV, nm)	Oscillator strength ( <i>f</i> )	Assignment	Character
O-CTA	$S_0 \rightarrow S_1$	2.60 (477.0)	1.3010	$H \rightarrow L$ (83%)	CT, $\pi-\pi^*$
	$S_0 \rightarrow S_2$	3.50 (353.8)	0.1112	$H-1 \rightarrow L$ (57%), $H \rightarrow L+1$ (38%),	CT, $\pi-\pi^*$
O-CT2A	$S_0 \rightarrow S_1$	2.28 (544.0)	1.5279	$H \rightarrow L$ (83%)	CT, $\pi-\pi^*$
	$S_0 \rightarrow S_2$	3.05 (406.0)	0.1894	$H-1 \rightarrow L$ (54%), $H \rightarrow L+1$ (42%),	CT, $\pi-\pi^*$
O-CT3A	$S_0 \rightarrow S_1$	2.05 (605.7)	1.7186	$H \rightarrow L$ (85%)	CT, $\pi-\pi^*$
	$S_0 \rightarrow S_2$	2.73 (454.9)	0.4716	$H \rightarrow L+1$ (68%), $H-1 \rightarrow L$ (27%)	CT, $\pi-\pi^*$

**Table 3.5** The excitation energies, oscillator strengths and molecular compositions for the 2 lowest states by TD-B3LYP/6-31 G (d, p) (solvent)

Molecules	State	Excitation energy (eV, nm)	Oscillator strength ( <i>f</i> )	Assignment	Character
O-CTPA	$S_0 \rightarrow S_1$	2.40 (515.6)	1.4406	$H \rightarrow L$ (88%)	CT, $\pi-\pi^*$
	$S_0 \rightarrow S_2$	3.17 (391.0)	0.3236	$H \rightarrow L+1$ (77%), $H-1 \rightarrow L$ (15%),	CT, $\pi-\pi^*$
O-CT2PA	$S_0 \rightarrow S_1$	2.16 (574.7)	1.6204	$H \rightarrow L$ (88%)	CT, $\pi-\pi^*$
	$S_0 \rightarrow S_2$	2.80 (442.9)	0.4683	$H \rightarrow L+1$ (82%), $H-1 \rightarrow L$ (9%)	CT, $\pi-\pi^*$



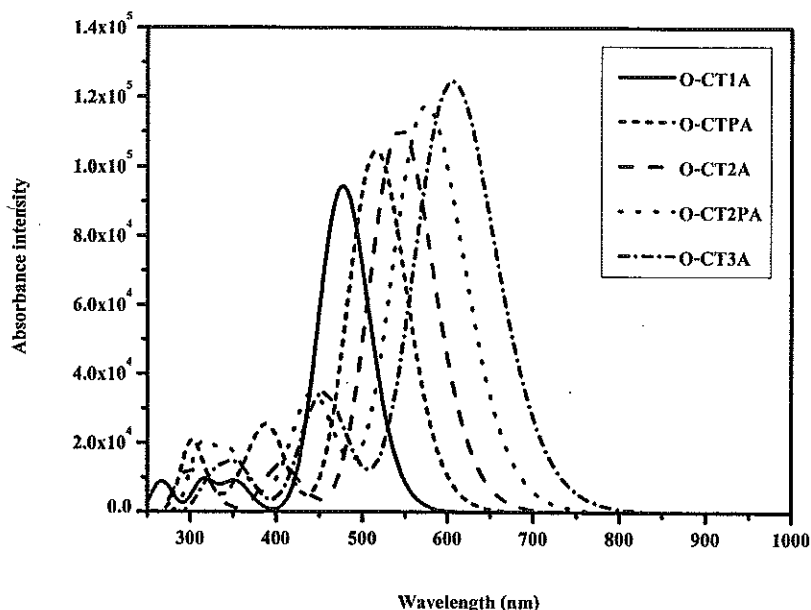


Figure 3.6 Calculated absorption spectra of O-CT1A, O-CT2A, O-CTPA, O-CT3A and O-CT2PA by B3LYP/6-31G (d,p)

### 3.3.2 *N*-Coumarin derivatives

#### 3.3.2.1 Optimized structure

The structures of organic dye used in this study are shown in Figure 3.7. The optimized geometries of N-CT2A and N-CT3A in the gas phase obtained by DFT/6-31G(d,p) are shown in Figure 3.8 and the selected inter-ring distances and dihedral angles are listed in Table 3.6. The dihedral angle of *N*-coumarin dye were investigated to understand the influence of the increasing thiophene number. The dihedral angle between C-T of N-CT2A and N-CT3A are -2.56 and 1.65 degree, respectively. For T-T dihedral angle were calculated to be 0.64 and 1.12 degree for N-CT2A and N-CT3A, respectively. The T-A dihedral angle of N-CT2A and N-CT3A are in range of 0.02-0.21 degree, respectively. From the calculated results, the dihedral angle of donor, linker and acceptor moieties in N-CT2A and N-CT3A are coplanar. It is suggesting that optimized structures are fully conjugated as demonstrated by the co-planarity of the donor and cyanoacrylic acid groups. It is interesting to compare the results of this report with those of the previous report of O-CT2A and O-CT3A involving the same linker and acceptor but different donor. The results revealed that the replacement of *O*-Coumarin by *N*-coumarin show

a similar dihedral angle between C-T dihedral angle of N-CT2A and N-CT3A and C-T dihedral angle of O-CT2A and O-CT3A, as shown in Table 3.1. The optimized geometry of N-CT2A is coplanar structure similar to those of O-CT2A this coplanar structure may have directly affected better electron injection via a smooth pathway from donor to acceptor moiety, Resulting in the better performance of DSCs with thiophene based dye.

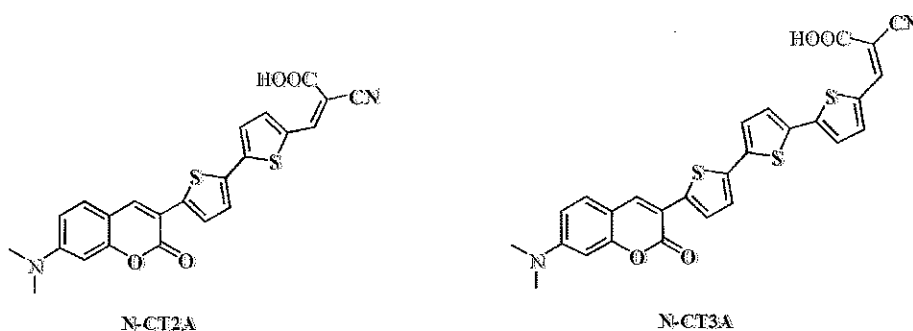


**Figure 3.7** Sketch map structure of target molecule N-CT2A and N-CT3A

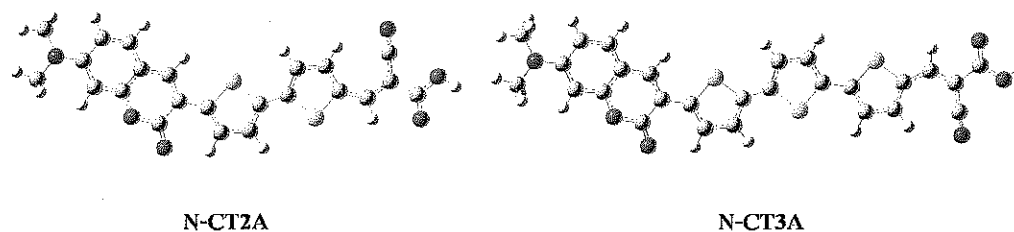


**Figure 3.8** The optimized structure N-CT2A and N-CT3A calculated by B3LYP/6-31G (d,p) level

**Table 3.6** The selected inter-ring distances and dihedral angles of N-CT2A and N-CT3A by B3LYP/6-31G (d,p).

Molecule		C-T	T1-T2	T2-T3	T-A
N-CT2A	Dihedral ( $\Phi$ )	2.56	0.64	-	0.02
	Distance ( $r$ )	1.46	1.44	-	1.43
N-CT3A	Dihedral ( $\Phi$ )	1.65	7.51	1.12	0.21
	Distance ( $r$ )	1.46	1.44	1.44	1.43

Note: C is coumarin, T is thiophene, A is acceptor

### 3.3.2.2 Electronic structure

To understand the electronic structure of *N*-coumarin dyes, N-CT2A and N-CT3A, molecular orbital and density of state were performed by using B3LYP/6-31G (d,p) level of theory. The frontier molecular orbitals of dyes are shown in Figure 3.9. The calculated HOMO level, the LUMO level percentage contribution of frontier molecular of N-CT2A and N-CT3A are listed in Table 3.7.

It can be seen that the HOMO level is a  $\pi$  orbital delocalized over the donor and linker unit, whereas the LUMO is  $\pi^*$  orbital localized in thiophene and cyanoacrylic group. Therefore, this distribution of the HOMO and LUMO is separated in the compounds. From the results indicating that the HOMO $\rightarrow$ LUMO transition can be considered as an intramolecular charge transfer (ICT) transition. To obviously explain the charge separation, the electron density of each part was shown in Table 3.7. Electron density distribution of HOMO state for N-CT2A is mainly located at the coumarin and the thiophene moiety which are calculated to be 50% and 42%, respectively. For the LUMO level, electron density distribution is mainly located at cyanoacrylic acid which is calculated to be 36%. From these calculation results, the excited electrons of N-CT2A transfers from the electron donor unit to the electron acceptor unit implying that the single excited state of these molecule could be considered as the intramolecular charge transfer along the  $\pi$ -conjugated skeleton.

For the N-CT3A, the HOMO level is a  $\pi$  orbital delocalized over the donor and  $\pi$ -spacer which the percentage contributions of coumarin are calculated to be 40% and 55%. The LUMO level is  $\pi^*$  orbital over  $\pi$ -spacer and acceptor unit, the percentage contributions of cyanoacrylic acid which are calculated to be 36%. It found that the excited electrons transfer from the coumarin to cyanoacrylic acid. It is suggesting that the excited state of these organic dye could be considered as the ICT along the  $\pi$ -conjugated backbone. Therefore, it is clearly concluded that thiophene ring is suitable linker for improving the dye efficiency of organic dye molecules. From the calculation results, the HOMO-LUMO gap of the dye N-CT2A and N-CT3A were computed by using B3LYP/6-31G(d,p). The results are listed in Table 3.8. The energy gap of N-CT2A was calculated to be 2.48 eV, while the energy gap of N-CT3A was calculated to be 2.30 eV. The energy level of N-CT2A and NCT3A as shown in Figure 3.10. It is found that the

HOMO-LUMO gap of N-CT3A is smaller than those of N-CT2A. The calculation study is suggesting that increasing the number of the thiophene units decrease the HOMO-LUMO gap.

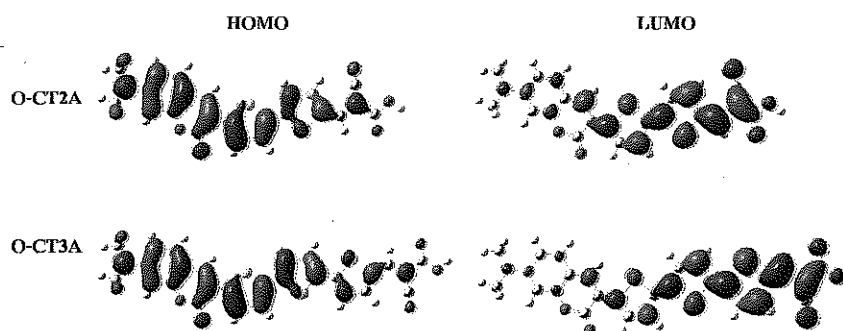


**Figure 3.9** Frontier molecular orbital of N-CT2A and N-CT3A calculated by B3LYP/6-31G (d,p) level of theory

**Table 3.7** Summarizes the energies and character of frontier orbital of N-CT2A and N-CT3A calculated by B3LYP/6-31G (d,p)

Molecule	Molecular orbital	Molecular Energy	percentage composition		
			Donor	thiophene	Acceptor
N-CT2A	LUMO	-2.79	15	49	36
	HOMO	-5.27	50	42	8
N-CT3A	LUMO	-2.82	7	58	36
	HOMO	-5.12	40	55	5

**Table 3.8** The calculated HOMO-LUMO energy gap of N-CT2A and N-CT3A

Molecule	$\Delta_{\text{HOMO-LUMO}}^a$ (eV)	Expt. <sup>b</sup> (eV)
N-CT2A	2.48	2.24
N-CT3A	2.30	2.15

<sup>a</sup>Calculations are performed with B3LYP/6-31G (d,p) in gas phase.

<sup>b</sup>Experimental  $\Delta_{\text{HOMO-LUMO}}$  estimated from the onset of the absorption spectra  $E_g$  (eV) =  $1240/\lambda_{\text{onset}}$  in dilute  $\text{CH}_2\text{Cl}_2$  solution.

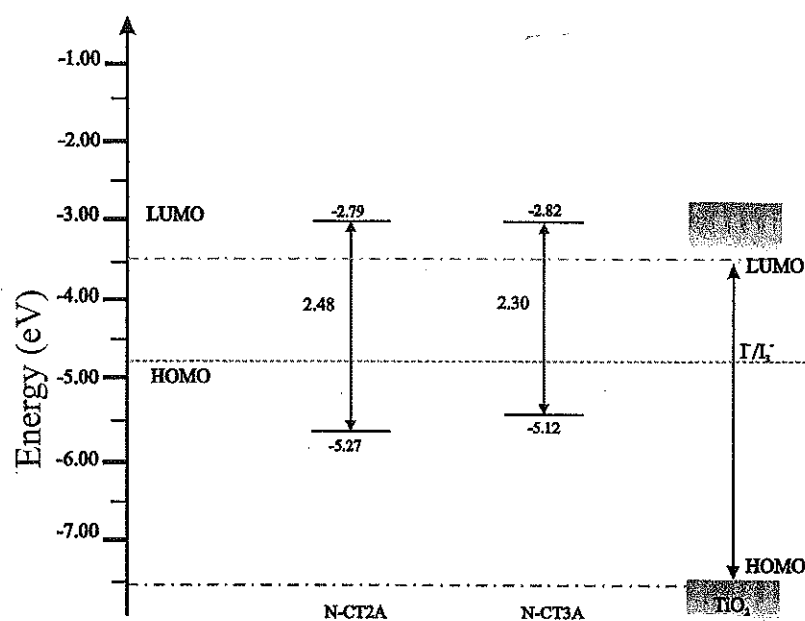


**Figure 3.10** Molecular orbital energy diagram of N-CT2A and N-CT3A

### 3.3.2.3 Absorbtion spectra

The investigation of D- $\pi$ -A structure, the molecular structure and excitation energy of the ICT states is an important point of discussion. Herein, theoretical calculations were performed to study on the ground-state structures of all organic dye. TDDFT calculations on a B3LYP/6-31G (d,p) level of theory show transitions with large oscillator strengths consistent with the absorption spectrum. The absorption spectra of all compounds are shown in Figure 3.11. Their optical characteristics are listed in Table 3.9.

The main absorption peak of N-CT2A and N-CT3A at 597.2 nm and 645.8 nm, that the absorption band could be attributed to the intramolecular charge transfer (ICT) between the donor and the acceptor, which is consistent with the assignment to the transition from the ground state ( $S_0$ ) to the first singlet excited state ( $S_1$ ). The absorption spectra are slightly red-shifted with the introduction of more thiophene units since the expansion of the  $\pi$ -conjugation length.

**Table 3.9** The excitation energies, oscillator strengths, and molecular compositions for the 2 lowest states by TD-B3LYP/6-31G (d,p) (solvent)

Molecule	State	Excitation energy (eV, nm)	Oscillator strength (f)	Assignment	Character
N-CT2A	$S_0 \rightarrow S_1$	2.08 (597.2)	1.4287	$H \rightarrow L$ (86%)	CT
	$S_0 \rightarrow S_2$	2.83 (437.6)	0.4933	$H-1 \rightarrow L$ (52%), $H \rightarrow L+1$ (43%)	CT, $\pi-\pi^*$
N-CT3A	$S_0 \rightarrow S_1$	1.92 (645.8)	1.5817	$H \rightarrow L$ (88%)	CT
	$S_0 \rightarrow S_2$	2.57 (481.5)	0.7794	$H-1 \rightarrow L$ (54%), $H \rightarrow L+1$ (40%)	CT, $\pi-\pi^*$

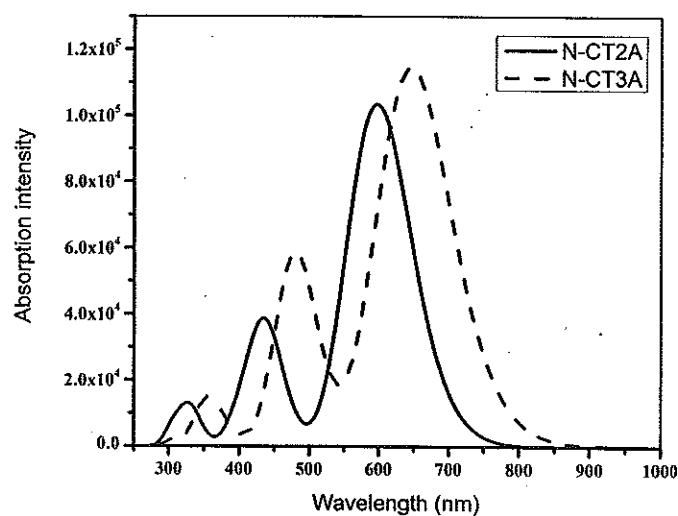


**Figure 3.11** Calculated absorption spectra of N-CT2A and N-CT3A by TD-B3LYP/6-31G(d,p)

### 3.4 Conclusion

For the coumarin derivative, the molecular structure and electronic properties were investigated. The structure of metal-free organic dyes containing of coumarin unit (*O*-coumarin and *N*-coumarin) as electron donor, thiophene and phenyl as linker and cyanoacrylic acid as electron acceptor. The influence of increasing thiophene units for improving the absorption spectra of coumarin derivatives and the difference linker (thiophene and phenyl) were investigated. Moreover, the effect of different donor between *O*-coumarin and *N*-coumarin, were studied. We found that the optimized geometries, the T-T dihedral angle of inker in O-CT2A and O-CT3A is smaller than the P-T dihedral angle in O-CTPA and O-CT2PA. From the calculation results, the coumarin dyes with thiophene-thiophene linker is more coplanar than that of the coumarin dyes with thiophene-phenyl linker. It is suggesting that the strong conjugated effects are form. Moreover the calculated results by TDDFT were compared with the experimental data. The calculation result is shown that the calculated data have the same tendency with the experiment. Beside the calculated absorption spectra of O-CT2A exhibit red-shifted compared to the absorption of O-CT1PA. It should be noted that improving conjugation system by the addition of thiophene unit was more suitable than phenyl unit For the optimized geometry of *N*-coumarin is coplanar structure similar to those of *O*-coumarin this coplanar may have directly affected better electron injection via a smooth pathway from donor to acceptor moiety. The main absorption peak of *N*-coumarin could be attributed to the intramolecular charge transfer (ICT) between the donor and the acceptor the absorption bands arising from ICT slightly red-shifted.

## CHAPTER 4

### *N,N*-DIMETHYLAMINOPHENYL DERIVATIVES

#### 4.1 Introduction

For the further development of highly efficient dye in DSCs, the dye must be designed to absorb most of the radiation of sun light in visible and near-IR region to produce a large photocurrent response. In addition, suitable energy level and location of HOMO and LUMO orbital of the dye are required to matching  $I/I_3$  redox potential and conduction band of the  $\text{TiO}_2$  semiconductor, respectively.

Another promising design strategy is replacement of coumarin unit with some other electron donor. The conjugated organic dye sensitizer that have *N,N*-dimethylaniline moieties as electron donor and a methine unit connecting with the cyanoacrylic acid group as the acceptor part were developed for use in dye sensitized solar cells. A maximum  $\eta$  of up to 6.8% was attained with dye based on NKX-2569 as shown in Figure 4.1. These molecules have simple structures and strongly electron donating suggests that organic dye is promising for use in DSCs in term of the possibility of low cost production [41].

Moreover, Yang and co-workers developed the new *N,N*-dimethylaniline containing thienothiophene D-ST as  $\pi$ -conjugation systems and rhodanine acetic acid as electron acceptor. This sensitizer showed good performance for DSCs and, especially, the DSCs based on D-ST achieved a good conversion efficiency of 6.2%. Although an elongation would contribute to a red shift in the absorption spectra, it would simultaneously cause two problems: it would complicate the synthetic produce, and second, it would decrease stability of the dye molecule due to the possibility of isomer formation [42]. Since *N,N*-dimethylaniline-base dye have been widely employed in DSCs but *N,N*-dimethylaniline dye containing thiophene have not been explored for DSCs. The introduction of  $\pi$ -conjugated ring unit such as phenyl and thiophene of coumarin dye expands of  $\pi$ -conjugation system and improve the stability of dye molecule



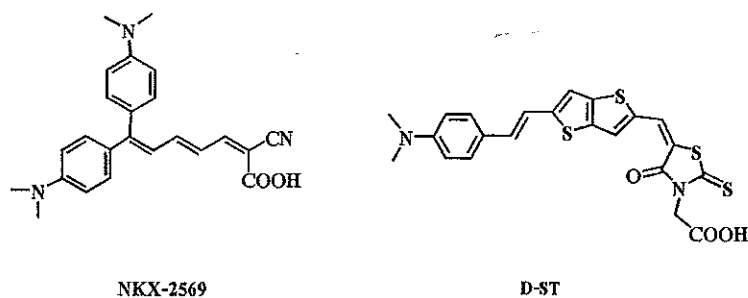


**Figure 4.1** *N,N*-dimethylaniline derivatives

Therefore, we are motivated to theoretically investigate the ground-state and excited-state electronic structures and optical properties of organic sensitizer for use in dye-sensitized solar cells. In this work, we have investigated the effect of conjugated spacer on *N,N*-dimethylaniline derivative by substitution different linker and increasing number of thiophene units namely PTPA, PT2A, PT2PA and PT3A as shown in Figure 4.2 to study the intramolecular charge transfer, optical properties and energy gap of the organic sensitizers. Knowledge of these series is useful for future improving the efficiency of organic dyes.

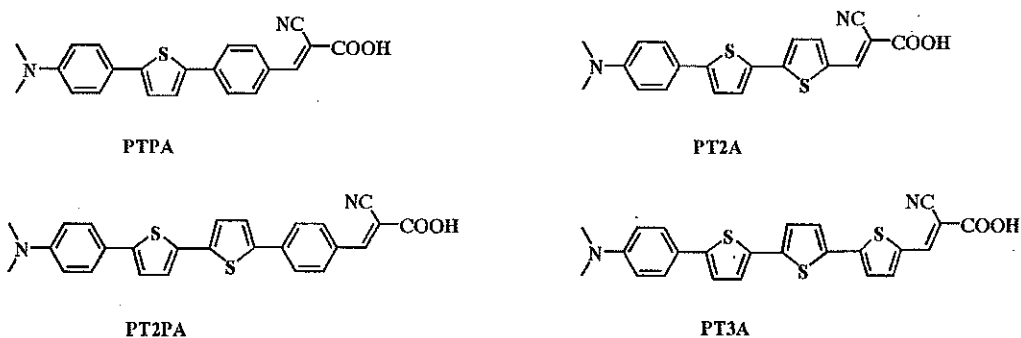


**Figure 4.2** Sketch map structure of target molecule PTPA, PT2A, PT2PA and PT3A

## 4.2 Method

To gain insight into the factor responsible for the absorption spectral, we perform DFT and TDDFT calculations on the ground state of organic dyes. The ground state structure of PTPA, PT2A, PT2PA and PT3A were optimized by the DFT method using the B3LYP functional with 6-31G (d,p) basis set. Electronic population of the HOMO and LUMO were calculated to show the position of localization of electron populations along with the calculated molecular orbital energy

diagram. The electronic absorption spectra require calculation of the allowed excitation and oscillator strengths, these calculations were carried out using TDDFT with the same basis set and exchange–correlation functional. The absorption spectra of all organic dyes were calculated using the Swizard program and the results were compared with the experimental data. Solvation effect for dichloromethane was included by means of the conductor–like polarizable continuum model (C-PCM). This computational approach allows us to provide a detailed assignment of the excited state involved in the absorption process. All calculations were carried out using the Gaussian 03 program package.

### 4.3 Results and discussion

The investigation of D- $\pi$ -A structure, the molecular structure and excitation energy of the ICT states is an important point of discussion. Herein, theoretical calculations were performed to study on the ground-state structures of all organic dyes.

#### 4.3.1 Optimized structure

The structures of organic dye used in this study are shown in Figure 4.2. The optimized geometries of PTPA, PT2A, PT2PA and PT3A in the gas phase shown in Figure 4.3 by the DFT method using the B3LYP exchange–correlation function, with 6-31G (d,p) basis set and the selected bond distances and dihedral angles are listed in Table 4.1.

We optimized the molecular structure in the gas phase obtaining the geometries of dye with thiophene unit, T- T dihedral angle were calculated to be -5.70 degree and -5.33 degree for PT2A and PT3A, respectively. It was found that the donor and acceptor moieties are fully conjugated as demonstrated by the co-planarity of the aryl amine and cyanoacrylic acid groups. When we replace the thiophene ring by phenyl ring, T-P dihedral angles were found to be 15.57 degree and -13.81 degree for PTPA and PT2PA, respectively.

Since steric repulsion between the hydrogen atoms of thiophene and phenyl, these units are not fully coplanar. It reveals that non planar structure affects the delocalization of electron from donor to acceptor cannot smoothly via non planar  $\pi$ -spacer. From this the investigated metal-free organic dyes exhibit coplanar conformation between the thiophene group of the  $\pi$ -conjugated linker. We believe that this coplanar molecular structure should improve the electron transfer from the electron-donor to the electron-acceptor in these dyes molecule. We have

also concluded that the  $\pi$ -conjugated chain can enhance the electron-transfer ability. Furthermore, organic dye with a more planar  $\pi$ -conjugated chain may have a better DSCs performance

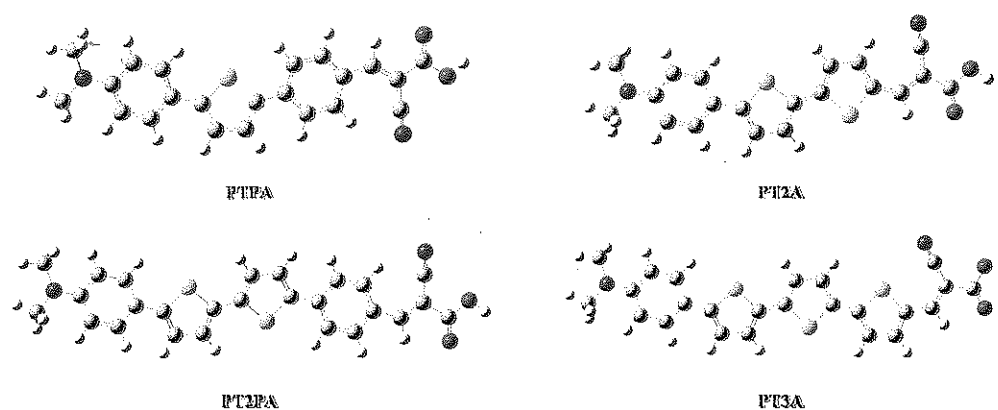


**Figure 4.3** The optimize structure of PTPA, PT2A , PT2PA and PT3A by calculated by B3LYP/6-31G (d,p) level of theory .

**Table 4.1** The selected inter ring distances and dihedral angles of PTPA, PT2A, PT2PA and PT3A by B3LYP/6-31G(d,p)

Molecule		D -P	P1-T1	T1-T2	T-P	T2-T3	P-A
PTPA	Dihedral ( $\Phi$ )	7.29	-22.83	-	15.57	-	0.69
	Distance ( <i>r</i> )	1.38	1.46	-	1.46	-	1.44
PT2A	Dihedral ( $\Phi$ )	-5.89	22.68	-5.70	-	-	0.29
	Distance ( <i>r</i> )	1.38	1.45	1.44	-	-	1.42
PT2PA	Dihedral ( $\Phi$ )	-8.25	24.51	4.08	-13.81	-	0.18
	Distance ( <i>r</i> )	1.38	1.46	1.44	1.46	-	1.45
PT3A	Dihedral ( $\Phi$ )	-4.98	19.02	-5.33	-	1.60	-0.06
	Distance ( <i>r</i> )	1.38	1.46	1.44	1.44	1.44	1.42

Note: D is dimethylaminophenyl, P is phenyl, T is thiophene, A is acceptor

### 4.3.2 Electronic structure

To gain insight into the geometrical electronic structures of the dyes, molecular orbital and density of state were calculated by using B3LYP/6-31G (d,p) level of theory. The frontier molecular orbitals of the dyes are shown in Figure 4.4. The calculated the HOMO and LUMO and percentage contribution of frontier molecular orbital of PTPA, PT2A, PT2PA and PT3A are listed in Table 4.2. The calculated electron distribution shows favorable directionality for inject electron from donor group to conduction band of the  $\text{TiO}_2$  via the bridge and anchoring group.

The electron density distribution of HOMO state for PTPA, PT2A, PT2PA and PT3A is mainly located at the donor and the  $\pi$ -conjugated linker moiety. Electron density of dimethylaniline in PTPA and PT2A are calculated to be 61% and 54% for HOMOs. The electron density of thiophene in PT2A is larger than phenyl in PTPA that are calculated to be 39% and 35% for PT2A and PTPA, respectively, while at the LUMOs level, the percentage contributions of cyanoacrylic acid are calculated to be 52% and 44% in for PTPA and PT2A. From these results, the excited electrons are shifted from the electron donor moiety to the electron acceptor unit implying that the single excited state of these molecule could be considered as the intramolecular charge transfer along the  $\pi$ -conjugated skeleton. Moreover, comparing between PTPA and PT2A, the DOS calculations have been shown percentage contribution of linker in both dyes were significantly different. These results confirm that adding phenyl rings affect to the  $\pi$ -spacer of these organic dyes due to the dihedral between thiophene and phenyl ring were not coplanar and therefore the ICT between phenyl rings cannot be induced as expected leading to the reduction of transferring electrons in anchoring group at the end. Therefore, these results are clearly concluded that thiophene ring is appropriate linker for improving the dye efficiency of our dye molecules.

Highly efficient DSCs require that the LUMO level of the dye molecules should be above the conduction band edge of  $\text{TiO}_2$  ( $E_{cb}$ ) to ensure an effective electron injection from the dye molecules to the conduction band of the  $\text{TiO}_2$  film and the HOMO level of the dye should be below the redox potential of  $\text{I}^-/\text{I}_3^-$  to ensure the regeneration of dye molecules. The calculated  $\Delta_{H-L}$  of PTPA, PT2A, PT2PA and PT3A is 2.56, 2.48, 2.34 and 2.26 eV, respectively, as listed in Table 4.3.

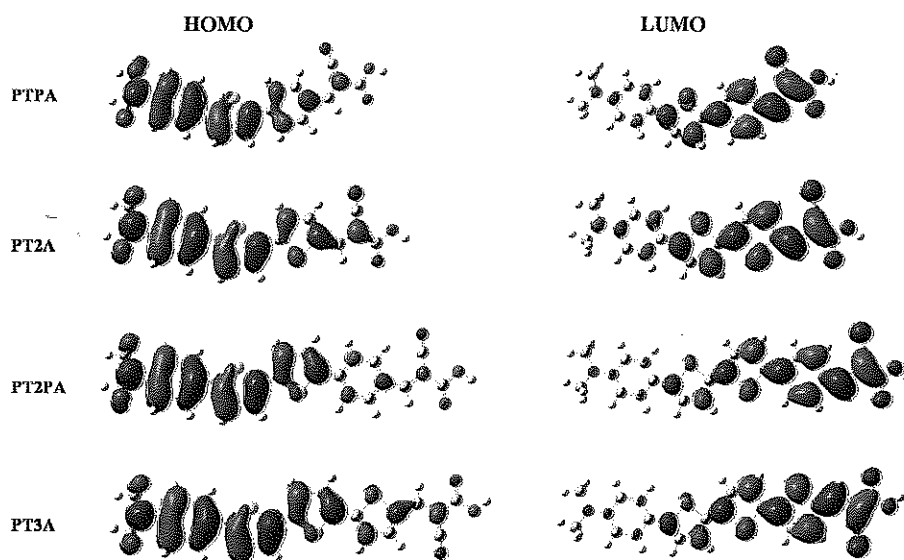


**Figure 4.4** Frontier molecular orbital of PTPA, PT2A, PT2PA and PT3A calculated by B3LYP/6-31G (d,p) level of theory

**Table 4.2** Summarizes the energies and percentage contribution of frontier orbital of PTPA, PT2A, PT2PA and PT3A calculated by B3LYP/6-31G (d,p)

Molecules	Molecular orbital	Molecular Energy (eV)	percentage composition		
			Donor	Linker	Acceptor
PTPA	LUMO	-2.51	4	44	52
	HOMO	-5.07	61	35	4
PT2A	LUMO	-2.61	5	52	44
	HOMO	-5.09	54	39	7
PT2PA	LUMO	-2.60	1	51	47
	HOMO	-4.93	48	50	2
PT3A	LUMO	-2.69	2	60	38
	HOMO	-4.94	43	52	4

The HOMO of PT2PA and PT3A is destabilized and LUMO is stabilized as compared to PTPA and PT2A. From the results, the HOMO-LUMO gap of PT2PA and PT3A is reduced due to increasing of the conjugation length. Furthermore, the results also indicate that the electronic structures of PTPA and PT2PA are very similar to PT2A and PT3A, but the HOMO-LUMO gap of PTPA and PT2PA is larger than those of PT2A and PT3A respectively. These results are found that substituent has remarkable influent on the LUMO level but a small effect on the HOMO. The LUMOs of PTPA and PT2PA with phenyl group are destabilized by 0.09-0.10 eV compare to the corresponding PT2A and PT3A.

The energy diagram of PTPA, PT2A, PT2PA and PT3A as shown in Figure 4.5. It was found that LUMO level of the PT2A and PT3A dye was closer the conduction band edge of  $\text{TiO}_2$  ( $E_{\text{cb}}$ ) than those of PTPA and PT2PA respectively suggesting that the excited electrons are injected into semiconductor. On the other hand the HOMO level of all organic dye suitably located under the redox potential that is appropriated for donation of electron from the  $\text{I}^-/\text{I}_3^-$  redox couple in the electrolyte solution. This showed that extension of linker by introduction of thiophene unit improve both the efficient electron injection from excited dye to the conduction band edge of  $\text{TiO}_2$  ( $E_{\text{cb}}$ ) and regeneration process in DSCs.

**Table 4.3** The calculated HOMO-LUMO energy gap of PTPA, PT2A, PT3A and PT2PA

Molecules	$\Delta_{\text{HOMO-LUMO}}^{\text{a}}$ (eV)	Expt. <sup>b</sup> (eV)
PTPA	2.34	2.13
PT2A	2.26	1.99
PT2PA	2.18	2.33
PT3A	2.01	N.A.

<sup>a</sup>Calculations are performed with B3LYP/6-31G (d,p) in  $\text{CH}_2\text{Cl}_2$  solution using Conductor-like Polarizable Continuum Model (C-PCM)

<sup>b</sup>Experimental  $\Delta_{\text{HOMO-LUMO}}$  estimated from the onset of the absorption spectra  $E_g$  (eV) =  $1240/\lambda_{\text{onset}}$  in dilute  $\text{CH}_2\text{Cl}_2$  solution

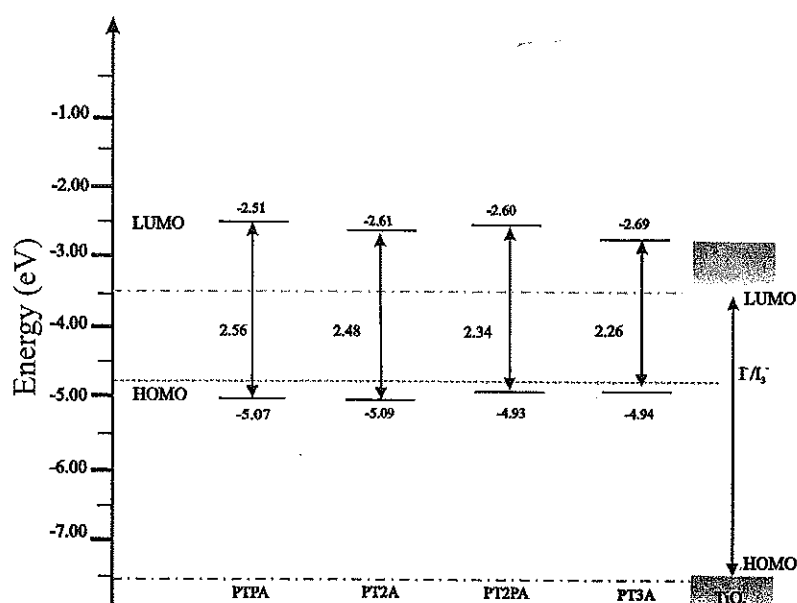


Figure 4.5 Molecular orbital energy diagram of PTPA, PT2A, PT2PA and PT3A

#### 4.3.3 Absorption spectra

TDDFT calculations on a B3LYP/6-31G (d,p) level of theory show transitions with large oscillator strengths consistent with the absorption spectrum. The UV-vis absorption spectra of all compounds are listed in Table 4.4. Their optical characteristics are shown in Figure 4.6, the main peak of PTPA, PT2A, PT2PA and PT3A is 586.6 nm, 610.8 nm, 651.7 nm and 694.7 nm, respectively. The organic dyes exhibit intense absorptions at around 587-698 nm that this band could be attributed to the electronic transition delocalized throughout the whole molecule with a charge-transfer character, which is consistent with the assignment to the transition from the ground state ( $S_0$ ) to the first singlet excited state ( $S_1$ ). Since the charge transfer absorption bands are very sensitive to the solvent polarity, we also measured the absorption in the solvent.

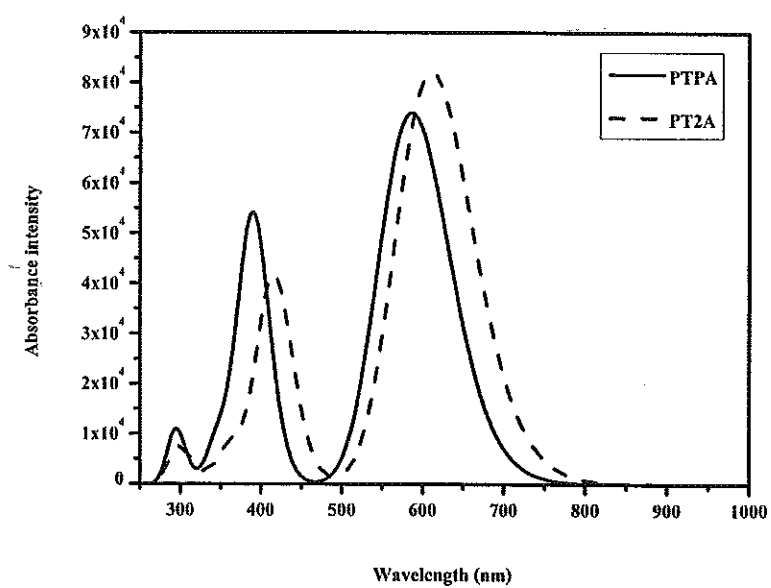
As depicted in Figure 4.6 the main peak at 586.6 nm and 610.8 nm for PTPA and PT2A respectively. The absorption spectra show that the calculated absorption spectra of PT2A with thiophene are red-shifted with respect to absorption spectra of PTPA with phenyl. Since thiophene-thiophene linker has smaller dihedral angle than thiophene-phenyl linker. The calculated results have the same tendency with the experiment. Moreover, the calculated absorption spectra of PT3A exhibit red-shifted compared to the absorption of PT2A due to

increasing the conjugation length. The sensitizer would expand the conjugation in the dye resulting in the wide absorption in the visible region. It should be noted that improving conjugation system by the addition of thiophene unit was more suitable than phenyl unit.

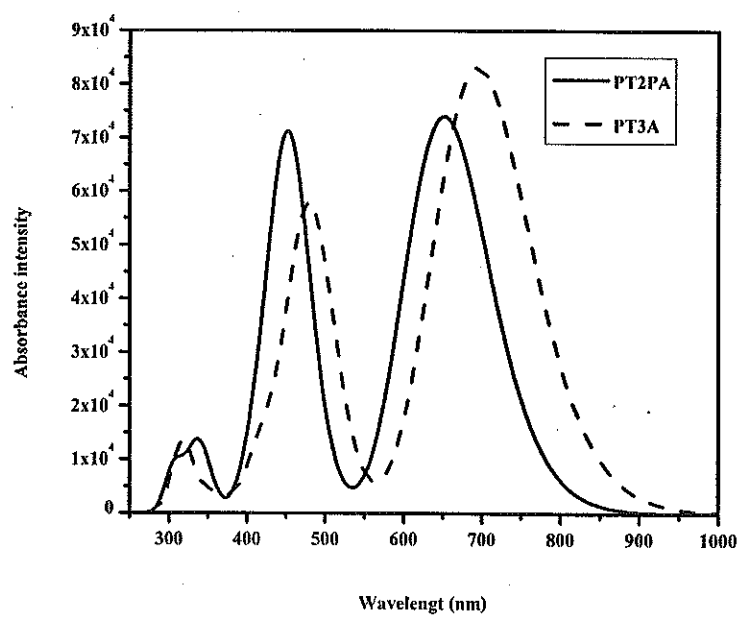
**Table 4.4** The excitation energies, oscillator strengths and molecular compositions for the lowest states by TD-B3LYP/6-31G (d,p) (solvent)

Molecules	State	Excitation energy (eV, nm)	Oscillator strength (f)	Assignment	Character
PTPA	$S_0 \rightarrow S_1$	2.11(586.6)	1.0215	H $\rightarrow$ L (89%)	CT
	$S_0 \rightarrow S_2$	3.18 (390.2)	0.7382	H-1 $\rightarrow$ L (79%), H $\rightarrow$ L+1 (13%)	CT, $\pi-\pi^*$
PT2A	$S_0 \rightarrow S_1$	2.03 (610.8)	1.1328	H $\rightarrow$ L (85%)	CT
	$S_0 \rightarrow S_2$	2.98 (415.7)	0.5756	H-1 $\rightarrow$ L (78%), H $\rightarrow$ L+1 (12%)	CT, $\pi-\pi^*$
PT2PA	$S_0 \rightarrow S_1$	1.90 (651.7)	1.0206	H $\rightarrow$ L (100%)	CT
	$S_0 \rightarrow S_2$	2.73 (454.7)	0.9268	H-1 $\rightarrow$ L (86%), H $\rightarrow$ L+1 (13%)	CT, $\pi-\pi^*$
PT3A	$S_0 \rightarrow S_1$	1.78 (694.7)	1.1477	H $\rightarrow$ L (100%)	CT
	$S_0 \rightarrow S_2$	2.58 (480.6)	0.7822	H-1 $\rightarrow$ L (89%), H $\rightarrow$ L+1 (10%)	CT, $\pi-\pi^*$





(a)



(b)

**Figure 4.6** (a) Absorption spectra of PTPA and PT2PA (b) calculated absorption spectra of PT2A and PT3A by TD-B3LYP/6-31G (d,p)

#### 4.4 Conclusion

We have investigated the effect of conjugated spacer on *N,N*-dimethylaminophenyl derivative by substitution difference linker and increasing number of thiophene of the organic sensitizers. Knowledge of these series is useful for future improving the efficiency of organic dyes. The calculation results shown that optimized geometries of dye with thiophene unit, T-T dihedral angle more planar than those of dye with phenyl unit. Furthermore the absorption spectra dyes with thiophene-thiophene linker is more red shift than that of the dyes with thiophene - phenyl linker. The sensitizer would expand the conjugation in the dye resulting in the wide absorption in the visible region. It should be noted that improving conjugation system by the addition of thiophene unit was more suitable than phenyl unit.

## CHAPTER 5

### CARBAZOLE-FLUORENE DERIVATIVES

#### 5.1 Introduction

Because of the strong emission and absorption properties, carbazole and their derivatives have been exploited as electroluminescent, non-linear optical (NLO) and photorefractive materials. The hole-transporting capability has been explored in OLEDs and, moreover, the wide band gap of carbazole has been utilized in constructing photovoltaic devices. Nagatoshi Koumura and co-worker designed and sensitized organic sensitizer based-on carbazole, MK1, MK2 and MK3, for application in dye-sensitized solar cells. It was found that the maximum value of 7.7% was obtained with the DSCs based-on MK-2 sensitizer show in Figure 5.1[43].

Moreover, Samuel G. Awuah and coworker report the synthesis, photophysical, electrochemical and theoretical properties of novel pyran-based organic dyes (D1, D2, and D3) show in the Figure 5.1 as well as their applications in DSCs for the first time [44]. The designed dyes possess a cyanoacrylic acid group as an acceptor and arylamine group as a donor group in a D- $\pi$ -A configuration.

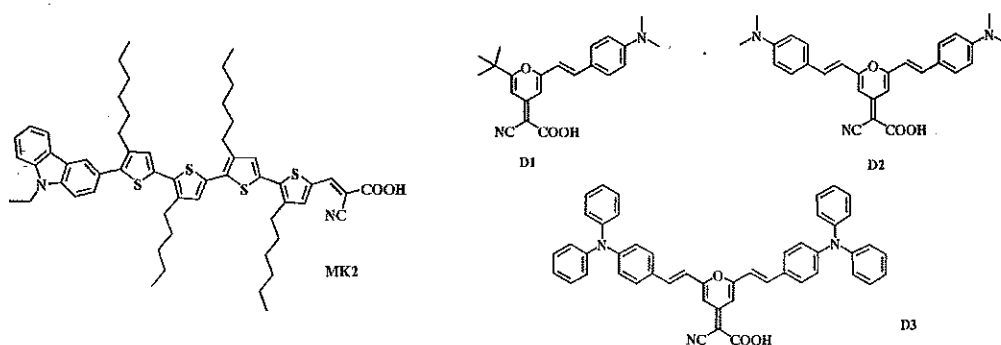


**Figure 5.1** Sketch map structure of molecule MK-2, D1, D2 and D3

The introduction of varying donor groups resulted in correspondingly different photophysical and electrochemical properties. The DSCs fabricated using dye D1 shown the highest photovoltaic performance with the overall conversion efficiency is 2.17%. The synthesized dyes with a pyran chromophore and arylamine donor groups showed potentials for applications in DSCs.

In this chapter, theoretical calculations were performed to study the ground-state structures and optical properties of carbazole-fluorene derivatives. The series of metal-free organic dyes containing carbazole act as electron donor, fluorene, phenyl and pyran act as linker. The influence of different acceptor, acrylic acid and cyanoacrylic acid were investigated.

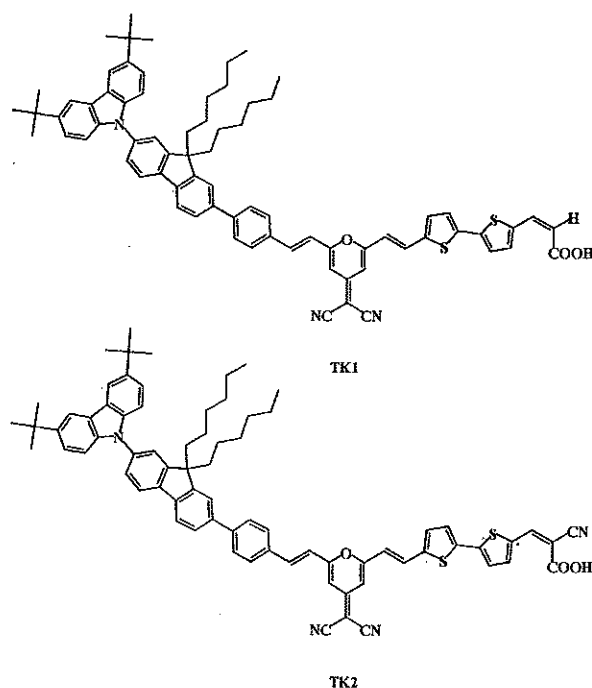


**Figure 5.2** Sketch map structure of target molecule TK1 and TK2

## 5.2 Method

To gain insight into the factor responsible for the absorption spectral, we perform DFT and TDDFT calculations on the ground state of organic dyes. The ground state structure of TK1 and TK2 were optimized by the DFT method using the B3LYP exchange–correlation function

with 6-31G (d,p) basis set. Electronic population of the HOMO and LUMO were calculated to show the position of localization of electron populations along with the calculated molecular orbital energy diagram. The electronic absorption spectra require calculation of the allowed excitation and oscillator strengths, these calculations were carried out using TDDFT with the same basis set and exchange–correlation functional. The absorption spectra of all organic dyes were calculated using the Swizard program and the results were compared with the experimental data. Solvation effect for dichloromethane was included by means of the conductor–like polarizable continuum model (C-PCM). This computational approach allows us to provide a detailed assignment of the excited state involved in the absorption process. All calculations were carried out using the Gaussian 03 program package.

### 5.3 Results and discussion

In the investigation of D- $\pi$ -A systems, the molecular structure of the ICT states is an important point of discussion. Herein, theoretical calculations were performed to study the ground-state structures of carbazole-fluorene dye.

#### 5.3.1 Optimized structure

We optimized the geometries of TK1 and TK2 in the gas phase obtaining the geometries shown in Figure 5.3 and the selected bond distances and dihedral angles are listed in Table 5.1. The dihedral angle of TK1 and TK2 dyes was determined C-F dihedral angle were calculated to be -54.03 degree and -54.72 degree, respectively. The T-A dihedral angle are calculated to be -0.18 degree and -0.01 degree. We found that the cyanoacrylic acid group was located to be coplanar with the thiophene. From the calculated results indicating that the linker and acceptor moieties are fully conjugated as demonstrated by the co-planarity of the linker and acceptor groups.

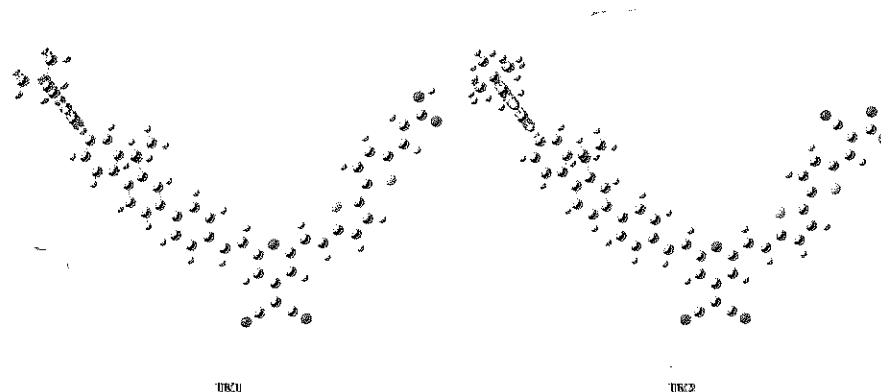


**Figure 5.3** The optimize structure of TK1 and TK2 calculated by B3LYP/6-31G (d,p) level

**Table 5.1** The selected bond distances and dihedral angles of TK1 and TK2 by B3LYP/6-31G (d,p)

Molecules		C-F	F-P	P-E	E-Py	Py-E	E-T	T-T	T-A
TK1	Dihedral ( $\Phi$ )	-54.03	-34.67	-0.62	2.93	-2.79	-0.79	1.90	-0.18
	Distance (r)	1.42	1.48	1.46	1.44	1.45	1.43	1.43	1.44
TK2	Dihedral ( $\Phi$ )	-54.72	-34.90	-1.46	-2.50	2.14	0.32	0.72	-0.01
	Distance (r)	1.42	1.48	1.46	1.44	1.45	1.44	1.43	1.43

Note: C is Carbazole, F is Fluorene, P is phenyl, E is ethane, Py is pyran, T is thiophene,

A is acceptor

### 5.3.2 Electronic structure

To gain insight into the geometrical electronic structures of the dyes, molecular orbital and density of state were performed by using B3LYP/6-31G (d,p) level of theory. The frontier molecular orbitals of the TK1 and TK2 dyes are shown in Figure 5.4 (a) and 5.4 (b). The HOMO level, LUMO level and percentage contribution of frontier molecular orbital TK1 and TK2 are listed in Table 5.2.

**Table 5.2** Summarizes the energies and percentage contribution of frontier orbital of TK1 and TK2 calculated by B3LYP/6-31G(d, p)

Molecules	Molecular orbital	Molecular Energy (eV)	$\Delta_{H-L}$	percentage composition				
				Cbz	Flu-Phe	Py	Thio	Cyn
TK2	LUMO	-3.07	-2.09	0	2	44	43	12
	HOMO	-5.17		80	19	1	0	0
TK2	LUMO	-3.40	-1.78	0	0	28	47	25
	HOMO	-5.20		80	19	1	0	0

Note: Cbz is Carbazole, Flu is Fluorene, Phe is phenyl, Py is pyran, Thio is thiophene, Cyn is acceptor

**Table 5.3** The calculated HOMO-LUMO energy gap of TK1 and TK2

Molecule	$\Delta_{HOMO-LUMO}^a$ (eV)	Expt. <sup>b</sup> (eV)
TK1	2.10	2.14
TK2	1.77	2.16

<sup>a</sup>Calculations are performed with B3LYP/6-31G (d,p) in gas phase

<sup>b</sup>Experimental  $\Delta_{HOMO-LUMO}$  estimated from the onset of the absorption spectra ( $E_g$  (eV) =  $1240/\lambda_{onset}$ ) in dilute  $CH_2Cl_2$  solution

The HOMO is a delocalized  $\pi$  orbital over the carbazole and fluorene unit while the LUMO is  $\pi^*$  orbital that localized in pyran unit, thiophene unit and cyanoacrylic unit. As list in Table 5.2 electron density distribution of HOMO state for TK1, electron density of carbazole and fluorene are calculated to be 80% and 19%. While at the LUMO level, the electron density of pyran and thiophene in TK1 are calculated to be 44% and 43%, respectively. The percentage contributions of cyanoacrylic acid are calculated to be 12%.

For the TK2, at HOMO level is a delocalized  $\pi$  orbital over the donor and  $\pi$ -spacer, while the LUMO level is  $\pi^*$  orbital that localized in  $\pi$ -spacer and acceptor unit. The percentage contributions of electron density of carbazole and fluorene are calculated to be 80% and 19%. While at the LUMO level the electron density of pyran and thiophene in TK1 are calculated to be 28% and 47%, respectively. The percentage contributions of cyanoacrylic acid are calculated to be 25%. These results indicate that electron density on cyanoacrylic acid unit of TK2 dye more than electron density on acrylic acid of TK1 dye. It is suggesting that TK2 dye might be easier injecting electron from acceptor to the conduction band of  $\text{TiO}_2$  providing higher efficient electron injection.

The energy gap of TK1 without CN was calculated to be 2.09 eV. While the energy gap of TK2 with CN was calculated to be 1.79 eV. The HOMO-LUMO gap of TK2 is smaller than those of TK1 indicating that difference acceptor affect to the HOMO-LUMO gap. The results are listed in Table 5.3 which clearly indicating that the energy gaps of dye is decreased when CN was introduced in to dye molecule. The one property which indicates a good dye-sensitizer is that the LUMO of dye should be located above and closed to the conduction band of  $\text{TiO}_2$ . The energy level diagram of TK1 and TK2 are shown in Figure 5.4. The LUMO level of TK2 with cyanoacrylic acid as anchoring group are closer to the conduction band of  $\text{TiO}_2$  than TK1 which have acrylic acid as anchoring group. These can be explained that the strong withdrawing CN group has ability in lowering LUMO level. The results also imply that TK2 would have suitable property for injection of electron from excited dye to conduction band of semiconductor  $\text{TiO}_2$ .



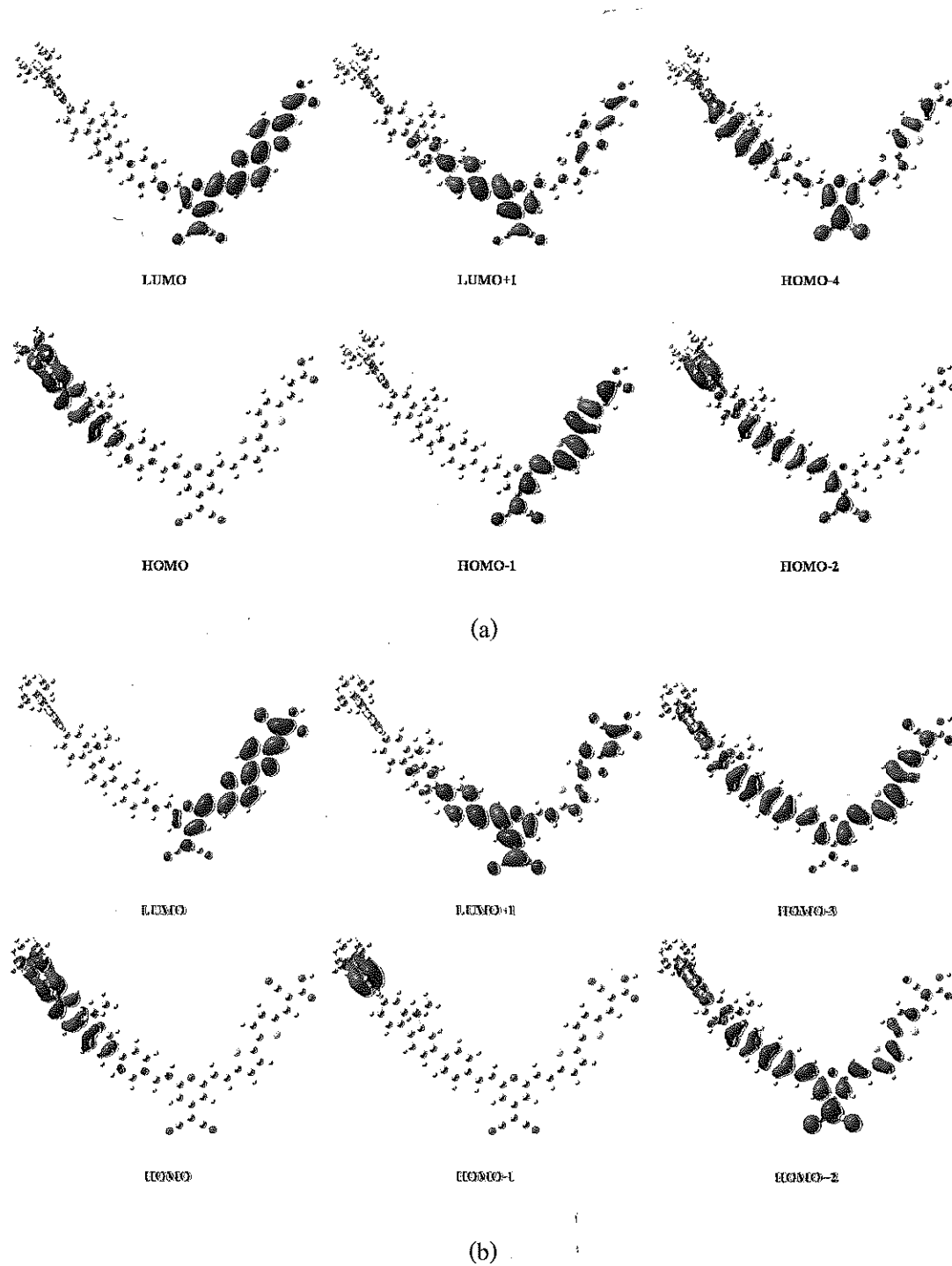


**Figure 5.4** (a) Frontier molecular orbital of TK1 and (b) frontier molecular orbital of TK2 calculated by B3LYP/6-31G (d,p) level of theory

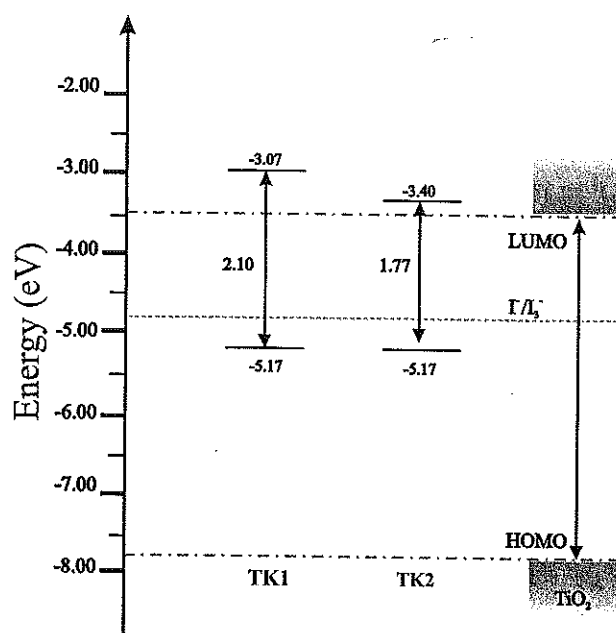


Figure 5.5 Molecular orbital energy diagram of TK1 and TK2

### 5.3.3 Absorption spectra

TDDFT calculations on a B3LYP/6-31G (d,p) level of theory show transitions with large oscillator strengths consistent with the absorption spectrum. The UV-vis absorption spectra of all compounds are shown in Figure 5.6. Their optical characteristics are listed in Table 5.4. The main absorption peak of TK1 and TK2 is 542.5 nm and 560.7 nm, respectively. The absorption spectra show that the calculated absorption spectra of TK2 with cyanoacrylic acid are red-shifted with respect to absorption spectra of TK1 with acrylic acid. These suggest that the dyes containing cyanoacrylic acid group as acceptor promise a better property since it is beneficial for absorbing the longer-wavelength light than TK1.

**Table 5.4** The excitation energies, oscillator strengths and molecular compositions for the lowest states by TD-B3LYP/6-31G (d,p) (solvent)

Molecules	State	Excitation energy (eV, nm)	Oscillator strength (f)	Assignment	Character
TK1	$S_0 \rightarrow S_2$	2.29 (542.5)	1.6468	H-1 $\rightarrow$ L (73%), H $\rightarrow$ L+1 (7%)	CT
	$S_0 \rightarrow S_3$	2.48 (500.3)	0.6230	H $\rightarrow$ L+1 (87%) H-1 $\rightarrow$ L (6%)	$\pi-\pi^*$
TK2	$S_0 \rightarrow S_2$	2.21 (560.6)	1.5163	H-3 $\rightarrow$ L (76%), H-2 $\rightarrow$ L (37%), H $\rightarrow$ L+1 (6%)	CT, $\pi-\pi^*$
	$S_0 \rightarrow S_3$	2.25 (551.2)	0.2780	H-2 $\rightarrow$ L (84%), H-1 $\rightarrow$ L (9%)	CT, $\pi-\pi^*$

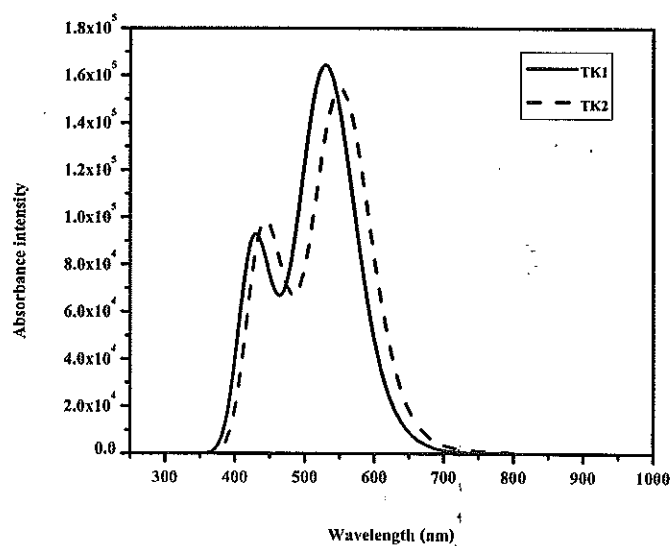


**Figure 5.6** Calculated absorption spectra of TK1 and TK2 by TD-B3LYP/6-31G (d,p)

#### 5.4 Conclusion

For carbazole-fluorene derivatives, the influence of different acceptor, acrylic acid and cyanoacrylic acid were investigated. From the calculation results, we found that the acrylic and cyanoacrylic acid group was located to be coplanar with the linker. It is indicating that the linker and acceptor moieties are fully conjugated as demonstrated by the co-planarity of the linker and acceptor. The absorption spectra of the dye with difference acceptor show that the calculated absorption spectra of TK2 with cyanoacrylic acid are red-shifted with respect to absorption spectra of TK1 with acrylic acid. These suggest that the dyes containing cyanoacrylic acid group as acceptor promise a better property since it is beneficial for absorbing the longer-wavelength light than the dyes containing cyanoacrylic acid group.

## CHAPTER 6

### COMPARISON OF COUMARIN, *N,N*-DIMETHYLAMINOPHENYL AND CABAZOLE BASED DYES

One of the most significant aspects in the development of dye-sensitized solar cells (DSCs) is the exploration and design of high-efficiency and low-cost dyes. In this chapter, we have reported a theoretical study of the structure and electronic properties of organic dyes with different donors.

#### 6.1. Coplanarity of the D- $\pi$ -A structure

To afford deeper insight into the geometrical and electronic properties of the dyes, the geometries of the molecules were optimized using density functional theory (DFT) with the B3LYP /6-31G(d) method as implemented in the Gaussian 03 program package. We selected the best dye form each series to represent coumarin, *N,N*-dimethylaminophenyl and cabazole based dyes, respectively as shown in Figure 6.1.

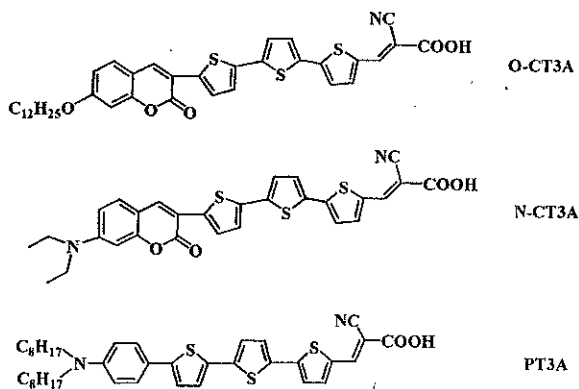


**Figure 6.1** The optimize structure of O-CT3A, N-CT3A and PT3A by calculated B3LYP/6-31G(d,p)

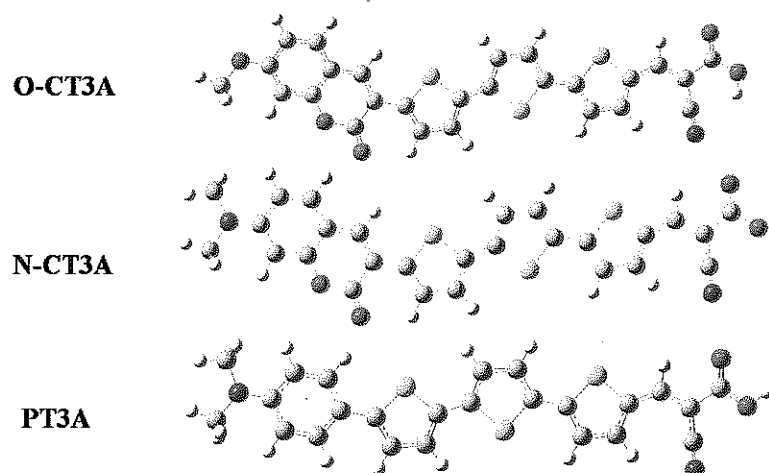


**Figure 6.2** The optimize structure of O-CT3A, N-CT3A and PT3A by calculated B3LYP/6-31G (d,p)

**Table 6.1** Selected inter-ring distances (Å) and dihedral angles (°) of O-CT3A, N-CT3A and PT3Acalculated by B3LYP/6-31G (d,p) calculations

Molecules		C-T	T1-T2	T2-T3	T1-P	T-A
O-CT3A	Dihedral ( $\Phi$ )	3.51	-9.94	3.69	-	-0.28
	Distance ( $r$ )	1.46	1.44	1.44	-	1.42
N-CT3A	Dihedral ( $\Phi$ )	1.65	-7.51	1.12	-	-0.21
	Distance ( $r$ )	1.46	1.44	1.44	-	1.43
PT3A	Dihedral ( $\Phi$ )	-4.98	19.02	-5.33	1.60	-0.06
	Distance ( $r$ )	1.38	1.46	1.44	1.44	1.42

C is coumarin, T is thiophene, A is acceptor

The optimize structure of O-CT3A, N-CT3A and PT3A display in Figure 6.2 the selected bond lengths and dihedral angles are listed in Table 6.1. The dihedral angle between C-T in O-CT3A, N-CT3A and PT3A are 3.51, 1.65 and -4.98 degree respectively. The calculation results show that the dihedral angle between donor and linker is coplanar. Moreover, T-A dihedral angle are found to be 0.06-0.20 degree indicating the cyanoacrylic acid group was located to be

coplanar with the thiophene. From the results, we found that the donor and acceptor moieties are fully conjugated as demonstrated by the co-planarity of the donor, linker and acceptor. No significant geometrical changes were found upon all of the dye molecules, indicating that all dyes the aromatic rings of the bridge between donor linker and the anchoring groups do not deviate from planarity. The perfection of the donor planarity is supposed to enhance the  $\pi$ -conjugated effect of the entire molecule and consequently improve the performance of organic dye as a sensitizer.

## 6.2 Intramolecular charge transfer

To gain insight into the geometrical and electronic structures of three dyes, molecular orbital and density of state were performed by using B3LYP/6-31G (d,p) level of theory. The frontier molecular orbital of the dyes are shown in Figure 6.3. The calculated the HOMOs level, the LUMOs level and percentage contribution of frontier molecular orbital of O-CT3A, N-CT3A and PT3A are listed in Table 6.2.

From the calculation results, it can be seen that the HOMO level is a delocalized  $\pi$  orbital over the donor and linker unit, whereas the LUMO level is  $\pi^*$  orbital which  $\pi$ -electron was localized in linker and acceptor group. Therefore, this distribution of the HOMO and LUMO is separated in the donor and acceptor part of compounds, indicating that the HOMO $\rightarrow$ LUMO transition can be considered as an intramolecular charge transfer (ICT) transition. To obviously explain the charge separation, the electron density of each part was shown in Table 6.2 Electron density distribution of HOMO state for O-CT3A, N-CT3A and PT3A is mainly located at the donor which is calculated to be 25%, 40% and 43% and the thiophene moieties are calculated to be 68%, 55% and 52%, respectively. These results indicate that the electron density of HOMO is mainly located on donor part. For the LUMOs level, the percentage contributions of cyanoacrylic acid are calculated to be 36%, 36% and 38% for O-CT3A, N-CT3A and PT3A, respectively, which is mainly delocalized on acceptor part. From these results, the excited electrons are shifted from the electron donor moiety to the electron acceptor unit implying that the single excited state of these molecules could be considered as the intramolecular charge transfer from donor to acceptor along through the  $\pi$ -conjugated skeleton.

In support of the assertion of charge transfer in Figure. 6.4 depicts the differential charge densities between the ground and excited state. The electron density difference map gives a visualization of electronic rearrangement for a transition, with red regions denoting an increasing of density and green regions representing a decreasing of density upon excitation. These plots have been generated using GaussView 3.0. As depicted in Figure. 6.4, the density decreasing (green) is mostly located on the donor and linker unit. This finding is consistent with a strong donor character of the *O*-coumarin, *N*-coumarin and *N,N*-dimethylaniline. On the other hand, the regions of density increment (red) look more localized on the acceptor moiety. This is expected to facilitate the charge separation of the dye sensitizer upon photoexcitation [45].

**Table 6.2** Summarizes the energies and character of frontier orbital of -CT3A, N-CT3A and PT3 calculated by B3LYP/6-31G (d,p)

Molecule	Molecular orbital	Molecular Energy (eV)	percentage composition		
			Donor	Linker	Acceptor
O-CT3A	LUMO	-2.80	7	58	36
	HOMO	-5.12	25	68	7
N-CT3A	LUMO	-2.82	7	58	36
	HOMO	-5.12	40	55	5
PT3A	LUMO	-2.69	2	60	38
	HOMO	-4.94	43	52	4



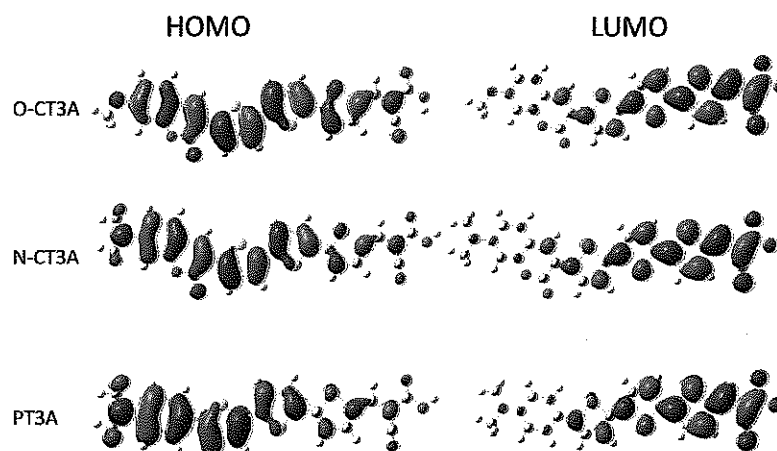


**Figure 6.3** Frontier molecular orbital of O-CT3A, N-CT3A and PT3A calculated by B3LYP/6-31G (d,p)

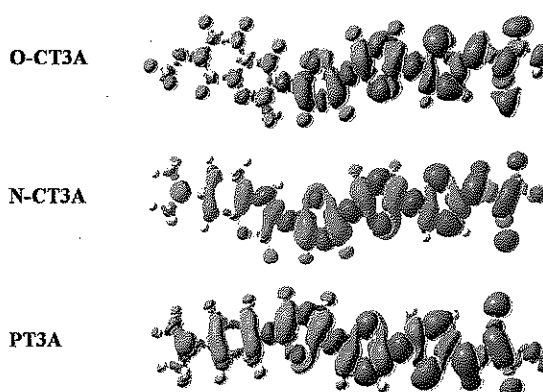


**Figure 6.4** The charge density difference of O-CT3A, N-CT3A and PT3A calculated by B3LYP/6-31G (d,p). The contour thresholds for molecular orbitals and density differences are 0.02 and 0.0004 a.u., respectively. The yellow and blue colors indicate a decrease and increase of charge densities, respectively.

### 6.3 Energy Gap

The energetic alignment of the HOMO and LUMO energy levels is crucial for an efficient operation of the dye in DSSCs. To ensure efficient electron injection from the excited dye into the conduction band of  $\text{TiO}_2$ . The LUMO level must be higher in energy than the conduction band edge. The HOMO level of the dye must be lower in energy than the redox

potential of the  $I/I_3^-$  redox couple for efficient regeneration of the dye cation after photoinduced electron injection into the  $TiO_2$  film. The calculated HOMO-LUMO energies follow the trends as found by electrochemical analysis and are listed in Table 6.3. The schematic energy levels of O-CT3A, N-CT3A and PT3A are shown in Figure. 6.5.

For comparison, dyes comprising the *N,N*-dimethylaniline group have significantly lower HOMO-LUMO gaps. The LUMO of three dyes are more negative than the conduction band of  $TiO_2$ , indicating that the electron injection process from the excited dye molecule to  $TiO_2$  conduction band is energetically favorable. From the calculation results are worth noting that the HOMO energy level of PT3A is more positive than redox potential relative to O-CT3A and N-CT3A, indicative of the more significant driving force for the reduction of the oxidized dye. These findings denote that the *N,N*-dimethylaniline donor in PT3A dye could enhance the driving force for the reduction of the oxidized dye, thus making the device performance of PT3A superior to that of O-CT3A and N-CT3A.

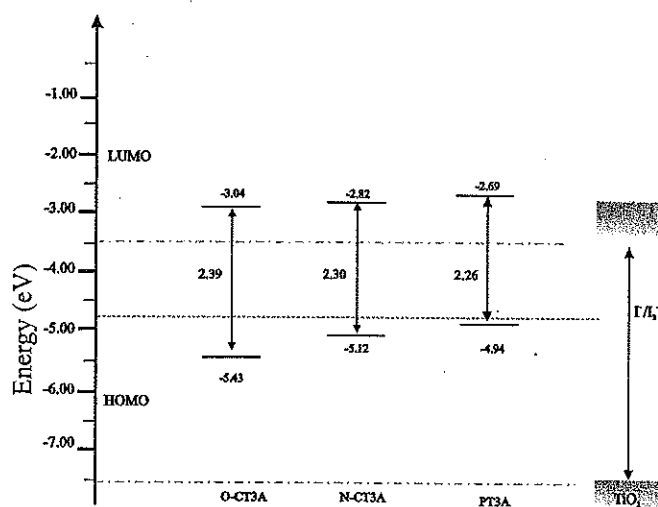


Figure 6.5 Frontier molecular orbital of O-CT3A, N-CT3A and PT3A calculated by B3LYP/6-31G (d,p)

**Table 6.3** The calculated HOMO-LUMO energy gap of O-CT3A, N-CT3A and PT3A

Molecule	$\Delta_{\text{HOMO-LUMO}}^a$ (eV)	Expt. <sup>b</sup> (eV)
O-CT3A	2.31	2.38
N-CT3A	2.30	2.15
PT3A	2.26	2.01

<sup>a</sup>Calculations are performed with B3LYP/6-31G (d,p) in gas phase.

<sup>b</sup>Experimental  $\Delta_{\text{HOMO-LUMO}}$  estimated from the onset of the absorption spectra  $E_g$  (eV) =  $1240/\lambda_{\text{onset}}$  in dilute  $\text{CH}_2\text{Cl}_2$  solution.

#### 6.4 Light Harvesting Efficiency

The UV-vis absorption spectra of all dyes are shown in Figure 6.6. The calculated maximum absorption wavelengths, oscillator strengths ( $f$ ), light harvesting efficiency (LHE), and electronic transition of O-CT3A, N-CT3A and PT3A are summarized in Table 6.4. All dyes absorb strongly in the region between 320 and 550 nm with a broad maximum between 430 and 520 nm. The strong absorption peak of O-CT3A, N-CT3A and PT3A at 605.7nm, 645.8 nm and 694.7 nm, that the absorption band could be attributed to the intramolecular charge transfer (ICT) between the donor and the acceptor, which is consistent with the assignment to the transition from the ground state ( $S_0$ ) to the first singlet excited state ( $S_1$ ). Notably, the absorption of PT3A red shift compared to O-CT3A and N-CT3A. Therefore, from the result assume that the introduction of *N,N*-dimethylaniline slightly increases the  $\pi$ -conjugation. Among these photosensitizers, due to strong electron donating ability of the diphenylamine unit, the PT3A dye with the *N,N*-dimethylaniline electron donor presents the longest maximum absorption wavelength which is an advantageous spectral property for light harvesting of the solar spectrum. Moreover, the influence of different electron donors affect to the light harvest capacity of the organic dye. The light-harvesting efficiency, LHE, related to the oscillator strength ( $f$ ) at a given wavelength is derived from the reciprocal absorption length via equation 57

$$\text{LHE} = 1 - 10^{-f} \quad (57)$$

The  $f$  is also in the same trend with the molar extinction coefficient, i.e. O-CT3A and N-CT3A have similar  $f$  and larger than that PT3A. The LHE factors are favorable for high electron injection efficiency from the excited states to the  $\text{TiO}_2$  conduction band and high photocurrent response. For PT3A dye, the least LHE factor ( $< 0.9263$ ) might affect to the light harvesting electron injection efficiency from the excited state to the conduction band of  $\text{TiO}_2$ .

From these results, PT3A has extended the absorption range into the near-IR region. However the light harvesting efficiency of PT3A dye is smaller than those of O-CT3A and N-CT3A, therefore the decreasing LHE parameter might affect to lower energy conversion efficiency of DSCs applications. We can conclude that N-CT3A is expected to be a promising dye with desirable energetic and spectroscopic parameters in DSCs field [46].

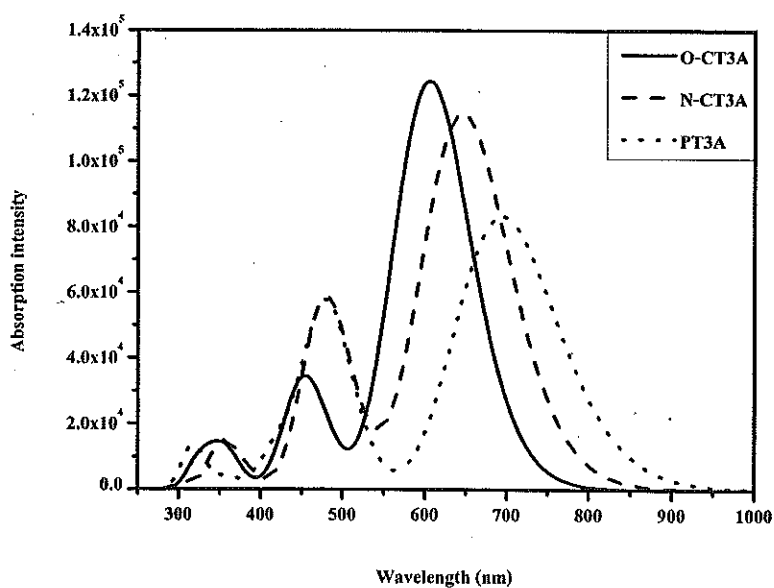


Figure 6.6 Calculated absorption spectra of O-CT3A, N-CT3A and PT3A by B3LYP/6-31G (d,p)

**Table 6.4** The excitation energies, oscillator strengths and molecular compositions for the 2 lowest states of O-CT3A, N-CT3A and PT3A by TD-B3LYP/6-31G (d,p)

Molecules	State	Excitation energy (eV, nm)	Oscillator strength (f)	light harvesting efficiency (LHE)	Assignment	Character
O-CT3A	$S_0 \rightarrow S_1$	2.05 (605.7)	1.7186	0.9809	$H \rightarrow L$ (85%)	$CT, \pi-\pi^*$
	$S_0 \rightarrow S_2$	2.73 (454.9)	0.4716		$H \rightarrow L+1$ (68%), $H-1 \rightarrow L$ (27%)	$CT, \pi-\pi^*$
N-CT3A	$S_0 \rightarrow S_1$	1.92 (645.8)	1.5817	0.9738	$H \rightarrow L$ (88%)	CT
	$S_0 \rightarrow S_2$	2.57 (481.5)	0.7794		$H-1 \rightarrow L$ (54%), $H \rightarrow L+1$ (40%)	$CT, \pi-\pi^*$
PT3A	$S_0 \rightarrow S_1$	1.78 (694.7)	1.1477	0.9288	$H \rightarrow L$ (100%)	CT
	$S_0 \rightarrow S_2$	2.58 (480.6)	0.7822		$H-1 \rightarrow L$ (89%), $H \rightarrow L+1$ (10%)	$CT, \pi-\pi^*$

## 6.5 $TiO_2$ adsorption

To gain insight into the electron injection capability of dyes, the adsorption of dyes on the  $(TiO_2)_{38}$  cluster was performed with DFT calculations using DMol<sub>3</sub> program [57] in Materials Studio version 5.5. The structure of  $(TiO_2)_{38}$  was comprised of 38  $TiO_2$  units which modeled a  $TiO_2$  nanoparticle, as in Jungsuttiwong's report. The  $(TiO_2)_{38}$  configuration was fully optimized using the generalized gradient-corrected approximation (GGA) method. The Perdew-Burke-Ernzerhof (PBE) [48] functional was used to account exchange-correlation effects with DNP basis set. The core electron was treated with DFT-semicore Pseudopotentials (DSPPs) [49]. After optimization, the adsorption energies ( $E_{ads}$ ) of dyes on the  $(TiO_2)_{38}$  cluster were obtained using the equation 58

$$E_{ads} = E_{dye} + E_{TiO_2} - E_{dye + TiO_2} \quad (58)$$

where  $E_{\text{dye}}$  was the total energy of isolated dye,  $E_{\text{TiO}_2}$  was the total energy of  $(\text{TiO}_2)_{38}$  cluster, and  $E_{\text{dye} + \text{TiO}_2}$  was the total energy of dye- $(\text{TiO}_2)_{38}$  complex. Following the above expression, the positive value of  $E_{\text{ads}}$  indicated a stable adsorption [50].

The optimized structures of dye- $\text{TiO}_2$  adsorptions are shown in Figure 6.7 and the important optimized bond length and adsorption energy ( $E_{\text{ads}}$ ) are listed in Table 6.2. The bond distances between 5c-Ti and O atom of dyes were calculated to be 1.97 Å and 2.19 Å for O-CT3A, 2.24 Å and 2.23 Å for N-CT3A, and 2.03 Å and 2.36 Å for PT3A. The adsorption energy ( $E_{\text{ads}}$ ) was calculated to be 19.23 kcal/mol, 20.43 kcal/mol and 23.45 kcal/mol for O-CT3A, N-CT3A and PT3A respectively. This suggests a slightly stronger binding of the dye complex. This could be a contributing factor to the better performance of O-CT3A, N-CT3A and PT3A.

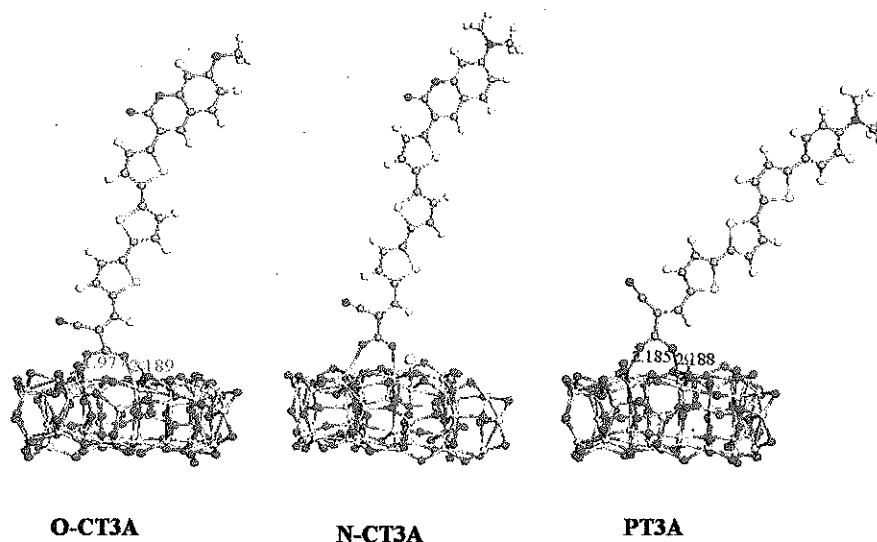


**Figure 6.7** Structure of O-CT3A, N-CT3A and PT3A adsorbed on  $(\text{TiO}_2)_{38}$  surface by Dmol<sup>3</sup> calculation

**Table 6.5** Selected bond length (Å) and adsorption energy (kcal/mol) of O-CT3A, N-CT3A and PT3A complex calculated by Dmol<sup>3</sup> calculation

Dyes	Ti-O1	Ti-O2	E <sub>ads</sub>
			(kcal/mol)
O-CT3A	1.97	2.19	19.23
N-CT3A	2.24	2.23	20.43
PT3A	2.18	2.19	23.45

## REFERENCES



## REFERENCES

- [1] B. Oregan and M. Grätzel. "A low-cost, high-efficiency solar cell based on dye-sensitized colloidal  $\text{TiO}_2$  films", Nature. 353: 737-740, 1991.
- [2] Q. S. Yu and et al. "An extremely high molar extinction coefficient ruthenium sensitizer in dye-sensitized solar cells: the effects of  $\pi$ -conjugation extension", The Journal of Physical Chemistry C. 113: 14559-14566, 2009.
- [3] T. W. Hamann and et al. "Advancing beyond current generation dye-sensitized solar cells", Energy & Environmental Science. 1: 66-78, 2008.
- [4] N. Martsinovich and A. Troisi. "Theoretical studies of dye-sensitized solar cells: from electronic structure to elementary processes", Energy & Environmental Science. 4: 4473-4495, 2011.
- [5] M. Grätzel. "Recent advances in sensitized mesoscopic solar cells", Accounts of Chemical Research. 42: 1788-1798, 2009.
- [6] C. Zhang and et al. "DFT and TDDFT study on structure and properties of organic dye sensitizer TA-St-CA", Current Applied Physics. 10: 77-83, 2009.
- [7] M. Grätzel. "Dye-sensitized solar cells", Journal of Photochemistry and Photobiology C: Photochemistry Reviews. 4: 145-153, 2003.
- [8] A. Hagfeldt and et al. "Dye-sensitized solar cells", Chemical Reviews. 110: 6595-6663, 2010.
- [9] F. De Angelis and et al. "Time-Dependent Density Functional Theory investigations on the excited states of Ru (II)-dye-sensitized  $\text{TiO}_2$  nanoparticles: the role of sensitizer protonation", Journal of the American Chemical Society. 129: 14156-14157, 2007.
- [10] M. Grätzel. "Conversion of sunlight to electric power by nanocrystalline dye-sensitized solar cells", Journal of Photochemistry and Photobiology A: Chemistry. 164: 3-14, 2004.
- [11] R. K. Kanaparthi, J. Kandhadi and L. Giribabu. "Metal-free organic dyes for dye sensitized solar cells: recent advances", Tetrahedron. 68: 8383-8393, 2012.

## REFERENCES (CONTINUED)

- [12] A. Mishra, M. Fischer and P. Bauerle. "Metal-free organic dyes for dye-sensitized solar cells: from structure: property relationships to design rules", Angewandte Chemie International Edition. 48: 2474-2499, 2009.
- [13] J. Preat and et al. "Enhanced efficiency of organic dye-sensitized solar cells: triphenylamine derivatives", The Journal of Physical Chemistry C. 113: 16821-16833, 2009.
- [14] H. Tian and et al. "Effect of different electron donating groups on the performance of dye-sensitized solar cells", Dyes and Pigments. 84: 62-68, 2010.
- [15] K. Hara and et al. "Molecular design of coumarin dyes for efficient dye-sensitized solar cells", The Journal of Physical Chemistry B. 107: 597-606, 2002.
- [16] T. Kitamura and et al. "Phenyl-Conjugated oligoene sensitizers for  $\text{TiO}_2$  solar cells", Chemistry of Materials. 16:1806-1812, 2004.
- [17] K. Hara and et al. "Oligothiophene-containing coumarin dyes for efficient dye-sensitized solar cells", The Journal of Physical Chemistry B. 109: 15476-15482, 2005.
- [18] S. Armas and et al. "Coumarin derivatives for dye sensitized solar cells: a TDDFT study", Physical Chemistry Chemical Physics. 14: 225-233, 2012.
- [19] W. Xu and et al. "Influence of acceptor moiety in triphenylamine-based dyes on the properties of dye-sensitized solar cells", Journal of Power Sources. 183: 792-798, 2008.
- [20] J. Xu and et al. "The effect of anchoring group number on molecular structures and absorption spectra of triphenylamine sensitizers : a computational study", Journal of Molecular Modeling. 18: 1767-1777, 2012.
- [21] J. Pei and et al. "Triphenylamine-based organic dye containing the diphenylvinyl and rhodanine-3-acetic acid moieties for efficient dye-sensitized solar cells", Journal of Power Sources. 187: 620-626, 2009.
- [22] Z. Wan and et al. "Influence of different arylamine electron donors in organic sensitizers for dye-sensitized solar cells", Dyes and Pigments. 95: 41-46, 2012.

## REFERENCES (CONTINUED)

- [23] H. Ham and Y. Kim. "Theoretical study of indoline dyes for dye-sensitized solar cells", Thin Solid Films. 518: 6558-6563, 2010.
- [24] H. Tian and et al. "Effect of different electron donating groups on the performance of dye-sensitized solar cells", Dyes and Pigments. 84: 62-68, 2010.
- [25] X. Cheng and et al. "Organic dyes incorporating the cyclopentadithiophene moiety for efficient dye-sensitized solar cells", Dyes and Pigments. 92: 1292-1299, 2012.
- [26] S. Singh and et al. "New triphenylamine-based organic dyes with different numbers of anchoring groups for dye-sensitized solar cells", The Journal of Physical Chemistry C. 116: 5941-5950, 2012.
- [27] C. Winder and N. Sariciftci. "Low band gap polymers for photon harvesting in bulk heterojunction solar cells", Journal of Materials Chemistry. 14: 1077-1086, 2004.
- [28] G. Zerza and et al. "Photoinduced charge transfer between Tetracyan O-Anthraquin O-Dimethane derivatives and conjugated polymers for photovoltaics", The Journal of Physical Chemistry A. 104: 8315-8322, 2000.
- [29] R. He and et al. "Quantum chemical study on excited states and charge transfer of oxazole [4,5-b]-pyridine derivatives", Science China Chemistry. 55: 1-11, 2012.
- [30] W. Nau "Modern molecular photochemistry of organic molecules", Chem Phys Chem. 12: 2496-2497, 2011.
- [31] J. M. Standard and B. Clark. "The Franck-Condon principle and Condon parabolas in a physical chemistry or quantum physics course", Journal of Chemical Education. 76: 1363-1366, 1999.
- [32] R. Chen and et al. "Effect of tetrahydroquinoline dyes structure on the performance of organic dye-sensitized solar cells", Chemistry of Materials. 19: 4007-4015, 2007.
- [33] J. Chang and et al. "Role of hydroxyl groups in the  $\text{NH}_x$  ( $x = 1-3$ ) adsorption on the  $\text{TiO}_2$  anatase (101) surface determined by a first-principles study", Langmuir. 26: 4813-4821, 2010.

## REFERENCES (CONTINUED)

- [34] Z. Cai-Rong and et al. "DFT and TDDFT study on organic dye sensitizers D5, DST and DSS for solar cells", Journal of Molecular Structure: THEOCHEM. 899: 86-93, 2009.
- [35] K. Srinivas and et al. "Novel 1,3,4-oxadiazole derivatives as efficient sensitizers for dye-sensitized solar cells: A combined experimental and computational study", Synthetic Metals. 161: 1671-1681, 2011.
- [36] Y. Kurashige and et al. "Theoretical investigation of the excited states of coumarin dyes for dye-sensitized solar cells", The Journal of Physical Chemistry A. 111: 5544-5548, 2007.
- [37] K. D. Seo and et al. "Coumarin dyes containing low-band-gap chromophores for dye sensitised solar cells", Dyes and Pigments. 90: 304-310, 2011.
- [38] J. Preat, D. Jacquemin and E. A. Perpète. "Theoretical investigations of the UV spectra of coumarin derivatives", Chemical Physics Letters. 415: 20-24, 2005.
- [39] S. Agrawal. and et al. "First-principles study of the excited-state properties of coumarin-derived dyes in dye-sensitized solar cells", Journal of Materials Chemistry. 21: 11101-11108, 2011.
- [40] S. Li and et al. "Novel organic dyes for efficient dye-sensitized solar cells", Chemical Communications. 26: 2792-2794, 2006.
- [41] Z. Wan and et al. "Triphenylamine-based starburst dyes with carbazole and phenothiazine antennas for dye-sensitized solar cells", Journal of Power Sources. 199: 426-431, 2012.
- [42] N. Koumura and et al. "Alkyl-functionalized organic dyes for efficient molecular photovoltaics", Journal of the American Chemical Society. 128: 14256-14257, 2006.
- [43] Z. Wang and et al. "Hexylthiophene-functionalized carbazole dyes for efficient molecular photovoltaics: tuning of solar-cell performance by structural modification", Chemistry of Materials. 20: 3993-4003, 2008.

## REFERENCES (CONTINUED)

- [44] S. G. Awuah and et al. "New pyran dyes for dye-sensitized solar cells", Journal of photochemistry and Photobiology A: Chemistry. 224: 116-122, 2011.
- [45] J Zhang. and et al. "How to design proper  $\pi$ - spacer order of the D- $\pi$ A dyes for DSSCs A density functional response", Dyes and Pigments. 95: 313-21, 2012.
- [46] W. Fan., D. Tan. and W. Deng. "Acene-Modified Triphenylamine Dyes for Dye-Sensitized Solar Cells: A Computational Study", Physical chemistry and chemical physics. 13: 2051-2060, 2012.
- [47] T. Yakhanthip and et al. "Theoretical investigation of novel carbazole-fluorene based D- $\pi$ -A conjugated organic dyes as dye-sensitizer in dye-sensitized solar cells (DSCs)", Journal of Computational Chemistry. 32: 1568-1576, 2011.
- [48] J.P. Perdew., K. Burke. and M. Ernzerhof. "Generalized Gradient Approximation Made Simple", Physical Review Letters. 77: 3865-3868, 1996.
- [49] B. Delley. "Hardness conserving semilocal pseudopotentials", Physical Review B. 66: 155125-155133, 2002.
- [50] S. Jungsuttiwong and et. al. "The effect of conjugated spacer on novel carbazole derivatives for dye-sensitized solar cells: Density functional theory/time-dependent density functional theory study", Journal of Computational Chemistry. 33: 1517-152, 2012.

## APPENDIX

**ROUTE KEYWORDS FOR CALCULATION IN THESIS  
ON GAUSSIAN03 PROGRAM**

**Geometry optimization calculation**

Ground state:

# opt b3lyp/6-31G(d,p)

Excited state:

# opt cis=(direct, root=1)/6-31G(d,p)

**Excitation energy, absorption wavelength and emission wavelength calculation**

TDDFT:

# td=(nstates=10,singlet) b3lyp/6-31G(d,p)

**Solvent**

# opt b3lyp/6-31G (d,p) scrf=(cpcm,solvent=dichloromethane)

**Density of state (DOS)**

# rb3lyp/6-31G (d,p) pop=full iop(3/33=1,3/36=-1)

### HOMO-LUMO GAPS CALCULATION

1. Open .log/.out file with Notepad Program
2. Find the last Alpha occ. and the first Alpha virt. Eigenvalues

Alpha occ. eigenvalues --	-0.42644	-0.42314	-0.41762	-0.40863	-0.40356
Alpha occ. eigenvalues --	-0.40038	-0.39824	-0.39525	-0.39187	-0.38447
Alpha occ. eigenvalues --	-0.38175	-0.37516	-0.37285	-0.36965	-0.36487
Alpha occ. eigenvalues --	-0.35988	-0.34674	-0.34119	-0.33127	-0.32607
Alpha occ. eigenvalues --	-0.31808	-0.29770	-0.28330	-0.27222	-0.26307
Alpha occ. eigenvalues --	-0.25998	-0.25557	-0.21951	-0.18295	
Alpha virt. eigenvalues --	-0.09996	-0.04689	-0.00635	-0.00203	0.00355
Alpha virt. eigenvalues --	0.01831	0.02010	0.02792	0.04080	0.06370
Alpha virt. eigenvalues --	0.07105	0.08593	0.09099	0.09306	0.10318
Alpha virt. eigenvalues --	0.10883	0.12021	0.12812	0.13362	0.14487
Alpha virt. eigenvalues --	0.15582	0.15774	0.16176	0.16394	0.16597

3. Calculate  $\Delta_{H-L}$  using below equation

$$\begin{aligned}
 \Delta_{H-L} &= \text{HOMO} - \text{LUMO} \\
 &= \text{Alpha virt. eigenvalues} - \text{Alpha occ. eigenvalues} \\
 &= -0.09996 - (-0.18295) \\
 &= 0.08299 \text{ a.u.} \\
 &= 0.08299 \times 27.211383 \approx 2.25 \text{ eV}
 \end{aligned}$$



## PLUBLICATIONS AND PRESENTATIONS BY AUTHOR

### Proceeding

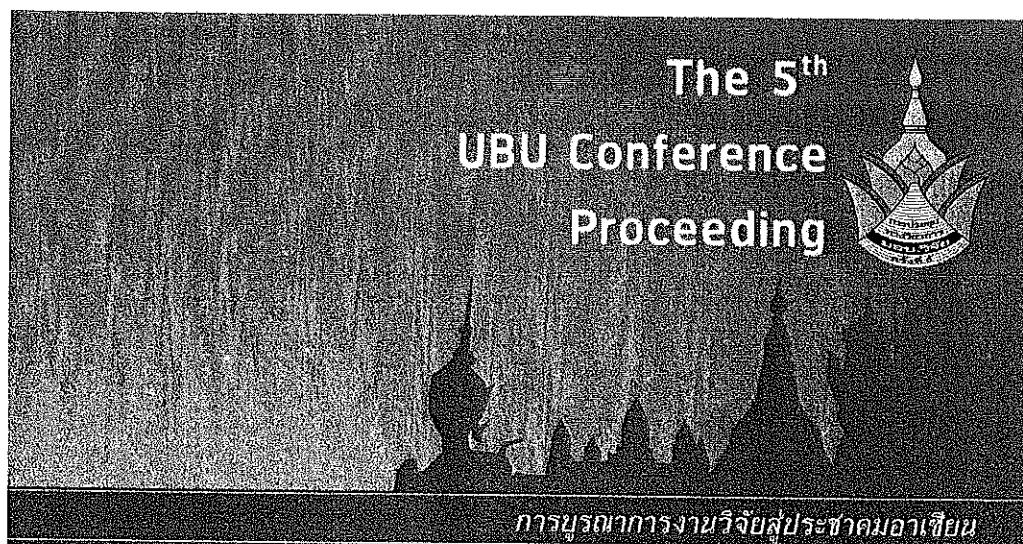
R. Rattanawan, S. Potjanasopa, T. Sudyoadsuk, T. Keawin, S. Saengsuwan, V. Promarak and S. Jungsuttiwong in the proceeding of UBRC5, Theoretical investigation of conformation and energies of Coumarine dye for Dye-sensitize Solar Cells, August 4-5, 2011, Sunee grand hotel and Convention Center, Ubon Ratchatani Thailand.

R. Rattanawan, D. Muenmart, S. Potjanasopa, T. Sudyoadsuk, T. Keawin, S. Saengsuwan, V. Promarak and S. Jungsuttiwong in the proceeding of PACCON2012 "DFT AND TDDFT study on conformation and energies studies of difference donor of organic dye for dye sensitized solar cells.", Pure and Applied Chemistry International Conference 2012 (PACCON2012), January 11-13, 2012, The Empress Hotel Chiang Mai, Chiang Mai, Thailand.

### Presentations

R. Rattanawan, S. Potjanasopa, T. Sudyoadsuk, T. Keawin, S. Saengsuwan, V. Promarak and S. Jungsuttiwong in the proceeding of UBRC5, Theoretical investigation of conformation and energies of Coumarine dye for Dye-sensitize Solar Cells, August 4-5, 2011, Sunee grand hotel and Convention Center, Ubon Ratchatani Thailand. (Oral presentation)

R. Rattanawan, D. Muenmart, S. Potjanasopa, T. Sudyoadsuk, T. Keawin, S. Saengsuwan, V. Promarak and S. Jungsuttiwong in the proceeding of PACCON2012 "DFT AND TDDFT study on conformation and energies studies of difference donor of organic dye for dye sensitized solar cells.", Pure and Applied Chemistry International Conference 2012 (PACCON2012), January 11-13, 2012, The Empress Hotel Chiang Mai, Chiang Mai, Thailand. (Poster presentation)



RESEARCH  
INTEGRATION  
*for* **A**SEAN  
COMMUNITY

ประชุมวิชาการ มอบ.วิจัย ครั้งที่ 5

เอกสารสืบเนื่องจากการประชุม

สาขา วิทยาศาสตร์และเทคโนโลยี

4 - 5 สิงหาคม 2554

ณ โรงแรมสุโขทัย แกรนด์ แอนด์ คอนเวนชั่น เซ็นเตอร์ จังหวัดอุบลราชธานี

การศึกษาโครงสร้างและพลังงานของสารสีย้อมไวแสงอินทรีย์คูมาริน  
เพื่อใช้ในเซลล์แสงอาทิตย์ชนิดสีย้อมไวแสง

Theoretical Investigation Of Conformation And Energies  
Of Coumarine Dye For Dye-Sensitize Solar Cells.

ธัญวดี รัตนวัน สิริพัทธา พจนโสภาค พริศศักดิ์ สุดขจรสุข ทินกร แก้วอินทร์  
สายันต์ แสงสุวรรณ วณิช พรมอารักษ์ และ ศิวพร จิระสุทธีวงศ์  
ศูนย์อิเล็กทรอนิกส์สารอินทรีย์และพลังงานทดแทน คณะวิทยาศาสตร์ มหาวิทยาลัยอุบลราชธานี  
Email: jslipom\_2000@yahoo.com

บทคัดย่อ

งานวิจัยนี้ได้ศึกษาสมบัติทางโครงสร้างและพลังงานของสีย้อมไวแสงอินทรีย์ที่ใช้เซลล์แสงอาทิตย์ชนิดสีย้อมไวแสง โดยอาศัยระเบียบวิธี DFT ที่ระดับ B3LYP/6-31G (d,p) ทำการคำนวณโครงสร้างที่สถานะพื้นและใช้ระเบียบวิธี TD-DFT ที่ระดับเดียวกันทำการคำนวณค่าพลังงานแถบช่องว่าง ( $E_{gap}$ ) และค่าการดูดกลืนแสงสูงสุด ซึ่งการคำนวณทั้งหมดใช้โปรแกรม Gaussian 03 ผลการคำนวณพบว่า โครงสร้างที่สถานะพื้น มีการจัดเรียงตัวของโมเลกุลในลักษณะที่แบนราบ ซึ่งส่งผลต่อการส่งผ่านอิเล็กตรอนจากหมู่ให้อิเล็กตรอนไปยังหมู่รับอิเล็กตรอน นอกจากนี้ ได้ทำการเปรียบเทียบค่าพลังงานแถบช่องว่างที่ได้จากการคำนวณกับค่าที่ได้จากการทดลอง พบว่ามีแนวโน้มที่สอดคล้องกันคือ ค่าพลังงานแสดงการเกิดเรดชิฟต์เมื่อความยาวคอนจูเกตเพิ่มขึ้น

คำสำคัญ : โมเลกุลสีย้อมไวแสงอินทรีย์ ดีเอฟที อนุพันธ์ของคูมาริน

Abstract

The geometries and energies of organic dye sensitizers for dye sensitize solar cells were investigated by using density functional theory (DFT). The ground state structures of organic dyes were optimized at B3LYP/6-31G (d,p) level, as implement in Gaussian 03 program. The first excitation energies ( $E_{gap}$ ) and maximal absorption wavelengths of organic dyes were performed by time-dependent density functional theory (TD-DFT) at the same basis set. The calculated results show that the ICT character involves primarily the promotion of electron from the HOMO to LUMO. The maximum absorption wavelength of dye sensitizers are in good agreement with the experimental data. Excitation energies are red - shifted with increasing of the conjugation lengths.

Keywords : organic dye sensitizers, DFT, Coumarin derivatives.

บทนำ

เซลล์แสงอาทิตย์ชนิดสีย้อมไวแสง คือเซลล์แสงอาทิตย์ชนิดหนึ่งซึ่งมีหลักการทำงานที่อาศัยกลไกทางปฏิกิริยาไฟฟ้าเคมีที่คล้ายคลึงกับการสังเคราะห์แสงของพืช ส่วนประกอบของเซลล์แสงอาทิตย์ชนิดสีย้อมไวแสงจะประกอบด้วยส่วนประกอบหลักๆ คือ กระจกนำไฟฟ้า สารที่ใช้ทำอิเล็กโทรดซึ่งเคลือบอยู่บนผิวกระจก ตัวสีย้อม (Dye) ซึ่งเคลือบบริเวณผิวของสารอิเล็กโทรด และสารละลายอิเล็กโทรไลต์ โดยเมื่อแสงตกกระทบที่ตัวสีย้อม จะมีการถ่ายพลังงาน

จากแสงไปยังโมเลกุลของตัวสีย้อม เพื่อกระตุ้นให้อิเล็กตรอนเคลื่อนที่จากผิวด้านนอกเข้าไปยังอิเล็กโตรดด้านใน ส่งผ่านไปยังวงจรจนนำไปสู่การเกิดเป็นกระแสไฟฟ้าขึ้น

ในปี ค.ศ. 1991 O' Regan และ Grätzel (B. O' Regan and M. Grätzel, Nature 353 (1991) 737) ได้พัฒนาเซลล์แสงอาทิตย์ชนิดสีย้อมไวแสง ภายใต้แสงอาทิตย์เทียม ที่ AM 1.5 โดยใช้สีกานาโนไทเทเนียมไดออกไซด์ (nanocrystalline  $\text{TiO}_2$ ) ที่มีลักษณะพหุรูป (fractal) แทนฟิล์มบางเรียบ (flat thin film) เพื่อให้สีย้อมไวแสงกลุ่มสารประกอบเชิงซ้อนของโลหะรูทีเนียมกับลิแกนด์กลุ่มพิรีดีน (Ru-polypyridine complex) เซลล์แสงอาทิตย์ชนิดนี้ ได้ถูกพัฒนาให้มีประสิทธิภาพในการเปลี่ยนพลังงานแสงเป็นพลังงานไฟฟ้าได้ถึง 10% ในปี ค.ศ. 1993 โดยใช้สีย้อมไวแสง ที่เป็นสารประกอบเชิงซ้อนของ ruthenium-bipyridine แต่เนื่องจากสารประกอบเชิงซ้อนของโลหะรูทีเนียมนั้นมีข้อจำกัด คือ เป็นวัสดุที่มีราคาแพง กระบวนการสังเคราะห์ทำได้ยาก และเกิดแก๊สพิษ จึงมีการพัฒนาสีย้อมไวแสงชนิดใหม่ขึ้นมาทดแทนเซลล์แสงอาทิตย์ชนิดสีย้อมไวแสงที่เป็นสารประกอบเชิงซ้อนของโลหะรูทีเนียม นำมาสู่เซลล์แสงอาทิตย์ชนิดสีย้อมไวแสงที่เป็นสารอินทรีย์ไม่มีโลหะเป็นองค์ประกอบ ซึ่งโมเลกุลสารอินทรีย์เหล่านี้มักเป็นโมเลกุลที่มีการคอนจูเกตและมีความเป็นขั้วสูง ยกตัวอย่างเช่น สารกลุ่มเพอร์ลีน ทอร์โฟริน และอนุพันธ์ของคูมาริน ที่มีข้อได้เปรียบกว่า คือ สังเคราะห์ง่าย ต้นทุนต่ำ และเป็นมิตรต่อสิ่งแวดล้อม จึงถูกนำมาใช้เป็นสีย้อมไวแสงอย่างแพร่หลายในปัจจุบัน

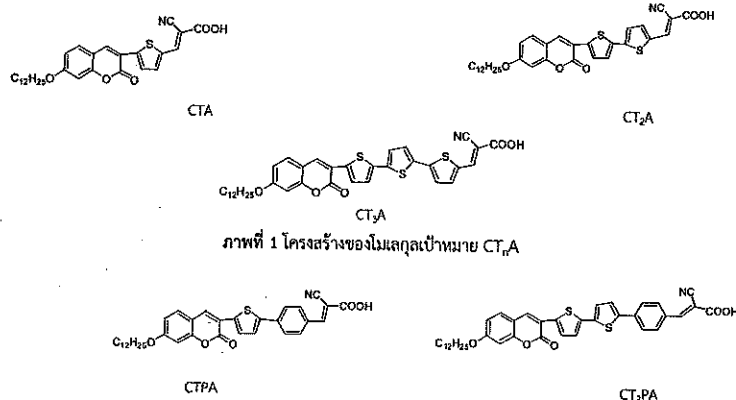
เพื่อให้เข้าถึงสมบัติในระดับโมเลกุลและกลไกสำคัญในการทำงานของเซลล์แสงอาทิตย์ชนิดสีย้อมไวแสง จึงได้มีการนำเอาการคำนวณทางเคมีควอนตัมโดยระเบียบวิธี Density functional theory (DFT) และ Time dependent density functional theory (TD-DFT) มาใช้ในการศึกษาสมบัติของโมเลกุล ข้อมูลที่ได้จากการศึกษาทางทฤษฎีนี้สามารถใช้ในการออกแบบ ทำนายแนวโน้มเกี่ยวกับสมบัติในการให้ และรับอิเล็กตรอน, สมบัติการดูดกลืนแสง, สมบัติการคายแสงและโครงสร้างของโมเลกุลที่เหมาะสมในการนำมาประกอบเป็นเซลล์แสงอาทิตย์ชนิดสีย้อมไวแสง ก่อนทำการทดลองในห้องปฏิบัติการจริง ส่งผลให้สามารถลดกระบวนการในการสังเคราะห์ นอกจากนี้ก็วิจัยสามารถลดค่าใช้จ่ายด้านสารเคมีและลดมลภาวะที่เกิดจากการสังเคราะห์ได้อีกด้วย ดังนั้นในการศึกษาวิจัยครั้งนี้ ผู้วิจัยมีความสนใจที่จะศึกษาการจำลองแบบโมเลกุล (Molecular modeling) และนำเอาระเบียบวิธีการคำนวณทางเคมีควอนตัมมาใช้ เพื่อศึกษาสมบัติทางโครงสร้าง สมบัติเชิงอิเล็กทรอนิกส์ และสมบัติเชิงแสงของโมเลกุลสีย้อมไวแสงที่เป็นสารอินทรีย์ที่มีโครงสร้างเป็นแบบ Donor- $\pi$ -Acceptor ซึ่งเป็นโมเลกุลสีย้อมไวแสงที่ทำหน้าที่ในการได้รับพลังงานแสงอาทิตย์ และส่งผ่านอิเล็กตรอนไปยังสารกึ่งตัวนำโลหะออกไซด์

#### อุปกรณ์และวิธีการ

คำนวณโครงสร้างโมเลกุลเพื่อทำนายสมบัติทางโครงสร้าง ระดับพลังงาน HOMO และ LUMO และสมบัติเชิงแสงของโมเลกุล โดยการปรับโครงสร้างที่สภาวะพื้นใช้ระเบียบวิธี Density functional theory (DFT) ซึ่งทฤษฎีกลศาสตร์ควอนตัมที่ใช้สำหรับคำนวณโครงสร้างทางอิเล็กทรอนิกส์ของระบบต่างๆ ทั้งที่เป็นอะตอมและโมเลกุล ในทฤษฎีนี้ สมบัติของอิเล็กตรอนสามารถอธิบายด้วยฟังก์ชันความหนาแน่นของอิเล็กตรอน ทำการคำนวณที่ระดับ B3LYP/6-31G(d,p) ซึ่งเป็นเบสซิสเซตที่ใช้ในการคำนวณ โดยเบสซิสเซตเหล่านี้คือชุดของฟังก์ชันทางคณิตศาสตร์ที่นำมารวมกันเพื่อสร้างเป็นออร์บิทัลเชิงอะตอม จากนั้นนำไปสร้างเป็นออร์บิทัลเชิงโมเลกุลและสร้างเป็นฟังก์ชันคลื่นรวมซึ่งอยู่ในสมการ Schrödinger จากนั้นนำโครงสร้างที่สภาวะพื้น มาคำนวณค่าพลังงานกระตุ้นด้วยระเบียบวิธี Time dependent-Density functional theory (TD-DFT) ที่ระดับ B3LYP/6-31G (d,p) ด้วยโปรแกรม Gaussian 03 จากนั้นทำการวิเคราะห์ผลของลักษณะโครงสร้างและพลังงานที่คำนวณได้ ทำนายสมบัติของโมเลกุล และเปรียบเทียบกับผลการทดลอง

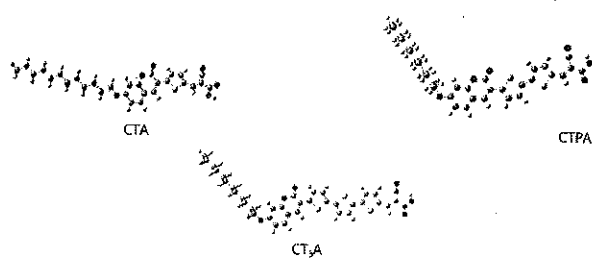
## ผลการวิจัย

โครงสร้างของโมเลกุลเป้าหมายประกอบด้วยโมเลกุลมีหมู่ให้อิเล็กตรอนคือ หนุคูมาริน (coumarin) มีหมู่เชื่อมต่อคือ หนุไทโอฟีน (thiophene) และหนุรับอิเล็กตรอนคือหนุไซยาโนอะคริลิก (cyanoacrylic acid) เรียกชื่อตามหนุฟังก์ชันคือ  $CT_nA$  ( $n=1-3$ ) ดังภาพที่ 1 และมีการแทนที่หนุไทโอฟีน ด้วยวงฟีนิล (phenyl) สำหรับโมเลกุล CTPA และ  $CT_2PA$  ดังแสดงได้ในภาพที่ 2 เนื่องจากโครงสร้างของโมเลกุลมีผลต่อประสิทธิภาพของโมเลกุลสีย้อมไวแสง งานวิจัยนี้จึงใช้ระเบียบวิธีทางเคมีควอนตัม เพื่อศึกษาเกี่ยวกับลักษณะทางโครงสร้างและค่าพลังงานของโมเลกุล

ภาพที่ 1 โครงสร้างของโมเลกุลเป้าหมาย  $CT_nA$ ภาพที่ 2 โครงสร้างของโมเลกุลเป้าหมาย คือ  $CT_nPA$ 

## 1. โครงสร้างที่เสถียรของโมเลกุลเป้าหมาย

จากการคำนวณทางเคมีควอนตัม เพื่อทำการปรับโครงสร้างที่เสถียรของโมเลกุลเป้าหมายทั้ง 5 โมเลกุล โดยใช้ระเบียบวิธี Density functional theory (DFT) ที่ระดับ B3LYP/6-31G (d, p) จะได้โครงสร้างที่เสถียรของโมเลกุลเป้าหมาย ดังแสดงได้ในภาพที่ 3 และภาพที่ 4 จากนั้นทำการวัดมุมไดฮีดรอล (dihedral angle) และความยาวพันธะ (bond length) ของแต่ละหนุที่เชื่อมต่อกัน ได้ผลดังแสดงในตารางที่ 1

ภาพที่ 3 โครงสร้างที่เสถียรของโมเลกุลเป้าหมาย คือ  $CT_nA$  คำนวณด้วยระเบียบวิธี DFT ที่ระดับ B3LYP/6-31G (d,p)



ภาพที่ 4 โครงสร้างที่เสถียรของโมเลกุลเป้าหมาย คือ CT<sub>2</sub>PA คำนวณด้วยระเบียบวิธี DFT ที่ระดับ B3LYP/6-31G (d, p)

ผลจากการวัดมุมระหว่างระนาบและความยาวพันธะเดี่ยวภายในโมเลกุล พบว่า มุมระหว่างระนาบของหมู่ให้อิเล็กตรอนและหมู่เชื่อมต่อ (C – T) ของโมเลกุล CTA, CT<sub>2</sub>A และ CT<sub>3</sub>A มีค่าเท่ากับ 22.17 , 1.33 และ 3.00 องศาตามลำดับ แสดงให้เห็นว่าการจัดเรียงตัวของโมเลกุล CTA เกิดการบิดหมุนมากที่สุด เนื่องจากมีหมู่เชื่อมต่อคือหมู่ไฮโดรเจนเพียงหมู่เดียว ซึ่งเมื่อเพิ่มจำนวนวงไฮโดรเจนในหมู่เชื่อมต่อ ทำให้โมเลกุลมีความแบนราบมากขึ้นอย่างมีนัยสำคัญซึ่งมีค่ามุมระหว่างระนาบเข้าใกล้ศูนย์นอกจากนั้น เมื่อพิจารณาขนาดของหมู่เชื่อมต่อของโมเลกุลทั้งสองชนิด (CT<sub>2</sub>A และ CT<sub>2</sub>PA) และทำการเปรียบเทียบ พบว่า มุมระหว่างระนาบของหมู่เชื่อมต่อ ของโมเลกุล CT<sub>2</sub>PA (T-P) มีค่าประมาณ 16-17 องศา ในขณะที่มุมระหว่างระนาบของหมู่เชื่อมต่อ ของโมเลกุล CT<sub>2</sub>A (Thi-Thi) มุมมีค่าเข้าใกล้ศูนย์ แสดงให้เห็นว่าการจัดเรียงตัวของโมเลกุลที่มีหมู่ไฮโดรเจนเป็นหมู่เชื่อมต่อมีความแบนราบมากกว่าโมเลกุลที่มีหมู่ไฮโดรเจน – ฟีนิลเป็นหมู่เชื่อมต่อ ดังนั้นถึงแม้ว่าวงฟีนิลเป็นวงอะโรมาติกที่มีคอนจูเกชันที่ดี แต่เมื่อนำมาเป็นหมู่เชื่อมต่อ จะส่งผลให้พันธะเดี่ยวที่เชื่อมต่อยาวขึ้นและเกิดการบิดหมุนได้ง่าย จึงไม่นิยมนำมาใช้เป็นหมู่เชื่อมต่อในโมเลกุล

ตารางที่ 1 คำนวณไดฮีดรอล (°) และความยาวพันธะ (Å) ของโมเลกุลเป้าหมาย คำนวณด้วยระเบียบวิธี

Density functional theory (DFT) ที่ระดับ B3LYP/6-31G (d, p)

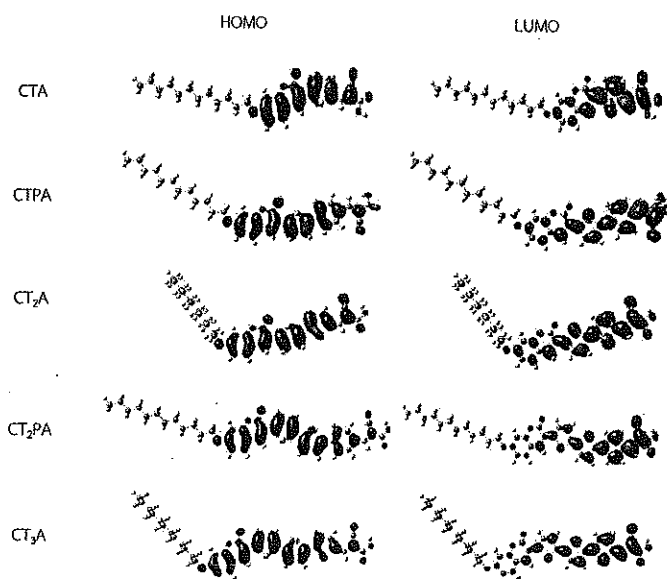
	C-T	Thi1-Thi2	Thi2-Thi3	T-A
CTA	22.17 (1.47)	-	-	1.42 (1.44)
CT <sub>2</sub> A	1.33 (1.46)	1.01 (1.44)	-	0.11 (1.42)
CT <sub>3</sub> A	3.00 (1.46)	2.73 (1.44)	3.61 (1.43)	0.17 (1.43)
	C-T	T-T	T-P	P-A
CTPA	5.01 (1.46)	-	16.79 (1.46)	2.97 (1.45)
CT <sub>2</sub> PA	2.34 (1.46)	0.71 (1.44)	16.77 (1.47)	0.78 (1.46)

C-T คือ ระบายระหว่างคาร์บอน – ไฮโดรเจน Thi1-Thi2 คือ ระบายระหว่างไฮโดรเจน1 และไฮโดรเจน 2  
Thi2-Thi3 คือ ระบายระหว่างไฮโดรเจน2 และไฮโดรเจน 3 T-A คือ ระบายระหว่างไฮโดรเจนและไนโตรเจนอะโรมาติก

## 2. แผนภาพระดับพลังงาน HOMO-LUMO

เมื่อทำการปรับโครงสร้างให้เสถียรที่สภาวะพื้นจากการคำนวณทางเคมีควอนตัมแล้ว จึงนำโครงสร้างที่เสถียรนี้ไปทำการแสดงแผนภาพระดับพลังงาน Highest occupied molecular orbital (HOMO) และ Lowest

unoccupied molecular orbital (LUMO) ด้วยโปรแกรม Gauss view ได้ผลดังแสดงในตารางที่ 2 และคำนวณเปอร์เซ็นต์การกระจายตัวของอิเล็กตรอนโดยใช้ระเบียบวิธี Density of state ผลที่ได้จากการคำนวณดังแสดงในตารางที่ 2



ภาพที่ 5 แผนภาพระดับพลังงาน HOMO และ LUMO ของโมเลกุลเป้าหมาย คำนวณด้วยระเบียบวิธี Density function theory (DFT) ที่ระดับ B3LYP/6-31G (d, p)

ตารางที่ 2 เปอร์เซ็นต์การกระจายตัวของอิเล็กตรอนที่ได้จากผล density of state คำนวณด้วยระเบียบวิธี Density functional theory (DFT) ที่ระดับ B3LYP/6-31G (d, p)

		Donor	linker	accepter
CTA	LUMO	26	31	43
	HOMO	58	30	12
CTPA	LUMO	17	41	42
	HOMO	38	55	6
CT <sub>2</sub> A	LUMO	18	47	35
	HOMO	30	58	12
CT <sub>2</sub> PA	LUMO	7	51	42
	HOMO	29	68	3
CT <sub>3</sub> A	LUMO	7	58	36
	HOMO	25	68	7

— ผลจากการคำนวณ พบว่าโครงสร้างของโมเลกุล ทั้ง 5 โมเลกุล ที่ระดับพลังงาน HOMO อิเล็กตรอนส่วนใหญ่กระจายตัวอยู่ที่หมู่ให้อิเล็กตรอนคือ หมู่คาร์บอนและหมู่เชื่อมต่อก็คือ หมู่ไฮดรอกซิลและหมู่ฟีนิล เมื่อถูกกระตุ้นไปที่ LUMO อิเล็กตรอนส่วนใหญ่อยู่ที่หมู่เชื่อมต่อ หมู่ไฮดรอกซิลและหมู่ฟีนิลรวมกันหมู่รับอิเล็กตรอนทั้งหมู่ไฮยาโนอะไครลิก ซึ่งแสดงให้เห็นว่าโมเลกุลมีการส่งผ่านอิเล็กตรอนได้ดี ตารางที่ 2 แสดงเปอร์เซ็นต์การกระจายตัวของอิเล็กตรอน ซึ่งมีค่าสอดคล้องกับแผนภาพการกระจายตัวของอิเล็กตรอนในภาพที่ 5 พบว่าที่ HOMO การกระจายตัวของอิเล็กตรอนส่วนใหญ่อยู่ที่หมู่ให้อิเล็กตรอนและหมู่เชื่อมต่อซึ่งมีค่าประมาณ 80-90% ในขณะที่ LUMO เปอร์เซ็นต์การกระจายตัวของอิเล็กตรอนที่หมู่รับอิเล็กตรอนมีค่าอยู่ในช่วง 35-45% แสดงให้เห็นว่าโมเลกุลมีการส่งผ่านอิเล็กตรอนจากระดับพลังงาน HOMO ไปยังระดับพลังงาน LUMO การทรานสิชันในลักษณะนี้เรียกว่า intramolecular charge transfer (ICT) ซึ่งเป็นการเคลื่อนที่ของอิเล็กตรอนจากหมู่ให้อิเล็กตรอนไปยังหมู่รับอิเล็กตรอน

### 3. คุณสมบัติการดูดกลืนแสง

เราสามารถคำนวณ คุณสมบัติทางอิเล็กทรอนิกส์ของโมเลกุลเป้าหมายโดยใช้ระเบียบวิธี TD-DFT ผลการคำนวณ ทำให้เราสามารถหาค่าพลังงานกระตุ้น (eV) ความยาวคลื่น (nm) Oscillator Strengths ( $f$ ) Composition in Terms of Molecular Orbital Contributions ได้ ดังแสดงในตารางที่ 3 และสเปกตรัมการดูดกลืนแสงที่ได้จากการคำนวณดังแสดงในภาพที่ 6 พบว่าความยาวคลื่นสูงสุดของโมเลกุล CTA, CTPA, CT<sub>2</sub>A, CT<sub>2</sub>PA และ CT<sub>3</sub>A ซึ่งมีค่าเท่ากับ 319.0, 477.6, 503.0, 548.4 และ 567.7 นาโนเมตร ตามลำดับ เป็นการทรานสิชันจาก HOMO → LUMO สามารถกล่าวได้ว่าทรานสิชันดังกล่าวเป็นแบบ intramolecular charge transfer (ICT)

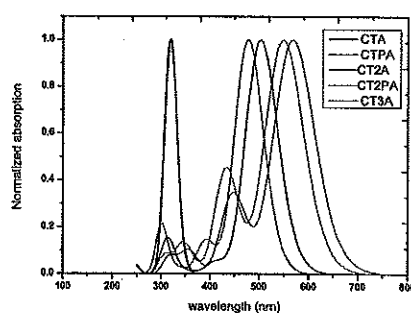
ตารางที่ 3 แสดงค่าพลังงาน (eV) ความยาวคลื่น (nm) Oscillator Strengths ( $f$ ) Composition in Terms of Molecular Orbital Contributions ที่ได้จากการคำนวณด้วยระเบียบวิธี TD-DFT

Molecules	Electronic transition	$\lambda_{max}$ (nm)	$f$	Main contribution H=HOMO, L=LUMO	$\lambda_{max}$ (nm) exp
CTA	S0→S1	319.0	1.4298	H-O→L+O (79%)	416
CTPA	S0→S1	477.6	1.4811	H-O→L+O (84%)	423
CT <sub>2</sub> A	S0→S1	503.0	1.6047	H-O→L+O (78%)	432
CT <sub>2</sub> PA	S0→S1	548.4	1.3925	H-O→L+O (86%)	425
CT <sub>3</sub> A	S0→S1	567.7	1.5452	H-O→L+O (82%)	439

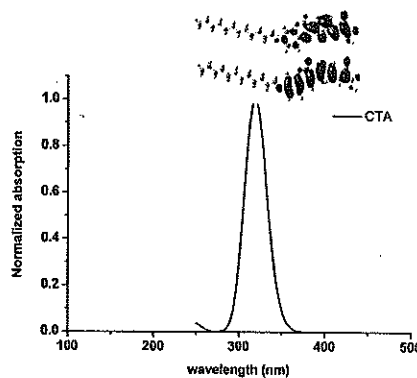
เมื่อเปรียบเทียบการสเปกตรัมการดูดกลืนแสงพบว่า สเปกตรัมการดูดกลืนแสงของโมเลกุล CT<sub>2</sub>A และ CT<sub>3</sub>A ที่มีหมู่ไฮดรอกซิลเป็นหมู่เชื่อมต่อ แสดงการเกิดเรดชิฟท์เมื่อเปรียบเทียบกับโมเลกุล CTPA และ CT<sub>2</sub>PA ที่มีหมู่ฟีนิลเป็นหมู่เชื่อมต่อ และยังพบว่าการเพิ่มจำนวนของไฮดรอกซิลของโมเลกุล CTA, CT<sub>2</sub>A, CT<sub>3</sub>A ยังส่งผลให้สเปกตรัมการดูดกลืนแสงเกิดเรดชิฟท์เช่นกันเนื่องจากการเพิ่มความยาวคอนจูเกชันของโมเลกุล นอกจากนี้เรายังสามารถทำนายลักษณะของการทรานสิชันจากสเปกตรัมการดูดกลืนแสงของโมเลกุลสีย้อมไวแสงได้ จากผลการคำนวณทาง TD-DFT ดังแสดงในตารางที่ 3 จากสเปกตรัมการดูดกลืนแสงของโมเลกุล CTA ดังแสดงในภาพที่ 6 พบว่า ที่ความยาวคลื่น 319 นาโนเมตร เป็นลักษณะการทรานสิชัน จาก HOMO → LUMO เมื่อพิจารณาจากแผนภาพการกระจายตัวของ



อิเล็กตรอน ดังพบว่าที่ระดับพลังงาน HOMO อิเล็กตรอนส่วนใหญ่กระจายตัวอยู่ที่หมู่อะโรมาติกซึ่งทำหน้าที่เป็นหมู่ให้อิเล็กตรอน คิดเป็นเปอร์เซ็นต์เท่ากับ 58 % และที่ระดับพลังงาน LUMO อิเล็กตรอนกระจายตัวอยู่ที่หมู่ไซยาโน - อะไโรลิก คิดเป็นเปอร์เซ็นต์ได้เท่ากับ 43% แสดงให้เห็นว่าโมเลกุลสีย้อมไวแสงมีการส่งผ่านอิเล็กตรอนจากหมู่ให้อิเล็กตรอนไปยังหมู่รับอิเล็กตรอน เป็นลักษณะของการทรานสิชันแบบ intramolecular charge transfer และพบว่าโมเลกุลสีย้อมไวแสงทั้ง 5 โมเลกุลมีลักษณะการทรานสิชันที่เหมือนกัน ซึ่งการทรานสิชันในลักษณะนี้ส่งผลดีต่อประสิทธิภาพของสีย้อมไวแสงเนื่องจากโมเลกุลของสีย้อมไวแสงสามารถส่งผ่านอิเล็กตรอนได้ดี



ภาพที่ 6 สเปกตรัมการดูดกลืนแสงของโมเลกุลเป้าหมาย ที่ได้จากการคำนวณด้วยเทคนิค TD-DFT



ภาพที่ 7 สเปกตรัมการดูดกลืนแสงของโมเลกุล CTA ที่ได้จากการคำนวณด้วยเทคนิค TD-DFT

#### 4. ค่าพลังงานแถบช่องว่าง ( $E_{gap}$ )

ค่าพลังงาน Excitation energy ของโมเลกุล สามารถคำนวณได้จากการใช้ระเบียบวิธี Time dependent-Density functional theory (TD-DFT) ซึ่งในงานวิจัยนี้ ทำการคำนวณที่ระดับ B3LYP/6-31G(d, p) ค่าพลังงานต่าง ๆ ที่ได้จากการคำนวณคือค่า excitation energy นั้นสามารถแสดงได้ดังตารางที่ 5 ผลการศึกษาพบว่า ค่าพลังงานแถบช่องว่างที่ได้จากการคำนวณด้วย ระเบียบวิธี TD-DFT ของโมเลกุล CTA, CTPA, CT<sub>2</sub>A, CT<sub>2</sub>PA, CT<sub>3</sub>A ดังแสดง

ในตาราง คือ 2.53 , 2.58 , 2.48 , 2.46 และ 2.38 eV ซึ่งมีแนวโน้มเช่นเดียวกับค่าพลังงานแถบช่องว่างที่ได้จากการทดลองคือ ค่าพลังงานแถบช่องว่างมีค่าลดลงเมื่อความยาวคอนจูเกตเพิ่มขึ้น

ตารางที่ 4 ค่าพลังงานที่ได้จากการคำนวณได้จากค่าความแตกต่างของระดับพลังงาน HOMO-LUMO ( $\Delta_{HL}$ ) คำนวณด้วยระเบียบวิธี TD-DFT//B3LYP/6-31G(d,p)

Molecules	HOMO(eV) <sup>a</sup>	LUMO(eV)	TD-DFT	Exp <sup>b</sup>
CTA	-5.85	-2.91	2.93	2.53
CTPA	-5.58	-2.78	2.60	2.58
CT <sub>2</sub> A	-5.52	-2.91	2.47	2.48
CT <sub>2</sub> PA	-5.36	-2.88	2.26	2.46
CT <sub>3</sub> A	-5.38	-2.99	2.18	2.38

<sup>a</sup> คำนวณด้วยระเบียบวิธี TD-DFT//B3LYP/6-31G(d,p)

<sup>b</sup> ค่าที่ได้จากการทดลอง [3]

#### สรุปและอภิปรายผล

จากการศึกษาทางทฤษฎีของสีย้อมไวแสงอินทรีย์ที่มีโครงสร้างของโมเลกุลเป้าหมายประกอบด้วย โมเลกุลหนูให้โอเลกตรอน คือ หมู่คาร์บอน มีหมู่เชื่อมต่อกับไฮโดรเจน และหมู่รับอิเล็กตรอนคือ โซยาโนอะไคลก เรียกว่าตามหมู่ฟังก์ชันคือ CT<sub>n</sub>A (n=1-3) และมีการแทนที่หมู่ไฮโดรเจน ด้วยวงฟีนิล สำหรับโมเลกุล CTPA และ CT<sub>2</sub>PA ซึ่งได้ศึกษาโครงสร้างที่เสถียรของโมเลกุล ระดับพลังงาน แผนภาพแสดงการกระจายอิเล็กตรอน และสมบัติทางแสงของโมเลกุลเป้าหมาย ผลการศึกษาพบโครงสร้างที่เสถียรซึ่งได้จากการปรับด้วยวิธี Density Functional Theory (DFT) ที่ระดับ B3LYP/6-31G (d,p) ของโมเลกุลเป้าหมายมีลักษณะการจัดเรียงตัวของโมเลกุลที่แบนราบ ที่ระดับพลังงาน HOMO มีการกระจายตัวของอิเล็กตรอนอยู่ที่หมู่คาร์บอนและไฮโดรเจน และที่ระดับพลังงาน LUMO มีการกระจายตัวของอิเล็กตรอนอยู่ที่หมู่โซยาโนอะไคลก ซึ่งมีการกระจายตัวของอิเล็กตรอนคล้ายกันทั้งห้าโมเลกุล ผลการคำนวณค่าพลังงานแถบช่องว่าง ( $E_g$ ) โดยการคำนวณผลต่างของระดับพลังงาน HOMO และ LUMO และผลจากการคำนวณด้วยระเบียบวิธีที่ 2 - คีเอฟที ซึ่งมีแนวโน้มของค่าพลังงานไปในทิศทางเดียวกันคือ ค่าพลังงานแถบช่องว่างมีค่าลดลงเมื่อความยาวคอนจูเกตเพิ่มขึ้น ผลของสมบัติการดูดกลืนแสงของโมเลกุล CTA , CTPA , CT<sub>2</sub>A , CT<sub>2</sub>PA , CT<sub>3</sub>A คือ 319.0 , 477.6 , 503.0 , 548.4 และ 567.7 nm ตามลำดับ ซึ่งเป็นการทรานส์ชันจาก HOMO→LUMO โดยมีลักษณะการทรานส์ชันแบบ intramolecular charge transfer (ICT) เปรียบเทียบค่าที่ได้จากการคำนวณ พบว่ามีความสอดคล้องกับผลการทดลองในห้องปฏิบัติการ จึงกล่าวได้ว่าระเบียบวิธีที่ 2 คีเอฟที สามารถนำมาประยุกต์ใช้ในการศึกษาคุณสมบัติของโมเลกุลสีย้อมไวแสงที่เป็นสารอินทรีย์ที่มีโครงสร้างเป็นแบบ Donor- $\pi$ -Acceptor ที่มีเพื่อนำไปประยุกต์ใช้เป็นโมเลกุลสีย้อมไวแสงในเซลล์แสงอาทิตย์ชนิดสีย้อมไวแสงได้

#### เอกสารอ้างอิง

- [1] วิเศษ พรหมอารักษ์ และคณะ. 2550 "เซลล์แสงอาทิตย์ชนิดสีย้อมไวแสง (Dye-Sensitized Solar Cells, DSSCs)". ว. มหาวิทยาลัยอุบลราชธานี(วิทย.) 9: 14-31.
- [2] O' Regan B., and Grätzel M., 1991. "A low-cost, high-efficiency solar cell based on dye-sensitized colloidal TiO<sub>2</sub> films" Nature 353: 737 - 740.

- [3] สิรินทรา พจนโสภา. 2554. การสังเคราะห์และพิสูจน์เอกลักษณ์ของสารอินทรีย์ สำหรับอุปกรณ์ออปโตอิเล็กทรอนิกส์. วิทยานิพนธ์ วิทยาศาสตร์มหาบัณฑิต: มหาวิทยาลัยอุบลราชธานี.
- [4] สิทธิศักดิ์ พลุมาตร. 2553. การศึกษาปัจจัยที่มีผลต่อค่าประสิทธิภาพของสีย้อมไวแสงอินทรีย์ชนิด D- $\pi$ -A ด้วยระเบียบวิธี DFT และ TD-DFT สำหรับเซลล์แสงอาทิตย์ชนิดสีย้อมไวแสง. วิทยานิพนธ์ วิทยาศาสตร์บัณฑิต: มหาวิทยาลัยอุบลราชธานี.

## DFT AND TDDFT STUDY ON CONFORMATION AND ENERGIES OF DIFFERENT DONOR OF ORGANIC DYE FOR DYE-SENSITIZED SOLAR CELLS

Rattanawalee Rattanawan, Duangratchaneekorn Muenmart, Sirintra Potjanasopa, Taweesak Sudyoasuk, Tinnagon Keawin, Sayant Saengsuwan, Vinich Promarak and Siriporn Jungsuttiwong\*

Center for Organic Electronics and Alternative Energy, Department of Chemistry, Faculty of Science,  
Ubon Ratchathani University, Warinckumrap, Ubon Ratchathani, 34190

\*Corresponding Author E-mail jsiriporn\_2000@yahoo.com, Tel. +66816922125

**Abstract:** In this study, the structures and energetic properties of coumarin derivatives forming D- $\pi$ -A system as the organic dye in dye-sensitized solar cells (DSCs) were investigated. The conjugated metal-free organic dye have been constructed based on different electron donor, *N*-coumarin and *O*-coumarin, connected to thiophene unit as linker and introduce cyanoacrylic acid as anchoring group. Density functional theory (DFT) and Time-dependent density functional theory (TDDFT) calculations have been performed on the organic sensitizers to gain insight into their structural, electronic, and optical properties. The ground state structure were optimized by DFT at the B3LYP/6-31G (d,p) level, as implemented in Gaussian 03 program. The first excitation energies ( $E_g$ ) and maximal absorption wavelengths of organic dyes were performed by TDDFT at the same optimized basis set. The optimized structure shows that the cyanoacrylic acid group is coplanar with respect to the thiophene unit, reflecting the strong conjugation across the thiophene-cyanoacrylic acid group. These results reveal that intramolecular charge transfer takes place through the donor coumarin to the linker and anchoring group. Furthermore, our results point out that the dye with *N*-coumarin as donor potentially improved performance of solar cell efficiency compared to *O*-coumarin dye. The good agreement between the experimental and TDDFT calculated absorption spectra of these sensitizers allowed us to provide a detail assessment of the main spectral feature of a series of dye sensitizers. These results provided useful information for the molecular engineering of efficient organic sensitizer.

### 1. Introduction

Dye-sensitized solar cell has been intensively studied as an alternative to the conventional solar cell because of its high photoelectric conversion efficiency, simple assemble technology and potential low cost. The ruthenium complexed photosensitizers such as the N3 and N719 compounds show a solar energy to electricity conversion efficiency of 10% on average. However, ruthenium complex dyes are not suitable for cost-effective and environmentally friendly photovoltaic system, because ruthenium is a rare and expensive metal, which limits the potentially wide application of these complexes. Due to this, metal free sensitizers are being investigated as alternative

sensitizers for dye-sensitized solar cells (DSC) applications.

Organic dyes have two major advantages in DSC. One is the high molar extinction coefficient for the organic dye due to its much higher oscillator strengths than those of metal complexes. Another advantage is that no noble metal like ruthenium is concerned in organic dye, this reduces the overall cost of the cell production. For further development of highly efficient dye in DSC the dye must be designed to absorb most of the radiation of sun light invisible and near-IR region to produce a large photocurrent response. In addition, suitable energy level and location of HOMO and LUMO orbitals of the dye are required to match the  $I/I^{3-}$  redox potential and conduction band edge level of the  $TiO_2$  semiconductor. Most of the reported highly efficient metal free dyes could be classified as electron donor acceptor  $\pi$ -conjugated (D- $\pi$ -A) compounds. These compounds have been found to possess photo induced intramolecular charge transfer (ICT) properties, which make these compounds have broad and intense absorption spectra in the visible region.

Among metal-free organic dyes, coumarin dyes have been subjected as strong candidates because of their good photoelectric conversion. The efficiency of DSC based on coumarin dyes are developed by Hara and co-workers in 2001 [1]. They increased  $\pi$ -conjugated system by insertion of a methine unit in C343 [2], which push the efficiency up to 5.6% (NKX-2311). Introducing of bulky substitution can prevent aggregation and yield the efficiency to 6.7% for NKX-2753 [3]. Recently, expanding  $\pi$ -conjugated system using thiophene moiety can reach the efficiency to 7.7% for NKX-2677 [4]. These works indicate that modifications of molecular structures are not limited and therefore higher efficiencies can be obtained.

Currently, molecular modeling techniques and especially quantum chemistry offer a competitive alternative for the interpretation of the experimental data. So the theoretical investigations of the physical properties of dye sensitizers are very important in order to disclose the relationship among the performance, structures and the properties, it is also helpful to design and synthesis novel dye sensitizers with higher performance.

Herein, we performed DFT/TDDFT calculation to provide a detailed characterization of the structural, electronic and optical properties of the organic sensitizers.

## 2. Materials and Methods

To gain insight into the factor responsible for the absorption spectral, we perform DFT and TDDFT calculations on the ground state of organic dyes. This computational procedure allows us to provide a detailed assignment of the excited state involved in the absorption process. The geometries in the gas phase were optimized by the DFT method using the B3LYP exchange – correlation function, with 6-31G (d,p) basis set in the Gaussian 03 program package [7]. Electronic populations of the HOMO and LUMO were calculated to show the position of localization of electron populations along with the calculated molecular orbital energy diagram. The electronic absorption spectra require calculation of the allowed excitation and oscillator strengths. These calculations were carried out using TDDFT with the same basis set and exchange – correlation functional.

## 3. Results and Discussion

In the investigation of D- $\pi$ -A systems, the molecular structure of the ICT states is an important point of discussion. Herein, theoretical calculations were performed to study the ground-state structures of coumarin dyes.

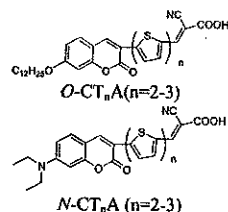


Figure 1. Sketch map of the structures of  $O-CT_nA$  and  $N-CT_nA$  ( $n=2-3$ )

### 3.1 Geometries of Ground State

The structures of the different donor moieties of the coumarin dyes used in this study are shown in Figure 1. We optimized the molecular structure of coumarin dyes in the gas phase and obtained the geometries as shown in Figure 2.

For dyes with the  $O$ -coumarin, The optimized structure shows that the cyanoacrylic acid group is coplanar with the thiophene, T-A dihedral angle are found to be  $0.02-0.21^\circ$ . Thus the strong conjugated effects are formed. This conjugation is very helpful for efficient transfer in conjugate chains. For the dyes with  $N$ -coumarin,  $N-CT_2A$  and  $N-CT_3A$ , it is noted that the optimized geometries of these compounds yield fully

planar geometry in the ground state. These results indicate that influence of different donor does not affect ground state structure of the dye.

Table 1. Selected important inter-ring distances in degree and bond length (in angstrom) of  $O-CT_nA$  and  $N-CT_nA$  calculated by B3LYP/6-31G (d,p) calculations

Molecules	C-T	T1-T2	T2-T3	T-A
$N-CT_2A$	2.56 (1.46)	0.64 (1.44)	- (1.44)	0.02 (1.43)
$N-CT_3A$	1.65 (1.46)	7.51 (1.44)	1.12 (1.44)	0.21 (1.43)
$O-CT_2A$	1.33 (1.46)	1.01 (1.44)	- (1.42)	0.11 (1.43)
$O-CT_3A$	3.00 (1.46)	2.73 (1.44)	3.61 (1.43)	0.17 (1.43)

Note: C is coumarin, T is thiophene, A is anchoring group

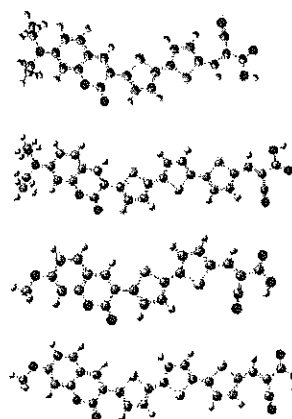


Figure 2. Optimized structures of  $N-CT_nA$  and  $O-CT_nA$  ( $n=2-3$ )

### 3.2 Frontier Molecular Orbital (FMO)

The frontier molecular orbitals of the coumarin dyes are shown in Fig. 3. The percentage composition of frontier molecular of  $N-CT_2A$ ,  $N-CT_3A$ ,  $O-CT_2A$  and  $O-CT_3A$  shown in Table 2. The highest occupied molecular orbital (HOMO) is a delocalized  $\pi$  orbital over the coumarin and thiophene unit, whereas, the lowest unoccupied molecular orbital (LUMO) is  $\pi^*$  orbital that localized in thiophene and cyanoacrylic

group. It is found that the percentage of comorin is about 25 – 50% while the percentage of contribution of cyanoacrylic is about 36 – 42%. The calculated results shows that the distribution of the HOMO and LUMO was separated in the compounds, indicating that the HOMO → LUMO transition can be considered as ICT transition. There were some electron transferred from the electron donor group to the electron acceptor group through chemical bonds. When the dye sensitizer was anchored to TiO<sub>2</sub>, the position of the LUMO close to the anchoring group enhance the orbital overlap with the titanium 3d orbitals and favors electron injection.

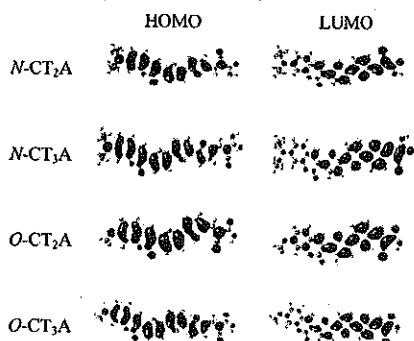


Figure 3. Molecular orbital surface of *N*-CT<sub>n</sub>A and *O*-CT<sub>n</sub>A (*n*=2-3)

Table 2. Energies and percentage composition of several frontier molecular orbitals of *N*-CT<sub>n</sub>A and *O*-CT<sub>n</sub>A (*n*=2-3)

Molecules		Donor	Thiophene	Acceptor
<i>N</i> -CT <sub>2</sub> A	LUMO	15	49	36
	HOMO	50	42	8
<i>N</i> -CT <sub>3</sub> A	LUMO	7	58	36
	HOMO	40	55	5
<i>O</i> -CT <sub>2</sub> A	LUMO	7	51	42
	HOMO	29	68	3
<i>O</i> -CT <sub>3</sub> A	LUMO	7	58	36
	HOMO	25	68	7

### 3.3 The lowest excitation energies ( $\Delta E_{\text{HOMO-LUMO}}$ )

Highly efficient DSCs require that the LUMO level of the dye molecules should be more negative than the conduction band edge of TiO<sub>2</sub> ( $E_{\text{cb}}$ ) to ensure an effective electron injection from the dye molecules to the conduction band of the TiO<sub>2</sub> film and the HOMO level of the dye should be more positive than the redox potential of  $\text{I}^-/\text{I}^{\cdot-}$  to ensure the regeneration of dye molecules.

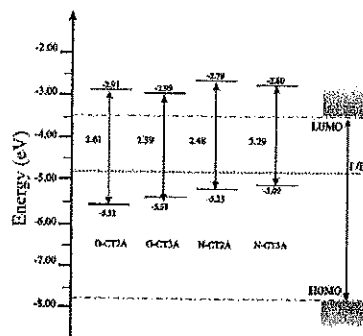


Figure 4. Schematic energy diagram of *N*-CT<sub>n</sub>A and *O*-CT<sub>n</sub>A (*n*=2-3)

As shown in Fig. 4, the calculated HOMO energy level was slightly higher, the LUMO energy level is a little lower, and the HOMO-LUMO gap was smaller, compared with those of *N*-coumarin and *O*-coumarin respectively, indicating the stronger electron donor ability of the *N*-coumarin than that of *O*-coumarin in the similar molecular structure. Moreover, increasing the number of the thiophene units increased the HOMO level and narrowed the HOMO-LUMO gap of the *N*-coumarin and *O*-coumarin dyes obviously.

### 3.4 Absorption spectra

TD-DFT calculations on a B3LYP/6-31G (d,p) level of theory show two transitions with large oscillator strengths consistent with the absorption spectrum. The UV-vis absorption spectra of all compounds are shown in Figure 5. Their photophysical characteristics are listed in Table 3. The absorption peaks of *O*-CT<sub>2</sub>A and *N*-CT<sub>2</sub>A existed at 503 and 541 nm; whereas *O*-CT<sub>3</sub>A and *N*-CT<sub>3</sub>A present an intense red-shift absorption peak at 567 and 593 nm due to their elongated conjugations. Coumarin-based dyes exhibited two intense absorptions in the ultraviolet region and one in the visible region.

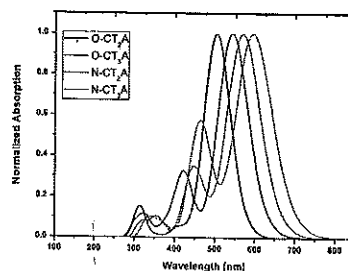


Figure 5. The absorption spectra of *N*-CT<sub>n</sub>A and *O*-CT<sub>n</sub>A (*n*=2-3)

Usually, the absorption bands at around 503–541 nm can be attributed to the  $\pi-\pi^*$  transition and bands at around 567–593 nm attributed to the ICT between the donor and the acceptor which was consistent with the assignment to the transition from the ground state ( $S_0$ ) to the first singlet excited state ( $S_1$ ) according to calculation results.

Table 3. Electronic transition, absorption wavelength and oscillator strength ( $f$ ) and excitation energy obtained by TDDFT at the B3LYP/6-31G(d,p)

Molecules	Electronic transition	$\lambda_{max}$ (nm)	Main contribution H→HOMO, L→LUMO	Character
N-CT <sub>2</sub> A	S <sub>0</sub> →S <sub>1</sub>	541.9 (1.3468)	H→L (82%)	ICT
	S <sub>0</sub> →S <sub>2</sub>	422.3 (0.4302)	H→L+1 (33%) H→L→L (41%)	$\pi-\pi^*$
N-CT <sub>3</sub> A	S <sub>0</sub> →S <sub>1</sub>	593.3 (1.4221)	H→L (85%)	ICT
	S <sub>0</sub> →S <sub>2</sub>	463.1 (0.8124)	H→L+1 (33%) H→L→L (40%)	$\pi-\pi^*$
O-CT <sub>2</sub> A	S <sub>0</sub> →S <sub>1</sub>	503.0 (1.6047)	H→L (78%)	ICT
	S <sub>0</sub> →S <sub>2</sub>	315.6 (0.1869)	H→L→L+1 (57%) H→L+2 (37%)	$\pi-\pi^*$
O-CT <sub>3</sub> A	S <sub>0</sub> →S <sub>1</sub>	567.7 (1.5452)	H→L (82%)	ICT
	S <sub>0</sub> →S <sub>2</sub>	358.6 (0.1321)	H→L+2 (63%) H→L→L+1 (25%)	$\pi-\pi^*$

The absorption bands arise from ICT slightly red-shifted with the introduction of more thiophene units due to the expansion of the  $\pi$ -conjugation length. Due to the strong push-pull systems, red shifts of the lower energy absorption band indicate that this band could be attributed to the electronic transition delocalized throughout the whole molecule with a charge-transfer character.

#### 4. Conclusions

The geometries, electronic structures, polarizabilities and optical properties of the N-coumarin and O-coumarin were studied by using density functional theory with hybrid functional B3LYP, and the UV-vis spectra were investigated by using TDDFT methods. The optimized geometries of these compounds yielded fully planar geometry in the ground state. The features of absorption spectra in visible and near-UV region were assigned, and the absorptions were all ascribed to the  $\pi-\pi^*$  transition and ICT between the donor and the acceptor according to the qualitative agreement between the experiment and the TDDFT calculations. When comparing those of N-coumarin and O-coumarin, the energy gap of N-coumarin was smaller than that of O-coumarin, indicating the stronger electron donor ability of the N-coumarin than that of O-coumarin. So this electron donor ability indicates that the choice of the appropriate donor in dye sensitizer is very important for improving the performance of DSCs.

#### Acknowledgements

The authors would like to express grateful acknowledgments to Department of Chemistry, Faculty of Science, Ubon Ratchathani University and Thailand Graduate Institute of Science and Technology (TGIST)

#### References

- [1] K. Hara, K. Sayama, Y. Ohga, A. Shinpo, S. Suga, H. Arakawa, *Chem. Commun.* (2001) 569–570
- [2] J.M. Rehm, G.L. McLendon, Y. Nagasawa, K. Yoshihara, J. Moser, M. Grätzel, *J. Phys. Chem. B* **100** (1996) 9577–9578
- [3] Z.-S. Wang, K. Hara, Y. Dan-oh, C. Kasada, A. Shinpo, S. Suga, H. Arakawa, H. Sugihara, *J. Phys. Chem. B* **109** (2005) 3907
- [4] K. Hara, M. Kurashige, Y. Dan-oh, C. Kasada, A. Shinpo, S. Suga, K. Sayama, H. Arakawa, *N.J. Chem.* **27** (2003), 783
- [5] Y. Kurashige, T. Nakajima, S. Kurashige, K. Hirao, *J. Phys. Chem. A* **111** (2007) 5544–5548
- [6] C.-R. Zhang, Z.-J. Liu, Y.-H. Chen, H.-S. Chen, Y.-Z. Wu, L.-H. Yuan, *THEOCHEM - J. Mol. Struct.* **899** (2009) 86–93
- [7] M. J. Frisch, Gaussian 03, Revision E. 01, Gaussian Inc., Wallingford, CT, 2004.

**VITAE**

<b>Name</b>	Miss Rattanawalee Rattanawan
<b>Date of Birth</b>	28 <sup>th</sup> April 1988
<b>Birth Place</b>	Si-Sa-Ket, Thailand
<b>Education</b>	B.Sc. (Chemistry), Ubon Ratchathani University, Ubon Ratchathani, Thailand (2010) M.Sc. (Chemistry), Ubon Ratchathani University, Ubon Ratchathani, Thailand (2010-2012)
<b>Address</b>	112/3 Moo. 5, Tambon Nong-krok, Amphor Maung, Si-Sa-Ket, Thailand, 33000
<b>Scholarship</b>	Thailand Graduate Institute of Science and Technology (TGIST) (2010-2012)